THE PLASTIC DEFORMATION OF AN IRON-MOLYBDENUM ALLOY

Thesis submitted for the degree of

Doctor of Philosophy

by

Rees David Rawlings

B.Sc.(Eng.) (London 1964)

June 1967

Department of Metallurgy,

Imperial College of Science
and Technology,

University of London.

ABSTRACT

The effect of precipitation of an intermetallic compound on the density, Young's modulus and, in particular, the deformation behaviour of an iron-11 at.% molybdenum alloy has been investigated.

In an attempt to determine the nature of the phase precipitated, the Fe-Mo system was examined by means of diffusion couples. It was confirmed that the R, ε and σ-phases are formed in this system but the existence of the Laves phase, λ, was not verified.

Prior deformation and the temperature of ageing altered the kinetics of ageing and the incremental hardness change; in contrast, the solution treatment temperature had very little effect on the ageing characteristics. Both the density and modulus increased with the precipitation of the intermetallic compound, and from these measurements time exponent values of 1.0 and 1.5 were obtained for the material aged with and without prior deformation.

Precipitation resulted in an increase in the proof stress, initial rate of work-hardening and the maximum stress sustained in compression, and a decrease in the work-hardening exponent and the strain to fracture at room temperature. The mechanical properties change only slightly with overageing.

The temperature dependence of the 0.2% proof stress at low temperatures of the solid solution and aged conditions was similar, indicating that precipitation altered the athermal stress but not the effective stress. The results below about 200°K for all conditions of the alloy were consistent with a theory for the Peierls' mechanism of plastic deformation. In the temperature range 200-500°K another activated process, or processes, were rate controlling but could not be identified. Above 500°K, over a temperature range which depended on the structural condition of the alloy, the deformation was relatively temperature independent. At more elevated temperatures the deformation for all forms of the alloy was again temperature dependent and was associated with a process with an activation energy similar to that for diffusion in Fe-Mo.

CONTENTS

Page

ABSTRACT 2

CHAPTER 1 INTRODUCTION 6

CHAPTER 2 THE IRON-MOLYBDENUM PHASE DIAGRAM 8

CHAPTER 3 THE AGEING CHARACTERISTICS OF Fe-11 At.% Mo ALLOY 17

3.1. Introduction 17

3.2. Experimental Procedure 17

3.2.1. Material and Specimen Preparation .. 17

3.2.2. Metallography and Hardness Measurements 18

3.2.3. Density Measurements 18

3.2.4. Young's Modulus Measurements 19

3.3. Results 21

3.3.1. Hardness, Density and Modulus Measurements 21

3.3.2. Metallography 24

3.4. Discussion 26

3.4.1. Hardness and Metallography 26

3.4.2. Density 29

3.4.3. Young's Modulus 31

3.4.4. Kinetics of Precipitation 32

CHAPTER 4 THE MECHANICAL PROPERTIES OF Fe-11 At.% Mo ALLOY 47

Page

4.1. Introduction 47

4.2. Experimental Procedure 48

4.3. Results 50

4.3.1. Room Temperature Behaviour 51

4.3.2. Effect of Temperature 52

4.4. Discussion 56

4.4.1. Room Temperature Properties 56

4.4.2. Effect of Temperature 57

4.4.3. Fracture Behaviour 59

CHAPTER 5 DEFORMATION PROCESS IN Fe-11 At.% Mo ALLOY .. 84

5.1. Introduction 84

5.2. Experimental Procedure 88

5.3. Results 88

5.3.1. Temperature Range 77^{o}-500^{o}K 88

5.3.2. Temperature Range 500^{o}-1100^{o}K 90

5.4. Discussion 92

5.4.1. Behaviour Below 500^{o}K 92

5.4.2. Athermal Behaviour 98

5.4.3. High Temperature Behaviour 101

CHAPTER 6 SUGGESTIONS FOR FURTHER WORK 124

ACKNOWLEDGEMENTS 127

APPENDICES 128

REFERENCES 132

CHAPTER 1

INTRODUCTION

Most studies of precipitation hardening phenomena have been carried out on face-centred cubic metals, particularly aluminium. Although interest has been developing - except for investigations of carbide and nitride precipitation - relatively little attention has been paid to body-centred cubic alloys.

It was felt that an extensive examination of the effect on the mechanical properties of the precipitation of an intermetallic compound in a pure, binary, b.c.c. alloy would provide a valuable assessment of the potential of precipitate hardening in these alloys, and also a useful comparison with the behaviour of f.c.c. alloys. It was decided to base the investigation on an iron alloy in preference to other b.c.c. alloys in order that the results might be more applicable to common industrial alloys. The main reasons for the choice of an iron-molybdenum alloy containing nominally 10 at.% molybdenum were

i. studies made by other workers (e.g. Sykes 1926 and 1940, Elsen and Wassermann 1961, Reiter and Hibbard 1955) provided useful background information;

ii. the high temperature αFe region is extensive, so allowing a wide range of solution treatment temperatures;

iii. the equilibrium volume fraction of precipitate in the temperature range 823-1073°K is about 0.18-0.26, depending on whether the ε or λ-phase is precipitated. Consequently any property change due to precipitation is likely to be of reasonable magnitude and therefore measurable; in comparison any side effects which might arise from trace amounts of interstitial impurities should be negligible.

The one disadvantage of using this alloy is the doubt concerning the structure and composition of the precipitate.

The problem of the uncertainty of the iron-rich part of the iron-molybdenum phase diagram is dealt with in more detail in the following chapter which reports the results of an examination of the system by means of diffusion couples. Chapter 3 is concerned with the data obtained from a study, which was preliminary to the main investigation of the mechanical properties, of the ageing characteristics of the alloy. The room temperature mechanical properties of the alloy after various thermal and thermo-mechanical treatments, and the temperature dependence of the mechanical properties for the alloy in four different structural conditions, are discussed in Chapter 4, whereas the operative thermally activated mechanisms of plastic deformation are analysed in Chapter 5.

CHAPTER 2

THE IRON-MOLYBDENUM PHASE DIAGRAM

There is some uncertainty concerning the number of intermetallic compounds that are formed in the iron-molybdenum system and this chapter reports the results of an examination of the system by means of diffusion couples.

The phase diagram according to Hansen (1958) has two intermetallic phases (Figure 2.1.). The ε-phase has a rhombohedral structure (Westgren 1936), and the composition of the molybdenum-rich boundary corresponds approximately to the formula Fe_3Mo_2, although the crystal structure is characterised by the formula Fe_7Mo_6. The σ-phase has a tetragonal structure (Bergman and Shoemaker 1954) and the molybdenum-rich boundary is thought to coincide with the composition FeMo.

The diagram constructed by Sinha et al. (1967) is more complex in that in addition to the ε (called μ by Sinha et al.) and σ-phases there are two other intermetallic compounds, R and λ (Fig. 2.2.). The earlier work of Bechtoldt and Vacher (1957), which showed that λ was an hexagonal Laves phase, Fe_2Mo, formed by a peritectoid reaction at about 1223°K, was confirmed by Sinha et al. The rhombohedral R-phase contains approximately 37.4 at.% Mo and decomposes eutectoidally at $1528^{\circ} \pm 10^{\circ}K$.

Diffusion couples were constructed by mechanically clamping a polished disc of molybdenum (3 mm thick, 6 mm diameter)

between two polished strips of iron (4 mm thick). The molybdenum was sintered high-purity molybdenum (99.97%) and the iron was deoxidised, Japanese electrolytic iron of approximately 99.96% purity. For heat treatments the couples were encapsulated in an argon atmosphere in silica. The specimens were quenched into water from the annealing temperature, sectioned and examined with a Cambridge Geoscan or a J.E.O.L. JXA3A electron-probe microanalyser. Microhardness tests were performed on the couples annealed at 1173° and 1593°K.

The results of the investigation are given in Table 2.1. The Laves phase was not observed in the two couples annealed below the peritectoid temperature 1223°K. This does not, however, preclude the existence of this compound as only positive diffusion couple results are really definitive: if a phase is not observed it may be argued that it is present in such a thin layer that it is not detected or that the annealing time was insufficient for the phase to nucleate. The back-scattered electron topographical image, with superimposed line scans for FeKα and MoLα radiations, of the interface of the 1173°K diffusion couple is given in Fig. 2.3. The plateau in the line scans corresponds to the ε-phase. This phase was also clearly distinguished by coloured, compound X-ray scanning pictures which were produced by the technique of direct colour synthesis (Jones et al. 1966) (Fig. 2.4.). At 1398°K, in agreement with

both phase diagrams and the work of Seebold and Birks (1960) on a couple annealed at 1373°K, only the ε-phase was formed. Although, due to experimental error, the absolute mean compositions of the ε-phase produced in the 1073°, 1173° and 1398°K diffusion couples differed, the homogeniety range in each case was only of the order of 1 at.% Mo.

The line scan across the interface of the couple annealed just above the eutectoid temperature, 1528°K, had two distinct plateaus. Point counts taken in the lower molybdenum content layer gave the composition of the molybdenum-rich side as 39.5 at.% Mo and the iron-rich side 37 at.% Mo. This large compositional variation was not consistent with the existence of the ε-phase only, and, since these two compositions corresponded well with those of the R and ε-phases it seemed most probable that both these phases were present and that they were separated by an ill-defined interface.

The results of the 1593°K anneal unambiguously confirmed the existence of the R-phase. The back-scattered electron compositional line scan (blue), superimposed on the absorbed electron image, is given in Fig. 2.5.; Fig. 2.6. shows a different field of view with the scan superimposed on the back-scattered electron topographical image. This couple was re-annealed at 1593°K, cooled in still air, and re-examined. The R-phase was again identified; this is in agreement with

the findings of Sinha et al. that the decomposition of this phase requires prolonged heat treatments.

Unfortunately it was impossible to study the intermetallic compounds formed at 1680°K as both the couples heat treated at this temperature parted at the interface.

The hardness of the R and ε-phases were similar; the mean of a number of microhardness tests gave H.V. = 955 and 1054 for the R and ε-phases respectively.

This investigation has confirmed that the R, ε and σ-phases are produced in the Fe-Mo system, but was unable to verify the existence of the Laves phase.

Table 2.1.

Temperature °K	Time hr.	Mean Composition (at.%Mo) and Thickness (10^{-4}cm.) of Phases					
		R-Phase		ε-Phase		σ-Phase	
		Composition	Thickness	Composition	Thickness	Composition	Thickness
1073	4.60×10^3			40	6		
1173	1.95×10^3			42.8	11		
1398	2.93×10^2			39.0	47		
1528	1.59×10^2	37.0	10	39.5	10	†	3
1593	1.40×10^2	36.6	10	41.6	15	†	5
1683	10 & 24	Specimens parted at interface					

† Present but composition not accurately measured.

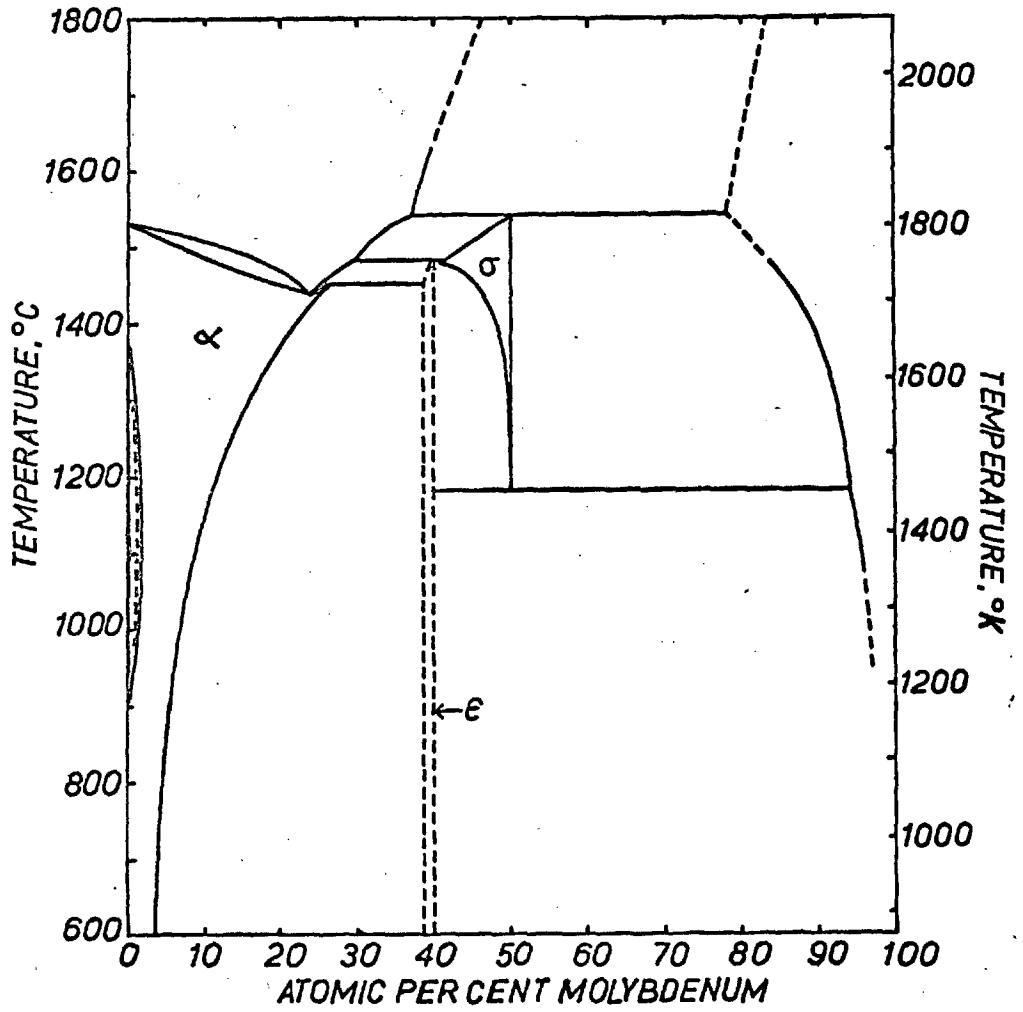

Fig. 2.1. Iron-molybdenum phase diagram according to Hansen.

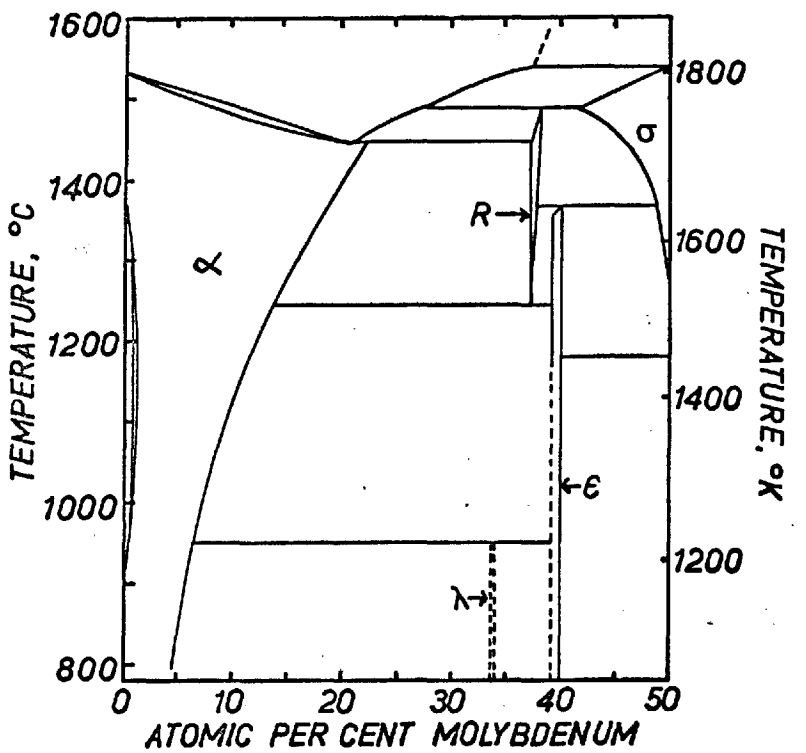

Fig. 2.2. Iron-rich part of the iron-molybdenum phase diagram according to Sinha et al.

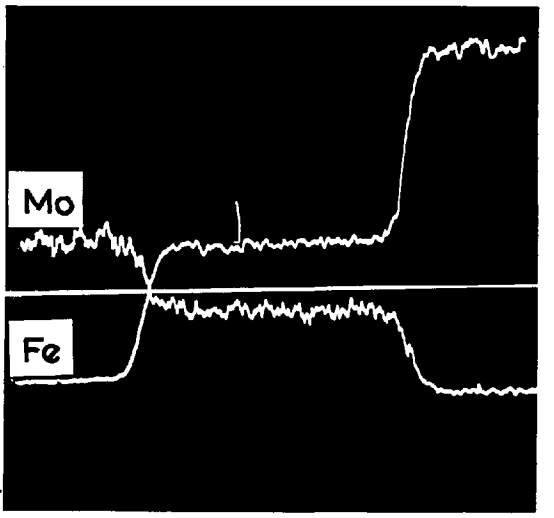

Fig. 2.3. FeMo Diffusion Couple 1944 hrs. at 1173°K.

Back-scattered electron picture with superimposed line scan for Fe K_α and Mo L_α radiation along a horizontal line. Magnification X2880.

Fig. 2.4. Coloured, compound X-ray scanning picture of the couple annealed at 1173°K. x 750.

Fig. 2.5. Back-scattered electron composition line scan superimposed on the absorbed electron image for the couple annealed at 1593°K. x 1200.

Fig. 2.6. Back-scattered electron composition line scan superimposed on the back-scattered electron topographical image for the couple annealed at 1593°K. x 1200.

CHAPTER 3

THE AGEING CHARACTERISTICS OF IRON-11 AT.% MOLYBDENUM ALLOY

3.1. Introduction

This chapter reports the results of a study of the effect of prior deformation, solution treatment temperature, and ageing temperature on the ageing characteristics of an Fe-11 at.% Mo alloy. As well as the hardness increase, the change in density and Young's modulus with ageing has been investigated.

3.2. Experimental Procedure

3.2.1. Material and Specimen Preparation

A 29 kg ingot of the alloy was cast at R.A.R.D.E., Fort Halstead, from deoxidised, Japanese electrolytic iron, and sintered, high purity, molybdenum (supplied by Murex Ltd.). The ingot was homogenised for six hours at 1473^{o}K and then worked, with intermediate anneals, into 6 mm and 16 mm diameter rods and 6 mm plate. Chemical analysis of the alloy gave, wt.% Mo 17.5 (11 at.%), C 0.003, Si 0.002, S 0.005, P <0.002 and O_2 0.0098.

Solution treatments were carried out under a dynamic argon atmosphere in a vertical, 'crusilite' element, furnace which had facilities for rapid quenching into iced water.

Except for the study of the effect of solution treatment temperature, all specimens were heat treated at 1573 $\pm$ 2°K for one hour. Salt baths were used for the ageing treatments.

Specimens for hardness, density and Young's modulus measurements were prepared from the stock rod or bar by machining and slitting with thin silicon carbide blades. A particular series of specimens were deformed prior to ageing in a Denison universal testing machine.

3.2.2. Metallography and Hardness Measurements

Specimens for optical metallography were mechanically polished on successively finer grades of diamond paste down to ¼μ. After polishing the specimens were etched in either alcoholic ferric chloride or in a 2% nital solution.

Vickers Diamond Pyramid hardness data were obtained using a 30 kg load. At least five impressions were averaged for each determination.

3.2.3. Density Measurements

Density measurements were made using a displacement technique in which each specimen was weighed in air and in

dibromoethane at 296°K. The specimens were cylindrical and weighed 3-4 gm ; all weighings were made on a balance reading to 1 x 10^{-5} gm. For each specimen the mean value of five weighings was used to calculate the density.

The density, ρ, of a specimen is given by:

$$\rho = \frac{W_A}{W_A - W_D} \cdot \rho_D \qquad (3.1.)$$

where W_A and W_D are the weights of the specimen in air and in dibromoethane respectively, and ρ_D is the density of the dibromoethane. ρ_D was evaluated using the displacement procedure and a standard nickel specimen. The error in an absolute density value was estimated to be 0.011% (Appendix I).

To obtain the density as a function of ageing time a single specimen was used and the density measured at various stages of ageing.

3.2.4. Young's Modulus Measurements

The Young's modulus of the alloy was determined over the temperature range 296°-520°K by recording the resonant frequency of the fundamental mode of the flexural vibrations of a plate specimen (Förster 1937). The apparatus* was similar to that

* The apparatus was constructed by D. C. Phillips of this department.

used by Wachtman and Lam (1959).

Young's modulus, E, is given by:

$$E = CWf^2 \qquad (3.2.)$$

where W is the weight of the specimen, f the resonant frequency and C a factor which depends upon the shape and size of the specimen, the mode of vibration, and Poisson's ratio. The value for C for flexural vibrations of prismatic bars can be calculated from the equation due to Pickett (1945):

$$C = 9.467 \times 10^{-1} \frac{1}{b} \left(\frac{\ell}{t}\right)^3 T_1 \qquad (3.3.)$$

where ℓ, t and b are the length, width and depth of the specimen respectively; T_1 is a correction factor which depends on the ratio of the radius of gyration across the width of the specimen and the length of the specimen, and on Poisson's ratio. For values of Poisson's ratio of 0, $\frac{1}{3}$ and $\frac{1}{6}$ Pickett gives equations from which T_1 can be calculated to five significant figures. Poisson's ratio of the alloy in all conditions was assumed to be $\frac{1}{3}$.

Specimens of nominal size 50.0 x 8.0 x 3.5 mm were machined from a solution treated sample of the alloy. Specimens of this size exhibited a resonant frequency of about 7000 c/s which was

the most stable frequency range of the oscillator. The specimens were weighed on a semi-micro balance and their dimensions measured with a micrometer. The estimated error of the technique was $\pm$ 0.33% (Appendix II).

The signal to noise ratio decreased with increasing temperature and above about 520^{o}K accurate measurement of the resonant frequency could no longer be made. The dimensions of the specimens were corrected for thermal expansion at elevated test temperatures by assuming a typical value for an iron alloy of 15 x 10^{-6} $^{o}K^{-1}$ for the coefficient of thermal expansion. This correction was small compared with the change in modulus with temperature.

The procedure for determining the modulus as a function of time of ageing at 923^{o}K was the same as that followed in the density investigation. The density data were used to correct for the change in the specimens dimensions as a result of the precipitation of the intermetallic compound.

3.3. Results

3.3.1. Hardness, Density and Modulus Measurements

Hardness measurements as a function of ageing time at different ageing temperatures are shown in Fig. 3.1. Discontinuities

which are often, but not always, associated with ageing that occurs via zones and intermediate precipitates were not observed. The alloy exhibited normal ageing behaviour, that is, the higher the ageing temperature the more rapid the attainment of peak hardness, but the lower the hardness value at the peak.

As found by Elsen and Wassermann (1961), deformation prior to ageing has a marked effect on the ageing characreristics of the alloy (Fig. 3.2.). The rate of hardening was increased by deformation of the solid solution; this is particularly apparent for the 748°K ageing treatment, where a large increase in hardness was observed for the deformed specimens. Prior deformation increased not only the rate of hardening but also the incremental change in hardness, ΔH.V. on ageing (Table 3.1.)

Table 3.1.

Ageing Temperature °K	% Def.	Time to Peak Hardness (Min)	Hardness HV		
			Solid Solution	Peak Hardness Condition	ΔH.V.
923	0	150	228	522	294
923	10	60	272	648	376
923	35	20	328	685	357
1073	0	3	228	390	162
1073	10	½*	272	542	270

* Shortest heat treatment given.

The hardness curves for specimens solution treated at 1473, 1573 and 1673°K and aged at 923°K are shown in Fig. 3.3. Although there was considerable scatter in the results it is clear that in the early stages of ageing the hardness was slightly greater the higher the solution treatment temperature. This was probably associated with the partial retention of the equilibrium vacancy concentration at the solution treatment temperature by the rapid quench into iced water; the excess vacancies would lead to enhanced diffusion in the early stages of ageing.

The density and Young's modulus of the alloy increased with the precipitation of the intermetallic compound (Figs. 3.4. and 3.5.). By comparing these curves with the appropriate hardness vs. time curves of Fig. 3.2. it can be seen that the maximum values of density, modulus and hardness were reached after the same ageing time. The density and modulus remained constant at the maximum value during overageing showing that there was not a change in the structure of the precipitate phase.

The increase in density after ageing for 10 minutes at 923°K as a function of prior deformation indicated that only a small amount of deformation was needed to increase markedly the kinetics of the precipitation process (Fig. 3.6.).

The modulus of the alloy in the solid solution, slightly aged (20 minutes at 923°K), aged to peak hardness (150 minutes

at 923°K) and overaged (2 x 10^3 minutes at 923°K) conditions decreased linearly with test temperature. The change in modulus, ΔE, plotted against temperature lie on the same straight line, within experimental error, for all conditions of the alloy (Fig. 3.7.). The slope of the graph is -5.5 x 10^8 dyne $cm^{-2}\ {}^{o}K^{-1}$ giving $\frac{\Delta E}{E}$ for the solid solution of approximately $-2.9 \times 10^{-4}\ {}^{o}K^{-1}$.

3.3.2. Metallography

Metallographic examination showed that precipitation had occurred throughout the grains for short ageing times (corresponding to a hardness increase of some 20 H.V.) at all temperatures. The amount of precipitate increased and became more uniform with ageing up to the peak hardness condition. The precipitate particles were larger the higher the ageing temperature; those formed during the 1073°K heat treatment were easily resolvable with the optical microscope and were rod and/or plate-like. No change in the structure with overageing could be detected at the low ageing temperatures, but the beginning of coalescence and spheroidisation was observed in the alloy aged for 475 minutes at 1073°K (Fig. 3.8.). After ageing for 2.8 x 10^5 minutes at this temperature, coalescence and spheroidisation had occurred to such an extent that the precipitate particles were no longer

elongated and the hardness had fallen to a value similar to that of the solid solution.

Precipitate-free zones were produced at the grain boundaries in the early stages of ageing at all heat treatment temperatures. The precipitation appeared to be more advanced at the edge of the zone than within the bulk of the grains (Fig. 3.9.). The zones decreased in size with ageing and in most instances had disappeared well before the peak hardness condition was reached (Fig. 3.10.). The zones were narrower the higher the solution treatment temperature. In the case of the highest ageing temperature, 1073^{o}K, marked precipitate-free zones were reformed after long heat treatments. These zones were associated with a large, continuous, grain boundary precipitate (Fig. 3.8.).

Precipitation occurred preferentially on the deformation structure, i.e. the twins and slip bands, of the specimens deformed prior to ageing. It has been suggested that both nucleation (Cahn 1957) and growth (Cottrell and Bilby 1949, Harper 1951) are increased when precipitation takes place on dislocations. Precipitate-free zones at grain boundaries were not formed in the early stages of ageing in specimens that were deformed prior to ageing. The ability of prior deformation to inhibit zone formation has also been reported in Al-Si and Al-Zn-Mg-Cu alloys (Rosenbaum and Turnball 1958 and 1959, Thomas 1960). However, zones were formed at grain boundaries

and at deformation twins on overageing at 1073°K.

As a consequence of the preferred precipitation on dislocations and twins, the deformation caused by the stresses set up during the rapid quench from the solution treatment temperature was revealed. Both slip and twinning took place in the surface regions of the specimens, but of particular interest are the twin interactions and the associated strain fields (Fig. 3.11.). Hornbogen (1961a) has studied the dynamic effects during twinning in Fe-19.5 at.% Mo and Fe-3.2 at.% P alloys; in addition to the interactions found by Hornbogen in Fe-Mo, an interaction between parallel twins which produced slip deformation between the narrow twins was observed (Fig. 3.12.). Since in the majority of cases there was no plastic strain between parallel twins it is possible that slip was only produced if the twins were formed simultaneously causing an interaction between the stress waves associated with both twins.

3.4. Discussion

3.4.1. Hardness and Metallography

The thermally activated process of precipitation from a supersaturated solid solution can be represented by the Arrhenius equation:

$$\frac{1}{t} = Ae^{\frac{-Q}{RT}} \qquad (.3.4)$$

where t is time of ageing, Q the average activation energy for precipitation, R the gas constant, T the ageing temperature and A a constant. A plot of the logarithm of the time to peak hardness against the reciprocal of the ageing temperature gave a straight line in accordance with this equation (Fig. 3.13.). By the method of least squares Q was calculated to be 53.1 kcal $mole^{-1}$.

The activation energy for the diffusion of molybdenum or iron in Fe-Mo solid solutions has not been measured, but Mokrov (1964) found that molybdenum in iron increased the activation energy for the formation of vacancies. This indicates that the activation energy for diffusion in Fe-Mo alloys, assuming a vacancy mechanism, is greater than that for self diffusion in iron, which is about 60 kcal $mole^{-1}$. Hence Q is lower than the expected value for the activation energy for diffusion. This may be experimental error or a genuine effect associated with excess vacancy enhanced diffusion in the a early stages of ageing, and/or the formation of concentration gradients in the matrix during precipitation which results in chemical diffusion. Elsen and Wassermann, using the same experimental technique, found that Q = 38 kcal $mole^{-1}$ for precipitation in a Fe-9.8 at.% Mo alloy.

Density is a measure of the amount of solute precipitated, hence, the density data of Fig. 3.4. shows that prior deformation does not induce a greater fraction of the solute to be precipitated. Consequently, the increase in ΔH.V.obtained by prior deformation must be the result of a change in precipitate size and distribution.

Precipitate-free zones formed in the early stages of ageing can be produced by solute denudation, or by slow ageing kinetics due to a vacancy-profile at the grain boundary (see for example Holl 1964, Nicholson and Lorimer 1966). Several scans across zones were made with an electron-probe microanalyser and a change in solute concentration was not observed. This, coupled with the fact that all the experimental observations can be interpreted on the basis of the vacancy-profile theory, suggested that the zones were due to low vacancy concentrations near the grain boundaries.

The precipitate-free zones adjacent to the grain boundaries and twins in the overaged conditions of the alloy, heat treated at 1073^{o}K, were clearly produced by the growth of the massive precipitate at the grain boundaries and twins by coalescence of neighbouring particles.

3.4.2. Density

In view of the doubt concerning the structure and composition of the compound precipitated, it was of interest to compare the experimental change in density on ageing with the theoretical change expected for the precipitation of the λ and ε-phases. The calculation was performed for the precipitation of the ε-phase in the form characterised by its crystal structure Fe_7Mo_6, and that corresponding to the chemical formula, Fe_3Mo_2.

The theoretical percentage change in volume was calculated for the ageing of 100 atoms of the solid solution to the equilibrium condition at 923°K. The equilibrium concentration of the matrix was taken as 2.4 at.% Mo (Abrahamson and Lopata 1966) and it was assumed, as suggested by Sinha et al., that in Fe_3Mo_2 the excess iron atoms occupy molybdenum sites. The relevant structural data are presented in Table 3.2. and the theoretical volume changes in Table 3.3.

The values for the percentage decrease in volume of 1.06, 0.81 and 1.16, for the precipitation of Fe_7Mo_6, Fe_3Mo_2 and Fe_2Mo respectively, are of the same magnitude as the experimental density increase of $0.94 \pm 0.01\%$. The agreement between theory and experiment is better in the case of the precipitation of the ε-phase. However, the theoretical volume changes for the two phases are very similar, and since the calculation depends on the accuracy of the lattice parameter values and to an even

Table 3.2.

Phase & Structure	Composition	Source of Lattice Parameter	Vol. of Structure Cell, $\AA^3$	No. of atoms or molecules per cell
Solid Solution b.c.c.	11 at.% Mo	Present work	24.42	2 atoms
Solid Solution b.c.c.	2.4 at.% Mo	Abrahamson & Lopata (1966)	23.76	2 atoms
ε Rhombohedral	Fe_7Mo_6	Arnfelt & Westgren (1935)	167.33	1 molecule
ε Rhombohedral	Fe_3Mo_2	Arnfelt & Westgren (1935)	167.33	1 molecule
λ Laves	Fe_2Mo	Bechtoldt & Vacher (1957)	150.56	4 molecules

Table 3.3.

Precipitate	Volume Occupied $\AA^3$			∴ % Change in Volume
	Matrix	Precipitate	Solid Solution	
Fe_7Mo_6	954.8	253.0	1220.7	-1.06
Fe_3Mo_2	916.3	294.5	1220.7	-0.81
Fe_2Mo	857.6	348.9	1220.7	-1.16

greater extent on the value taken for the equilibrium concentration of the matrix, this result cannot be taken as definitive.

3.4.3. Young's Modulus

The mean value of the Young's modulus for the three specimens tested in the solid solution condition was $19.49 \pm 0.22 \times 10^{11}$ dyne cm^{-2}. A comparison with the modulus of iron is difficult due to the variation in the data for iron in the literature (Table 3.4.), but it is apparent that molybdenum has very little effect on the modulus of iron. The possibility that there is a reduction in the modulus with the addition of molybdenum would be in keeping with the bigger solute atoms causing large internal strains.

The increase in the modulus of the alloy on ageing was presumably a mixture effect, the hard precipitate particles having a greater modulus than the matrix. Increases in Young's modulus with ageing have also been observed in aluminium alloys (Dudzinski et al. 1948, Dudzinski 1952).

Table 3.4.

Reference	Young's Modulus x 10^{-11} dyne cm^{-2}
Tietz and Wilson 1961	19.36
Metals Handbook A.S.M. 1948	20.76 $\pm$ 0.34
" " " "	20.28
Cleaves and Heigel 1942	19.93 $\pm$ 0.34
Cleaves and Thompson 1936	20.96 $\pm$ 0.49
Mean	20.26

3.4.4. Kinetics of Precipitation

The kinetics of a precipitation reaction can be analysed using the equation suggested by Wert (1949):

$$1 - W = \exp\{-(\frac{t}{s})^{d}\} \qquad (3.5.)$$

where W is the fraction of solute precipitated at time t, d and s are constants; d is called the time exponent.

Using the density and modulus results straight line graphs were obtained for log $\ell n(\frac{1}{1-W})$ plotted against log t in accordance with equation 3.5. (Fig. 3.14.). The time exponent derived (by the method of least squares) for the material aged without prior deformation from the density and modulus measurements

was 1.47 and 1.64 respectively. The fact that d was approximately 1.5 indicated that the particles must have grown from initially negligible dimensions with constant eccentricity (Ham 1958). d values of 1.5 have been determined for other systems with non-spherical precipitate, e.g. Al-Cu where the precipitate particles are disc-shaped (Lankes and Wassermann 1950, Guinier 1952).

Prior deformation reduced the value of d to 1.08, which was in agreement with the value d = 1 predicted by Ham (1959) for precipitation on dislocations.

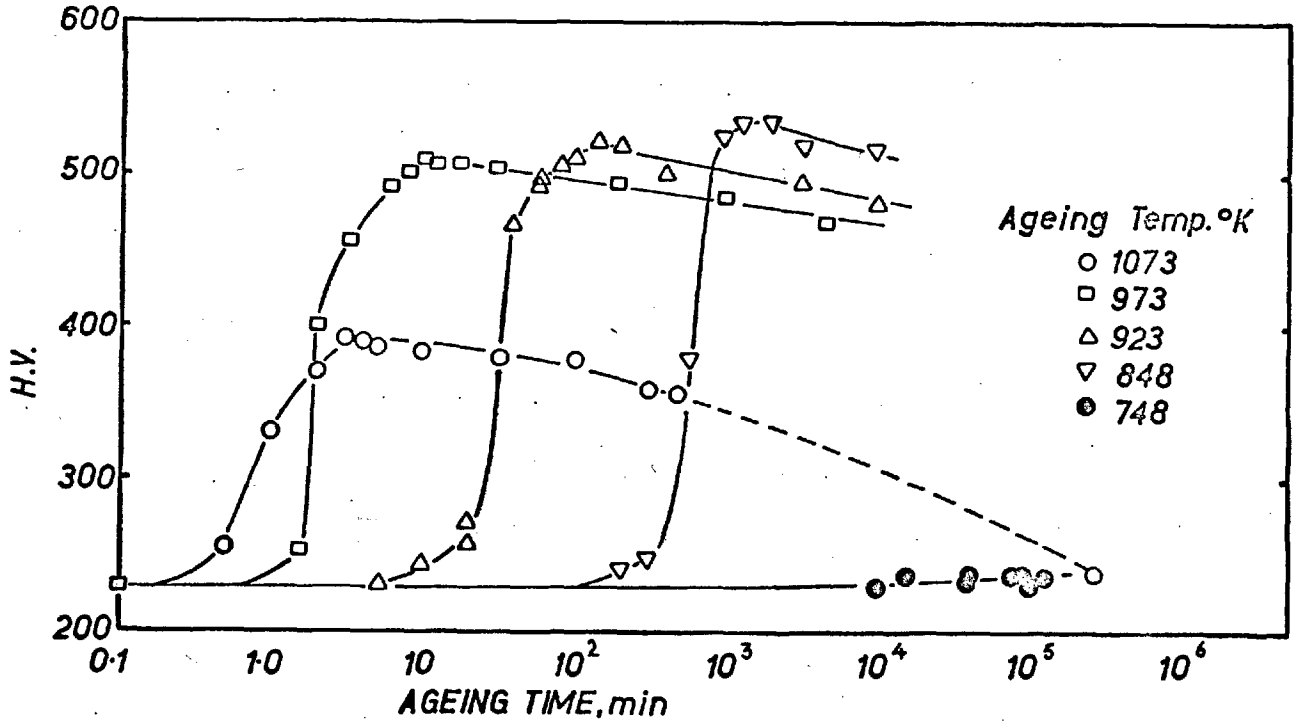

Fig. 3.1. Effect of temperature on the ageing behaviour.

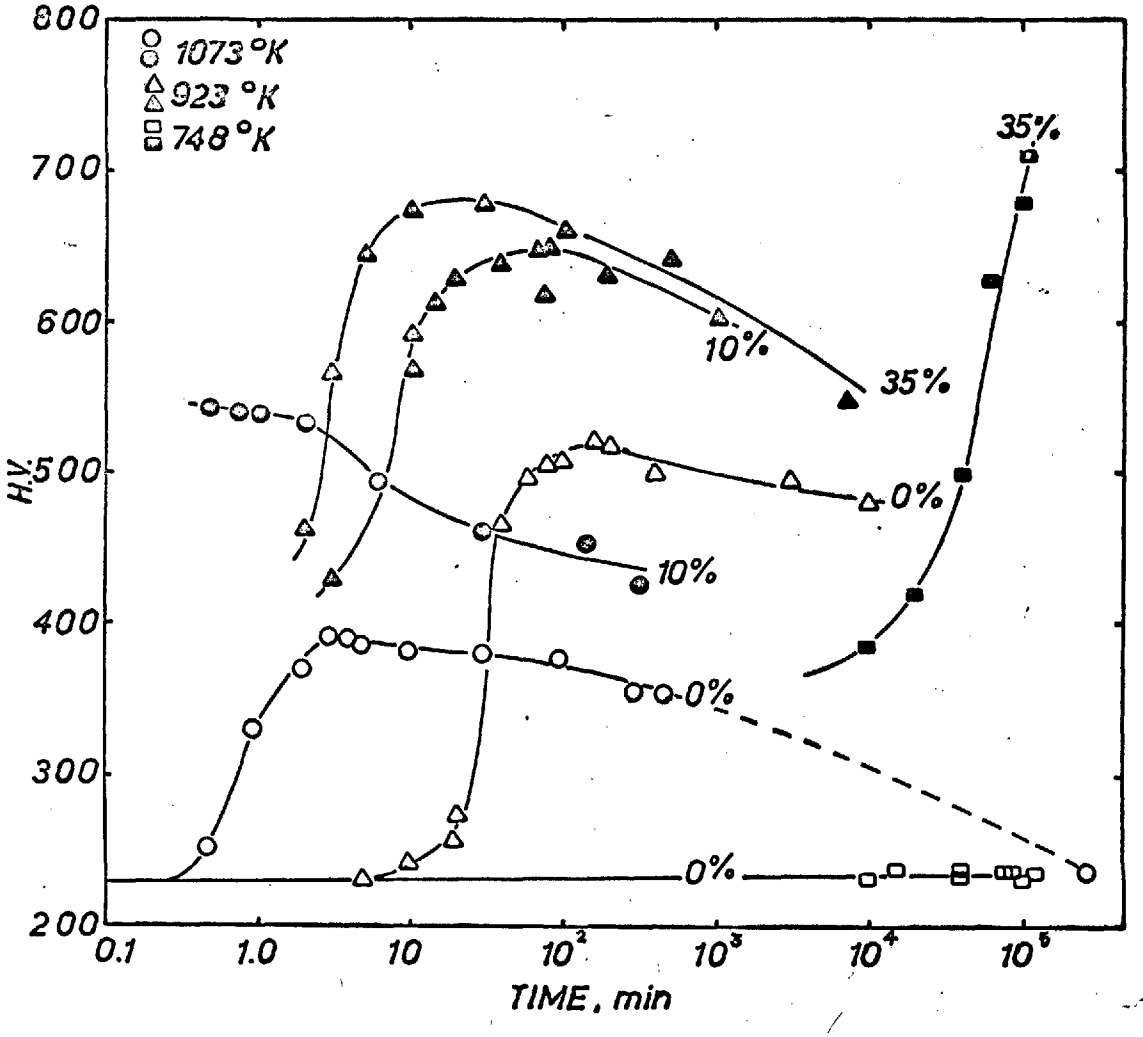

Fig. 3.2. Effect of prior deformation on the ageing behaviour.

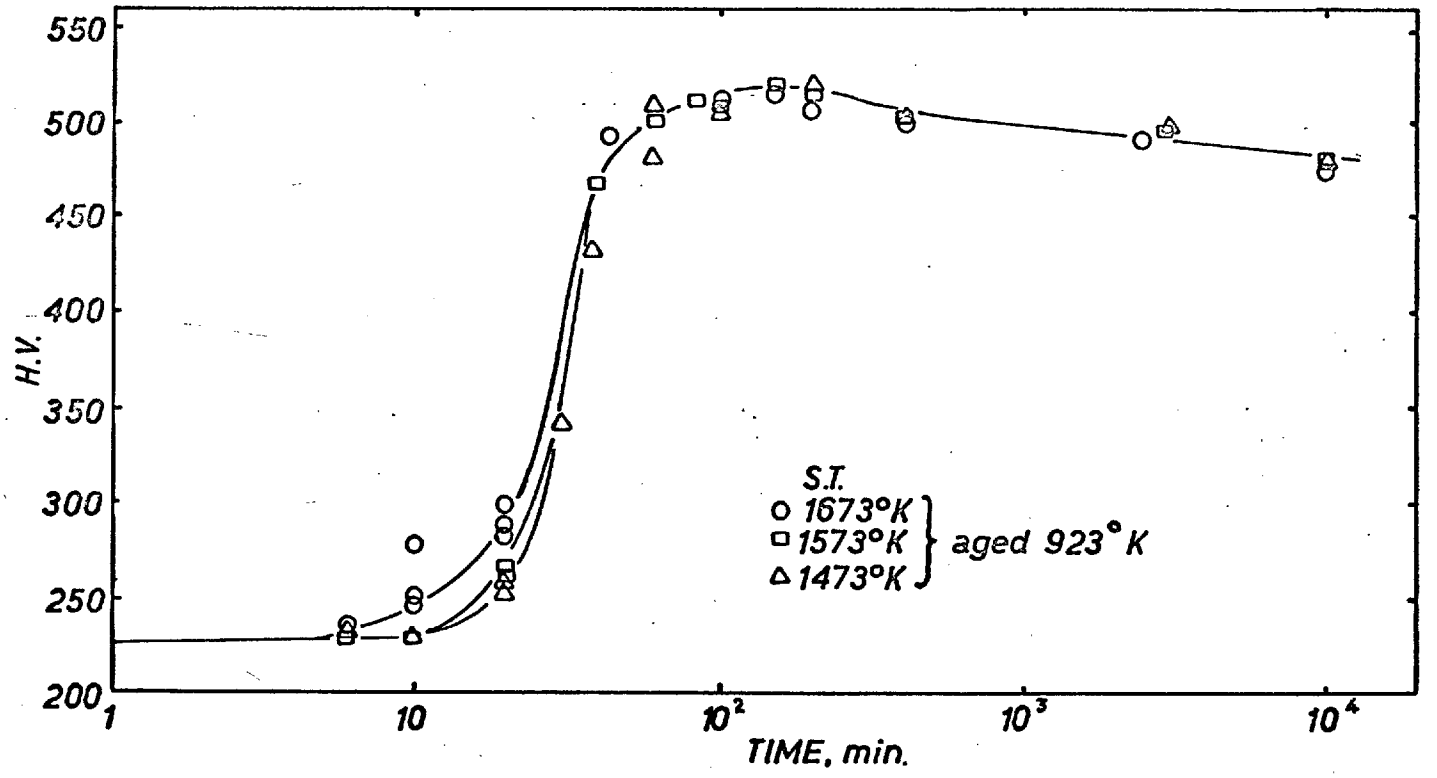

Fig. 3.3. Effect of solution treatment temperature on the ageing behaviour.

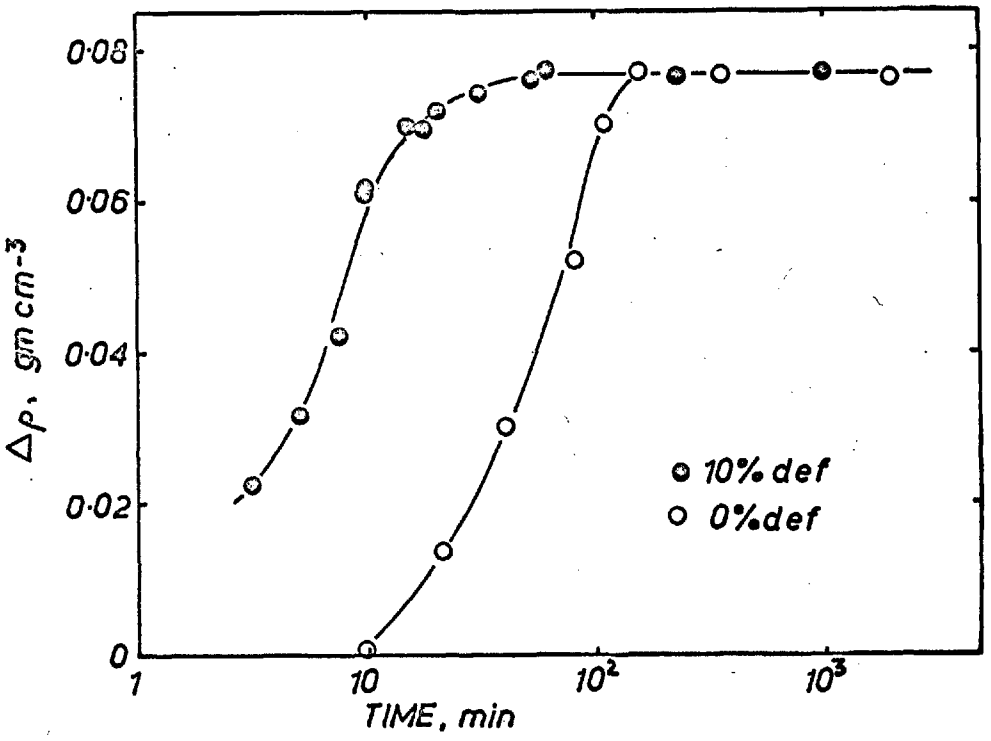

Fig. 3.4. Change in density as a function of ageing time at 923°K.

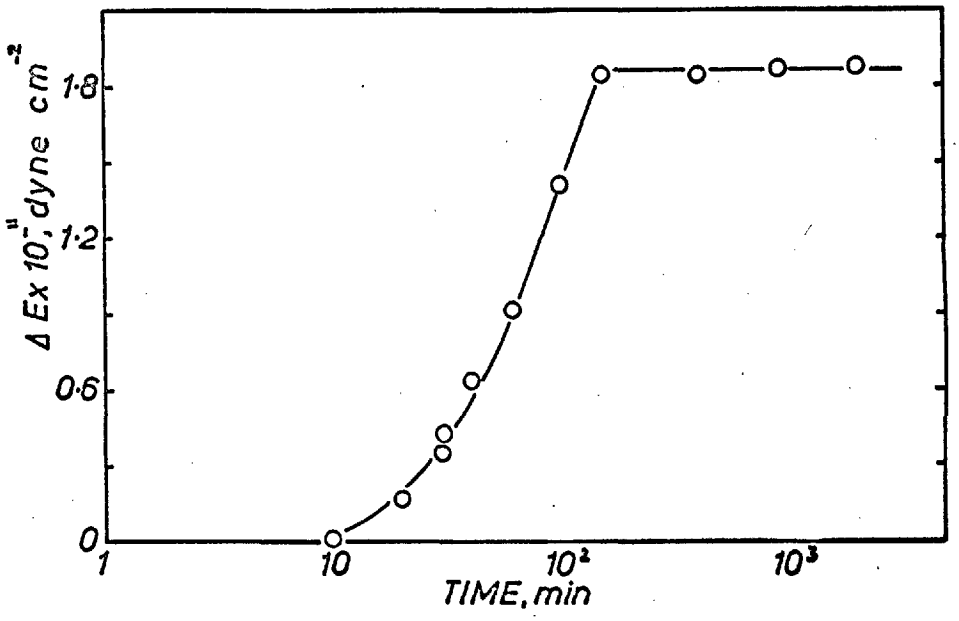

Fig. 3.5. Change in Young's modulus as a function of ageing time at 923°K.

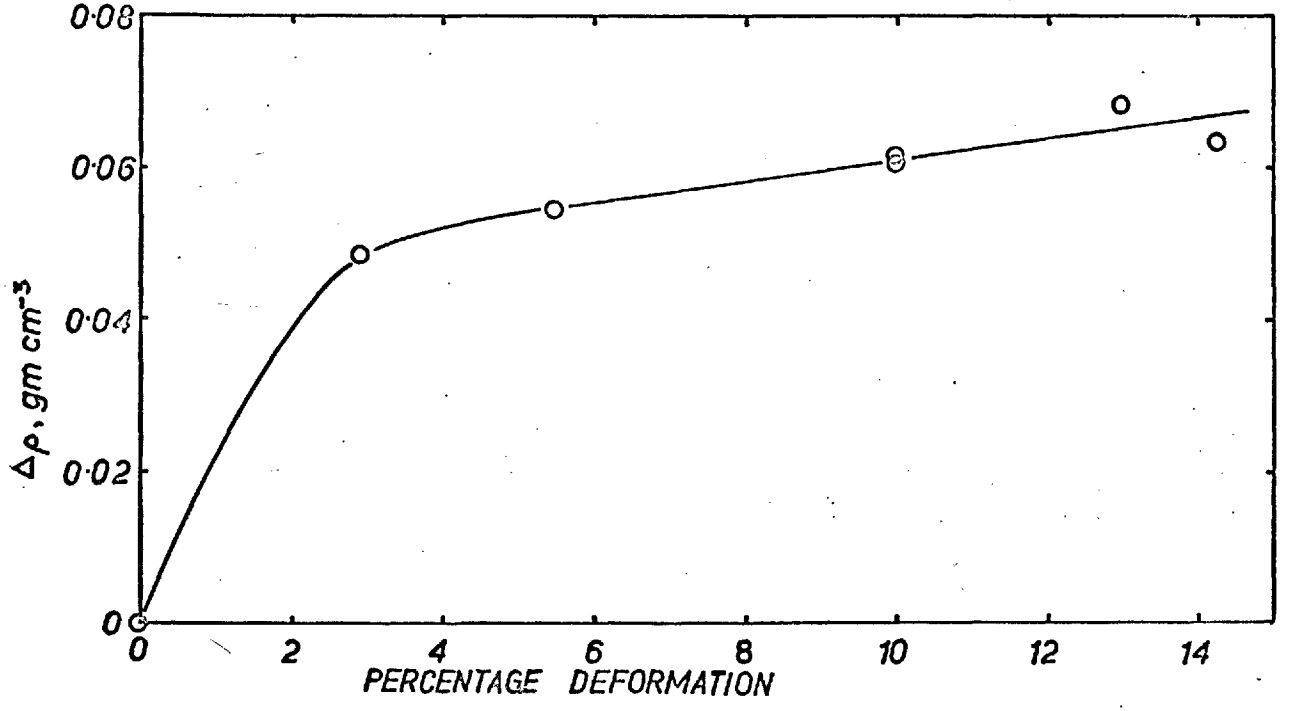

Fig. 3.6. Effect of prior deformation on the change in density of specimens aged for 10 minutes at 923°K.

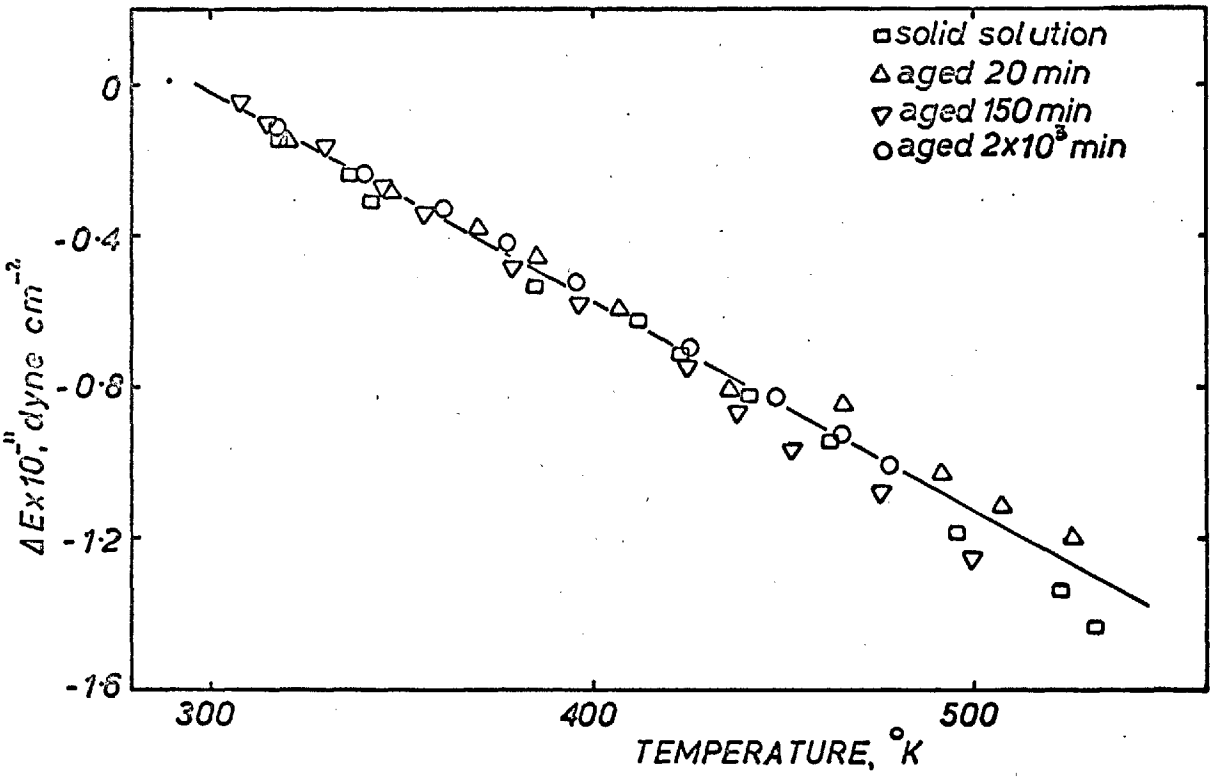

Fig. 3.7. Normalised plot of the change in Young's modulus with temperature of specimens aged to different conditions at 923°K.

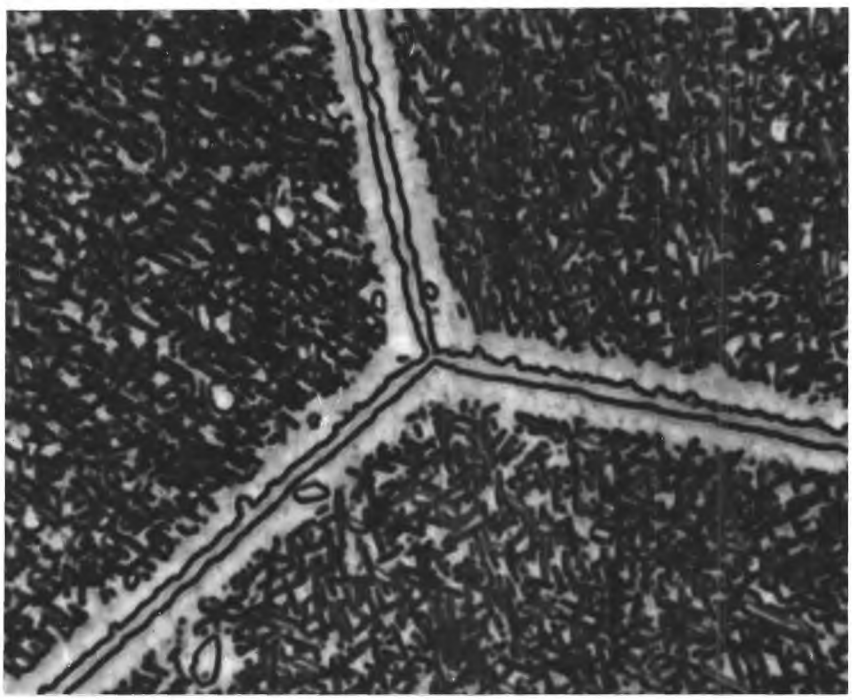

Fig. 3.8. Micrograph of the alloy aged 475 minutes at 1073°K showing elongated precipitate particles, the beginning of coalescence and speroidization, and the continuous grain boundary precipitate associated with the grain boundary denuded zone. x 2250.

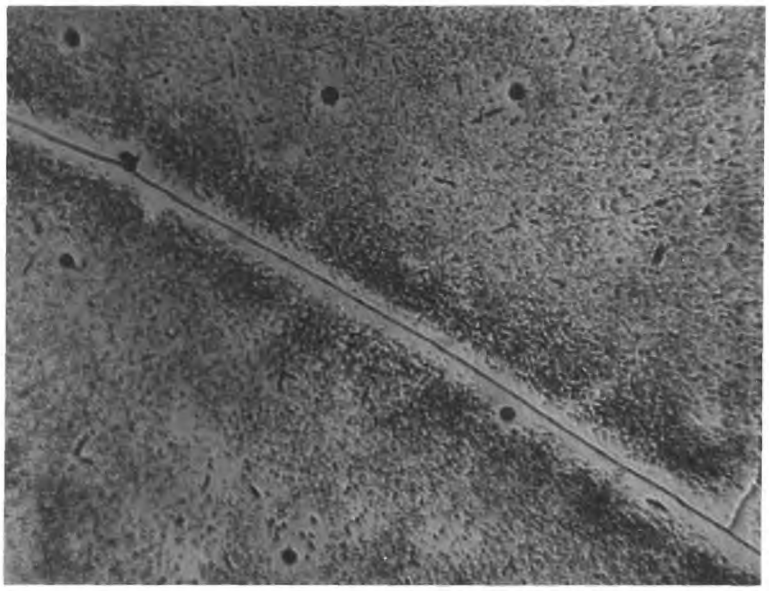

Fig. 3.9. Precipitate-free zone produced by ageing for 20 minutes at 923°K. x 750.

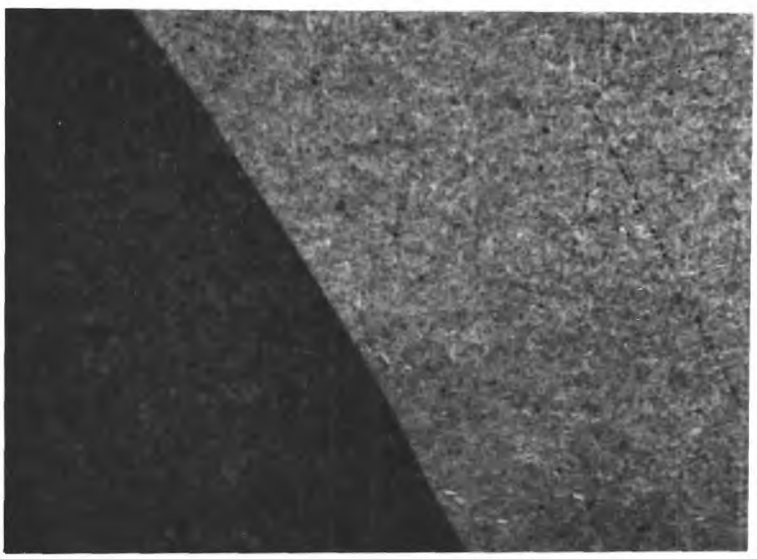

Fig. 3.10. Absence of precipitate-free zone in a specimen aged 60 minutes at 923°K. x 1000.

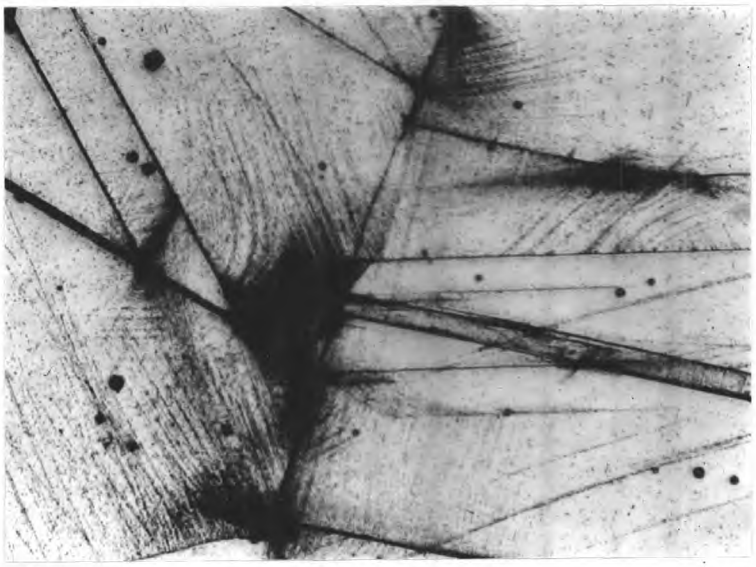

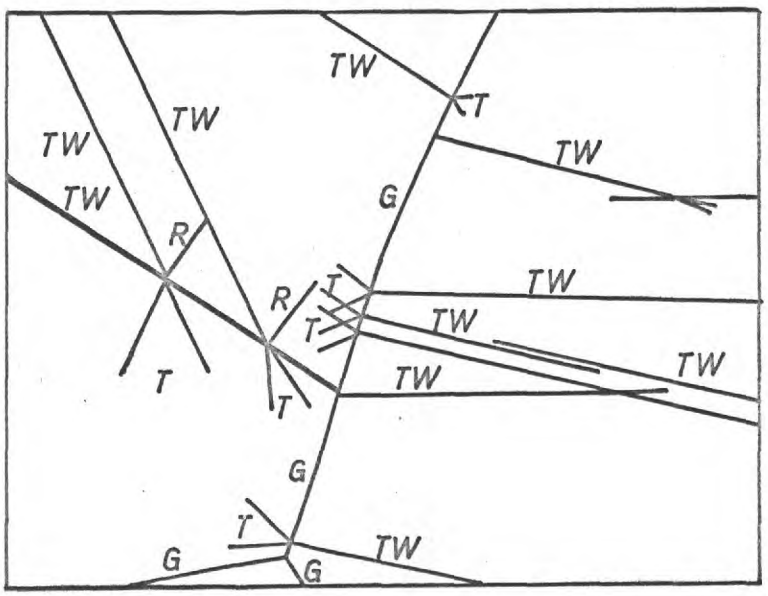

TW=Twin T=Transmitted wave
G=Grain boundary R=Reflected wave

Fig. 3.11. Quenching twins revealed by ageing 1.3×10^5 minutes at $748^{\circ}K$. x 525.

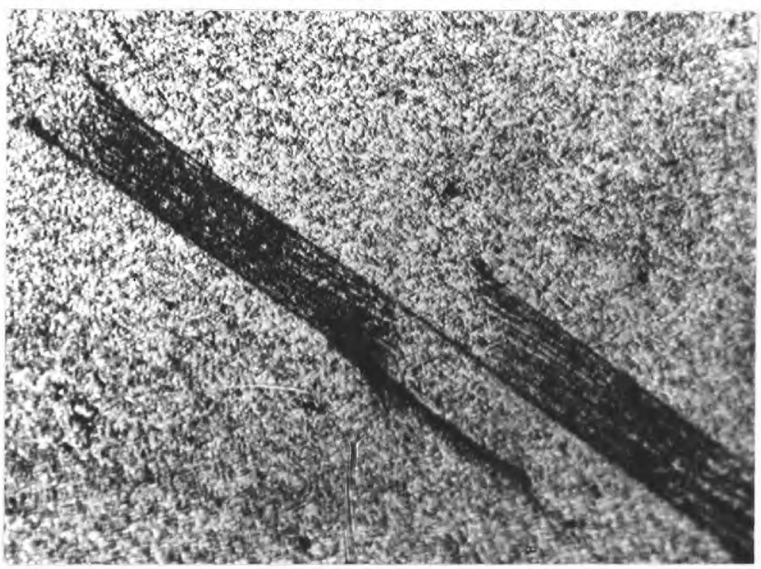

Fig. 3.12. Interaction between parallel twins. Aged 20 minutes at 923°K to reveal the deformation. x 525.

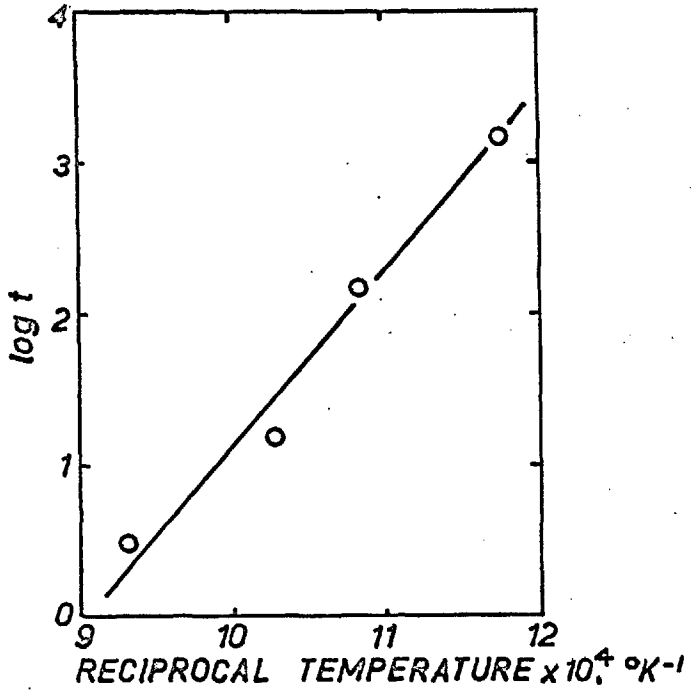

Fig. 3.13. Plot of the logarithm of the time to peak hardness against reciprocal of the ageing temperature.

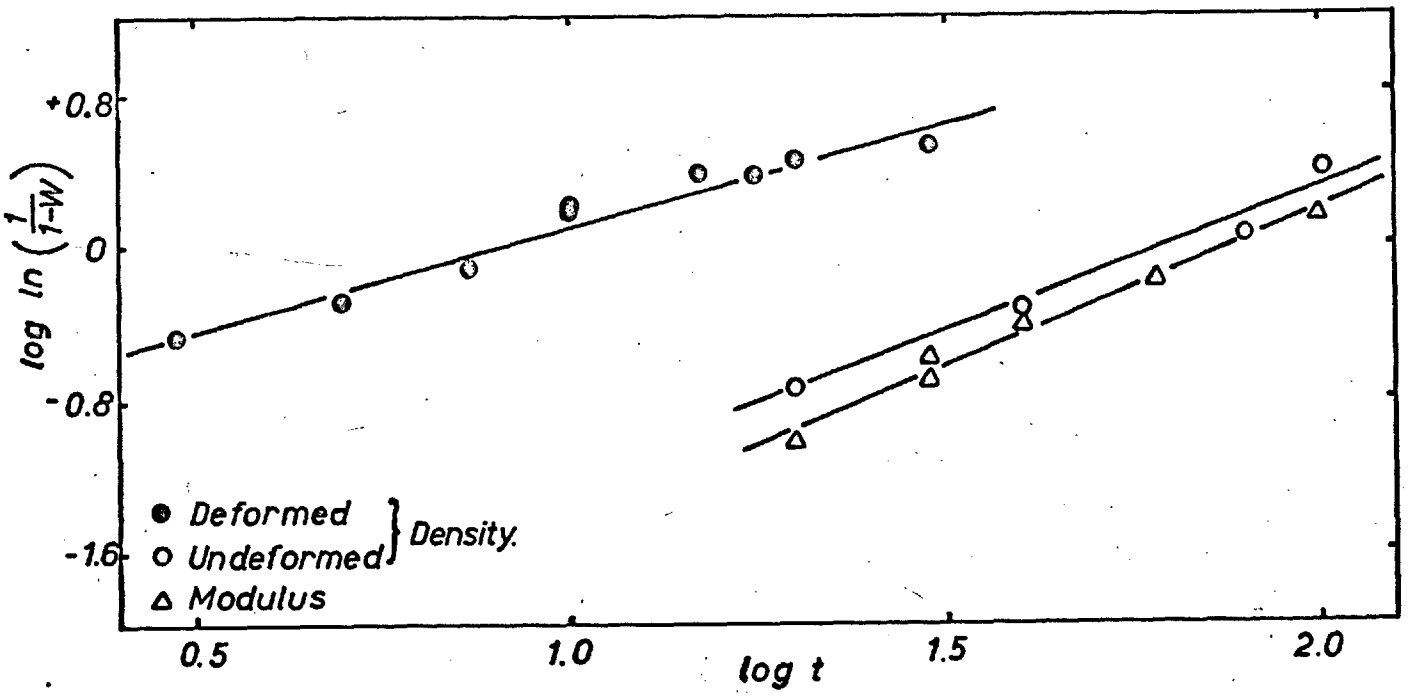

Fig. 3.14. Graph representing the ageing kinetics of the alloy with and without prior deformation.

CHAPTER 4

THE MECHANICAL PROPERTIES OF IRON-11 AT.% MOLYBDENUM ALLOY

4.1. Introduction

This chapter is concerned with a study of the room temperature deformation behaviour of the Fe-11 at.% Mo alloy after various thermal and thermo-mechanical treatments. In addition, the mechanical behaviour of certain structural conditions of the material has been investigated over the temperature range 77-1100^{o}K.

Several workers (Sykes 1926, Reiter and Hibbard 1955 and Coldren et al. 1964) have shown that precipitation of the intermetallic compound increases the tensile strength and decreases the ductility of Fe-Mo at room temperature. However, except for the tensile strength values of Sykes and hardness measurements (e.g. Sykes 1926 and 1940, Elsen and Wassermann 1961), no survey of mechanical properties as a function of time at a given ageing temperature has been made. Also, the effect of deformation prior to ageing has only been investigated by means of hardness data (Elsen and Wassermann 1961).

The tensile behaviour at elevated temperatures of Fe-Mo alloys of various compositions has been studied by Reiter and Hibbard and Coldren et al. However, tests were only performed on the solid solution and one aged condition of the material for

each composition, and only over the limited temperature range 800-1250°K. The same workers have also investigated the creep properties at 922°K.

4.2. Experimental Procedure

The production of the bulk material and the heat treatment procedures were as described in the previous chapter. After heat treatment the average grain diameter, determined by the linear intercept method, was 7×10^{-1} mm.

The available data on the mechanical properties of Fe-Mo alloys indicated that an alloy containing 11 at.% Mo would be brittle when tested at room temperature in the aged condition. Also, in common with other b.c.c. metals, the tendency to fail in a brittle manner would probably increase at sub-zero temperatures. Thus, compression was chosen as the main deformation mode as more plastic strain can be introduced into a brittle material by compression since, in general, the applied stress inhibits the propagation of cracks.

A floor model Instron tensile machine was adapted for compression testing by jigs which were attached to the underside of the cross-head beam. The construction and operation of these jigs has been described in an earlier paper (Pascoe et

al. 1967, Appendix III). Standard liquid coolants and an electrically heated oil bath were used for tests in the temperature range 77-475°K while higher temperature tests were performed in an argon atmosphere in a double wound Nichrome resistance furnace.

Compression specimens of nominal size 2.5 x 2.5 x 6.0 mm were cut longitudinally from the 6 mm diameter stock rod after heat treatment. To study the effect of prior deformation 10 mm lengths of the stock rod were deformed at a high strain rate in a Denison universal testing machine, heat treated and compression specimens prepared. The structural conditions chosen to investigate the effect of temperature on the mechanical properties were the solid solution, slightly aged (20 minutes at 923°K), aged to peak hardness (150 minutes at 923°K) and overaged (2×10^3 minutes at 923°K) conditions. All tests were carried out at a basic shear strain rate $\dot{\gamma}$, of 7.14×10^{-5} sec $^{-1}$; $\dot{\gamma} = 1.43 \times 10^{-3}$ sec $^{-1}$ was also used for some of the solid solution specimens.

A few room temperature tests were performed in tension at $\dot{\gamma} = 5.32 \times 10^{-5}$ sec $^{-1}$. The specimens had a gauge length of 8 mm and a cross sectional area of approximately 3 mm ^{2}. Unless stated otherwise the results reported are for compression tests.

4.3. Results

The initial yielding was not accompanied by a yield drop for any condition of the alloy in the temperature range studied. The yield stress, σ_{YS}, taken as the stress at which the first deviation from a linear stress-strain relationship was observed, was found to be rather irreproducible, especially when the initial rate of work-hardening was high. Consequently all results are quoted as 0.2% proof stresses, σ_{PS}. The behaviour of the yield and proof stresses were similar as a function of ageing time and test temperature.

The maximum stress, σ_m, and the corresponding strain, ε_m, attained during a test were recorded. Below 800°C these parameters can be taken as a measure of the fracture stress and the strain to fracture.

Holloman (1945) and Holloman and Lubahn (1947) have shown that for many metals the stress, σ, at a constant strain rate and temperature, increases with strain, ε, according to:

$$\sigma = k\varepsilon^n \qquad (4.1.)$$

where k and n are material constants referred to as the strength coefficient and the work-hardening exponent respectively. This equation was obeyed, with one exception, for all conditions of the alloy when $0.006 < \varepsilon < \varepsilon_m$.

The initial rate of work-hardening, represented by the difference in the proof and yield stresses, was used as a measure of the stress-strain behaviour at low strains.

4.3.1. Room Temperature Behaviour

The effect of ageing on typical room temperature stress-strain curves is shown in Fig. 4.1. As found in f.c.c. age-hardening systems (e.g. Al-Cu Hart 1953, Cu-Cr Hart and Hibbard 1955) at higher strains, i.e. $\varepsilon > 0.03$, all the flow curves are essentially parallel. There was an increase in the strength of the alloy as a result of the precipitation of the inter-metallic compound; the loss of strength on overageing was small (Fig. 4.2.). Besides the increase in strength, changes in the initial rate of work-hardening and the work-hardening exponent with ageing were noted (Figs. 4.3. and 4.4.).

σ_m and ε_m, for the alloy deformed 10% and aged at 923°K and well-aged at 923°K without prior deformation, plotted as a function of time of ageing are given in Figs. 4.5. and 4.6. Specimens aged at 1073°K and for less than 150 minutes at 923°K did not crack during deforming to strains approaching 0.1. Also shown are the fracture stresses obtained from the tensile tests. The solid solution exhibited some ductility (ε = 0.03-0.05) whilst the aged material was completely brittle and had a

fracture stress lower than the yield stress in compression. The failure of the solid solution was transcrystalline and the aged material predominately intercrystalline. The yield and proof stresses of the solid solution were the same value for tension and compression.

The data obtained from tests on a series of specimens given different amounts of prior deformation and aged for 10 minutes at 923°K are illustrated in Figs. 4.7. and 4.8. The proof stress, maximum stress in compression and initial rate of work-hardening increased and the work-hardening exponent and strain to fracture decreased the greater the amount of prior deformation.

4.3.2. Effect of Temperature

The effect of temperature on the flow curves of the alloy in the solid solution condition is shown in Fig. 4.9. At 77°K a large drop in stress, accompanied by an audible click, always occurred in the early stages of a test. Two tests were discontinued, one before and one immediately after the drop in stress. Metallographic examination revealed that the deformation structure of the former consisted of straight slip bands (Fig. 4.10.) whilst deformation twinning had taken place throughout the specimen that had undergone the drop in load (Fig. 4.11.).

Sometimes this initial burst of twinning occurred without any previous measurable plastic deformation. Polycrystalline niobium behaves in a similar manner when tested at 77°K (Farrell and Evans 1965). Small discontinuities in the stress-strain curves, again accompanied by audible clicks, were observed at higher strains and were also attributed to twin formation. As for carbon steels (Maiden 1959) there was no correlation between the initial twinning stress and strain rate; all the initial twinning stresses were in the stress range 83 ± 11 kg mm^{-2}. However, the frequency of the smaller bursts of twin formation was greater the higher the strain rate.

The flow curves of the solid solution at all temperatures below 900°K, other than at 77°K, were similar in form. Above 900°K the stress increased to a maximum, σ_m, and then gradually decreased. The aged material did not twin at 77°K, but with this exception the flow curves were of the same form as obtained for the solid solution.

Below 500°K the temperature dependence of σ_{PS} for the four structural conditions of the alloy investigated was similar (Fig. 4.12.). This similarity was also shown by plots of σ_{PS} at 77 and 296°K against ageing time; the difference between the proof stresses at the two temperatures was approximately constant for all conditions of the alloy (Fig. 4.13.). In this temperature region it was found that σ_{PS} of the solid solution was

greater the higher the strain rate (Fig. 4.14.).

The athermal region extended over a wider temperature range for the solid solution and slightly aged than for the well-aged conditions of the alloy. The increase in strength at 960°K of the solid solution was due to precipitation while the specimen was reaching the test temperature.

Considerable scatter was obtained for the work-hardening exponent, but within experimental error the temperature dependence of n for the two well-aged conditions of the alloy could be represented by a single curve (Fig. 4.15.). Similarly, except at 77°K, the values for the solid solution and the slightly aged material were approximately the same at a given temperature. The high value of n for the solid solution at 77°K was thought to be the result of the twinning; twin formation effectively corresponds to a reduction in grain size and Smith et al. (1954) found that n was larger the smaller the grain size. The tendency for n to decrease with decreasing temperature below 500°K has also been observed for Fe-Al_2O_3, Fe-C (Felberbauer et al. 1964) and Fe-C alloys (Smith et al. 1954). The specimen aged 20 minutes and tested at 890°K rapidly work-hardened at higher strains, due to precipitation during the test, and equation 4.1. was not obeyed.

Below 900°K there was very little effect of temperature on the initial rate of work-hardening; above this temperature

$\sigma_{PS} - \sigma_{YS}$ was the same for all conditions of the alloy and was more temperature dependent (Fig. 4.16.).

The graph of the maximum stress, σ_m, sustained by the alloy as a function of temperature consisted of three distinct regions (Fig. 4.17.). Below 400°K failure occurred by transcrystalline and intercrystalline cracking. The amount of transcrystalline cracking decreased with increasing temperature until in the temperature range 400-800°K failure was completely intercrystalline and σ_m was relatively constant. The grain boundary brittleness in this temperature range was so acute that often surface grains were pushed out of the specimen (Fig. 4.18.). Above 800°K catastrophic failure did not take place and hence σ_m does not represent a fracture stress. ε_m decreased with temperature in this high temperature region (Fig. 4.19.) but at lower temperatures the scatter in the results masked any temperature dependence of this parameter. Grain boundary sliding was observed in the high temperature region.

The effect of ageing on σ_m and ε_m for specimens tested at 77°K is given in Fig. 4.20.

4.4. Discussion

4.4.1. Room Temperature Properties

The fact that no yield drops were observed for the solid solution indicated that the carbon content of the alloy was low. It has been shown (Edwards et al. 1940, Reiter and Hibbard 1955) that the addition of molybdenum to iron does not counteract the effects of carbon in causing yield points.

The form of the room temperature, σ_{PS}, versus ageing time curves were similar to the hardness versus ageing time curves discussed in the previous chapter. In particular, the proof stress and hardness reached maximum values after the same time of ageing.

The most marked effect of precipitation of the intermetallic compound on the flow curves at room temperature was the rapid work-hardening at low strains. The precipitate particles in Fe-Mo are rods or platelets and it is possible that the increase in the initial rate of work-hardening was accentuated by the elongated nature of the particles. Steels for example, exhibit a much more rapid initial rate of work-hardening if the structure is pearlitic than if the structure is spheroidised (Bain 1939).

As the strength of the alloy increased with the precipitation of the intermetallic compound so the work-hardening exponent decreased. This correlated with the work of Gensamer (1946)

which showed that for iron based alloys of a variety of structures and compositions the greater the strength the lower n; however, as Fig. 4.21. shows, at room temperature the decrease in n was small for σ_{PS} greater than 100 kg mm^{-2}. The initial rate of work-hardening increased with strength and, like n, the change in $\sigma_{PS} - \sigma_{YS}$ for $\sigma_{PS} > 100$ kg mm^{-2} was small (Fig. 4.22.).

4.4.2. Effect of Temperature

Hornbogen (1961b) found that the incidence of twinning increased with the concentration of molybdenum in Fe-Mo solid solutions. Thus, the absence of twinning at 77^{o}K in the aged conditions of the alloy, where the molybdenum concentration of the matrix was reduced, is explicable. In addition, precipitation in itself has been shown to hinder twinning (Lenhart 1955 and Corderoy 1962).

With the strain rates employed for obtaining mechanical properties data in the present investigation, deformation twins were only formed in the solid solution at 77^{o}K. However, twinning can be induced at higher temperatures by increasing the strain rate. For example, specimens that were deformed prior to ageing at a high strain rate twinned at room temperature; also twins were formed as a result of the stresses set up during the rapid quench from the solution treatment temperature (Chapter 3).

It has been reported that Fe-Mo solid solutions of relatively low molybdenum content exhibit strength inversion at low temperatures, i.e. at 77°K the yield stress of the solid solution is less than that of unalloyed iron (Rees et al. 1954, Nunes 1966). This effect was not observed in the present work.

The large temperature dependence of the proof stress for the alloy in the solid solution and aged conditions in the low temperature region was typical of b.c.c. metals. Unlike many f.c.c. alloys containing a dispersed phase the increase in flow stress over that of the solid solution was approximately temperature independent. It is concluded that precipitation increased the thermal component of the flow stress but did not affect to any large extent the thermally activated component of stress.

The loss of strength above about 700°K for the well-aged conditions of the alloy will be discussed in detail in the following chapter. Suffice at this stage to state that the temperature dependence of the proof stress in this temperature range is thought to be due to the thermally activated movement of dislocations past the large precipitate barriers. Even though the structure of the various specimens tested at 960°K and above must have varied considerably, the values of each of the properties measured, i.e. σ_{PS}, $\sigma_{PS} - \sigma_{YS}$, n and σ_m, were the same for all specimens at a given temperature. Thus, the precipitate was no longer an effective barrier to dislocation motion.

The maximum in the stress-strain curves at these temperatures is thought to be associated with grain boundary sliding. Two specimens, which were essentially bi-crystals with angles between the grain boundary and compressive axis of 45° and 90°, were tested at $960^{\circ}K$. ε_m was lower for the specimen with the 45° boundary as would be expected if ε_m was due to grain boundary sliding; however the values for ε_m for both specimens were within the scatter obtained for the polycrystalline material.

4.4.3. Fracture Behaviour

The smallest tensile stress, σ, able to propagate an atomically sharp crack of length 2c is given by the Griffith's formula (Griffith 1920), corrected for the plastic deformation at the tip of the crack:

$$\sigma = \left(\frac{2E\gamma'}{\pi c}\right)^{\frac{1}{2}} = \left(\frac{2E\gamma}{\beta\pi c}\right)^{\frac{1}{2}} \qquad (4.2.)$$

where E is Young's modulus, γ' the total energy required per unit increase in area of the crack, γ the surface energy per unit area and β a correction factor for the plastic work done; $\beta = \left(1 - \frac{2E\alpha}{\pi c}\right)$ where α is a constant (McLean 1962). Although the intercrystalline failure of the specimens aged less

than 60 minutes at 923°K may be attributed to precipitate-free zones at the grain boundaries (Chapter 3), this cannot account for the brittle behaviour of the well-aged material in which zones were not observed. Rather the catastrophic failure in these specimens was thought to be due to either fracture of the grain boundary precipitate or to failure at the precipitate-matrix interface. For fracture at the precipitate-matrix interface γ is given by:

$$\gamma = \gamma_P + \gamma_m - \gamma_{P-M} \qquad (4.3.)$$

where γ_P and γ_m are the surface energies of the precipitate and matrix respectively and γ_{P-M} the precipitate-matrix interfacial energy. The precipitate, whether the λ or ε-phase, was non-coherent with the matrix and therefore γ_{P-M} was large so effectively reducing γ. Additional evidence for cracking associated with the precipitate was obtained from the compression tests at room temperature on the alloy deformed prior to ageing. These specimens cracked at grain boundaries and at the twins that were formed during the prior deformation (Fig. 4.23.); in the previous chapter it was noted that twins were preferred sites for precipitation.

In compression, failure did not occur for specimens aged at 1073°K and tested at room temperature or for the solid solution at any temperature. The likelihood of brittle failure is

enhanced the greater the stress and it was found that the maximum stress sustained by any specimen aged at 1073^{o}K was only of the same order as the minimum stress recorded for fracture in compression for any condition of the alloy. Thus, it seems that the ductility of these specimens was due to the low stress levels needed for plastic deformation. The same reasoning, coupled with the absence of harmful precipitate at the grain boundaries, accounts for the ductility of the solid solution.

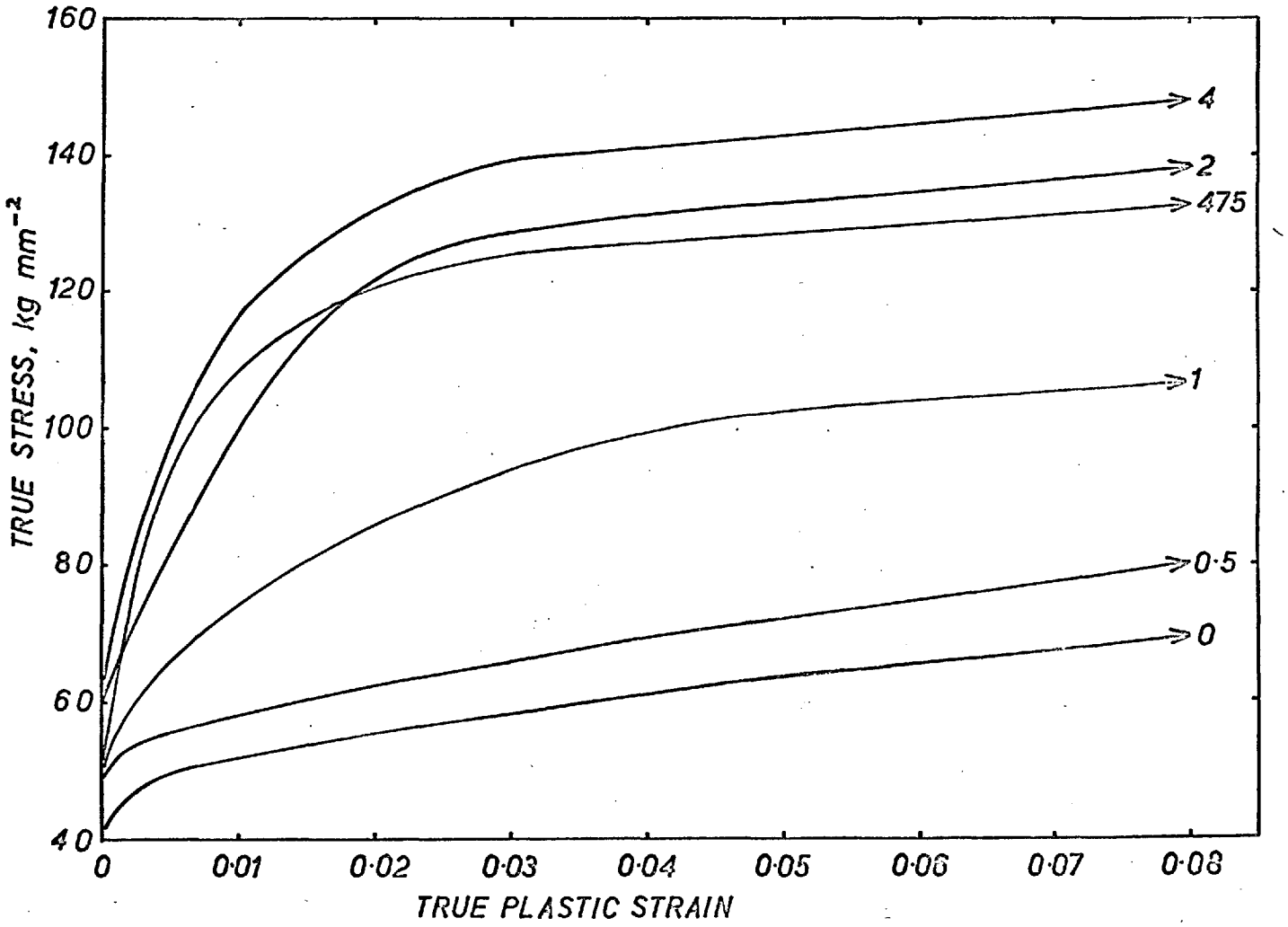

Fig. 4.1. Room temperature stress-strain curves for the alloy aged 0.5, 1, 2, 4 and 475 minutes at 1073°K.

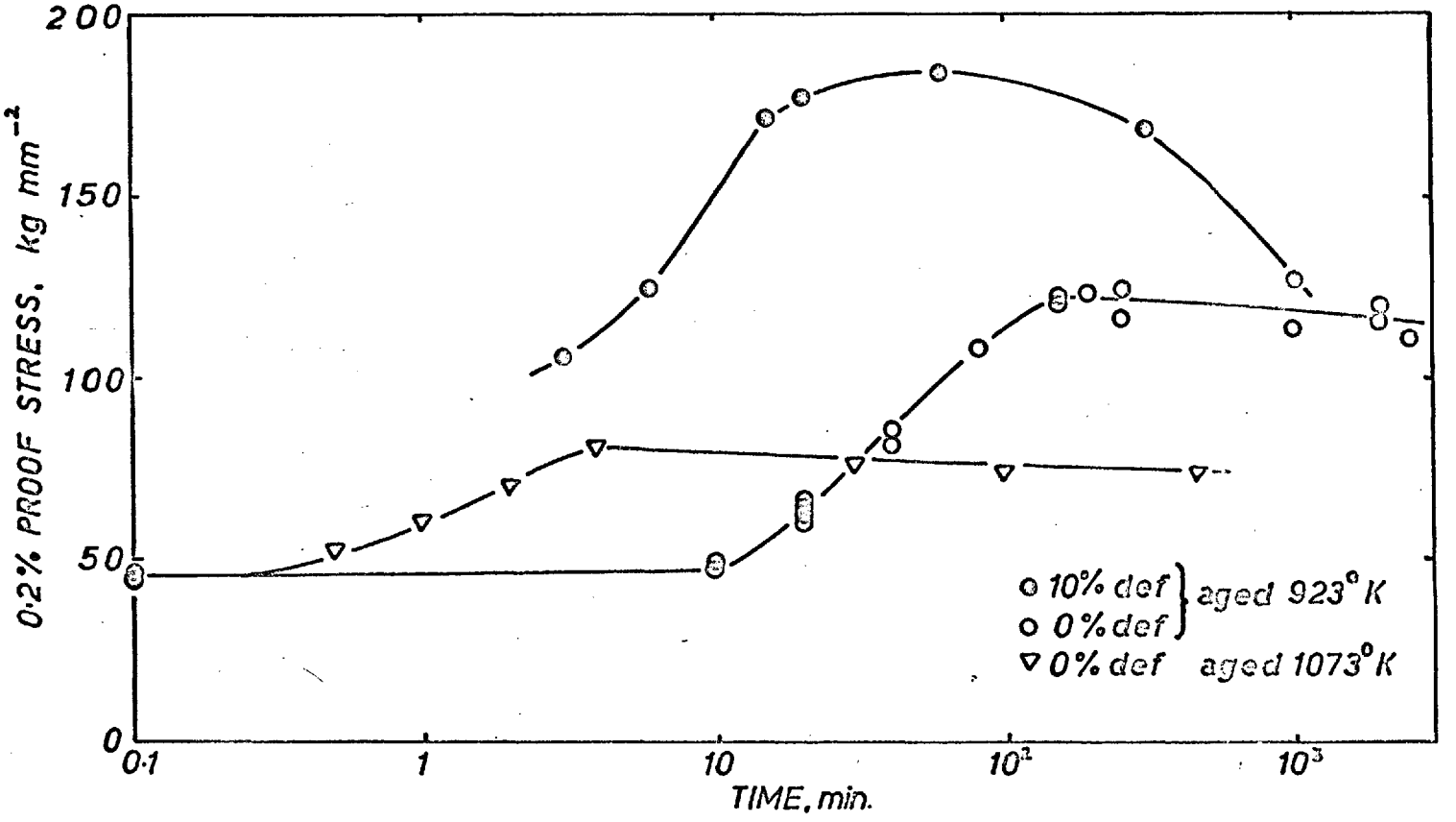

Fig. 4.2. The 0.2% proof stress as a function of ageing time.

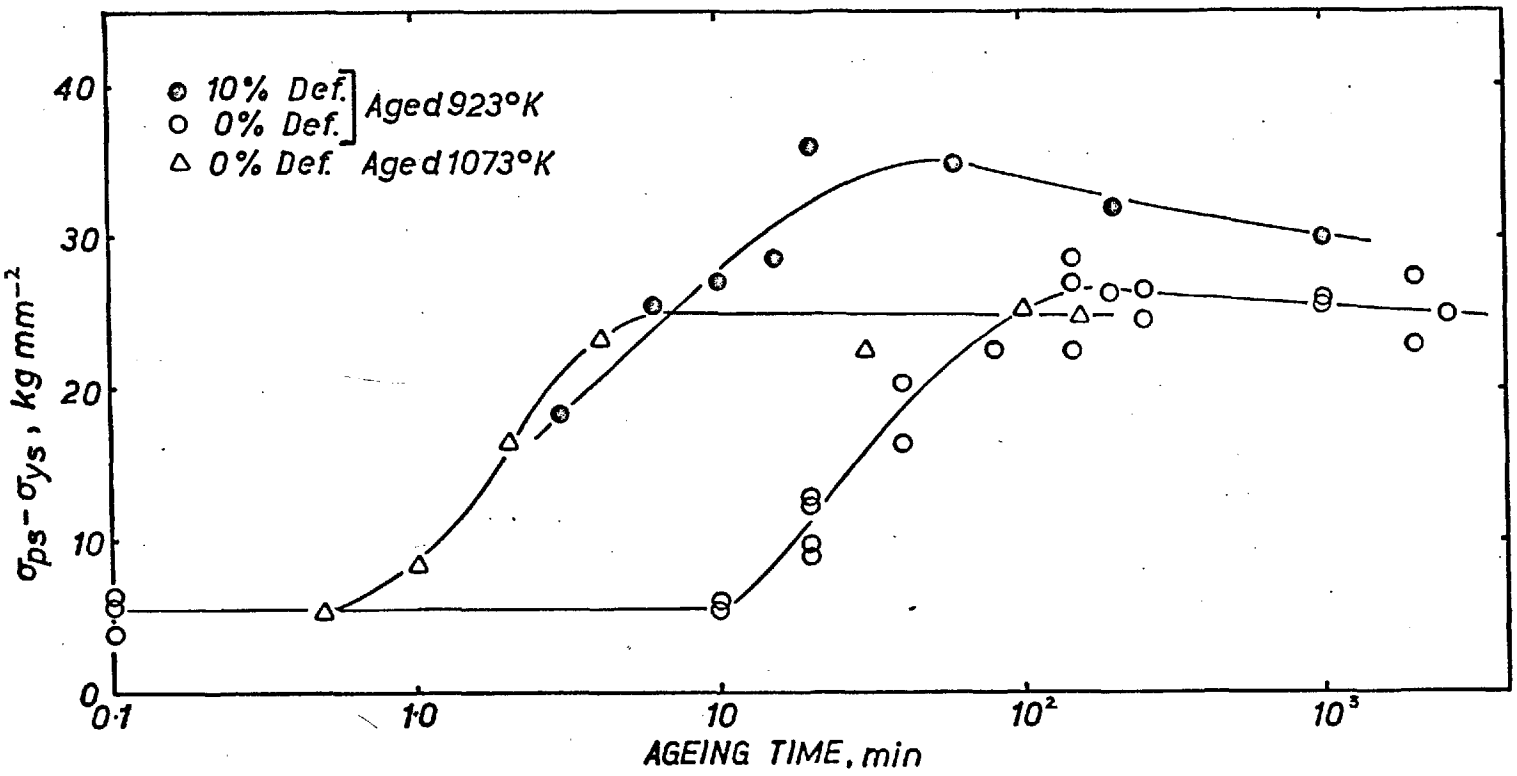

Fig. 4.3. Initial rate of work-hardening as a function of ageing time.

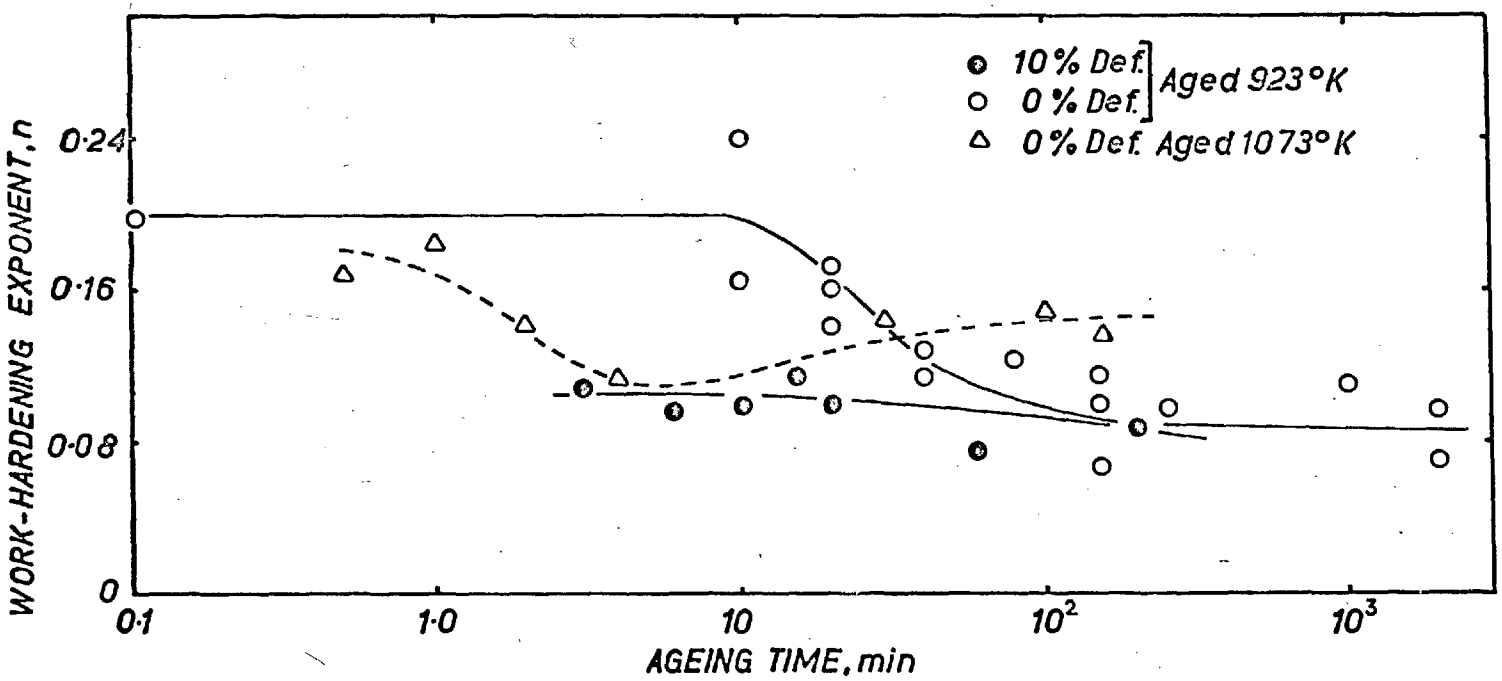

Fig. 4.4. Work-hardening exponent as a function of ageing time.

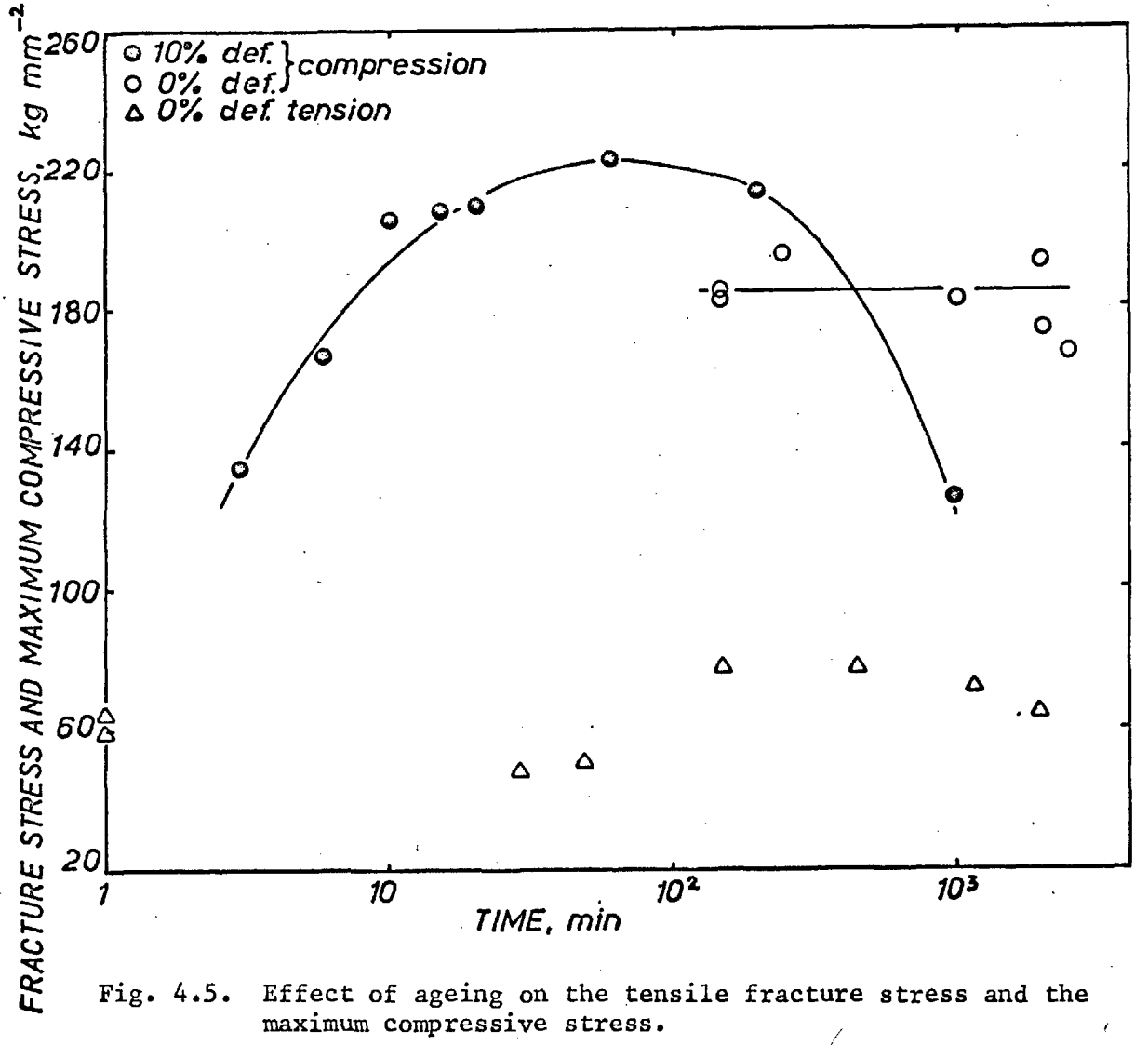

Fig. 4.5. Effect of ageing on the tensile fracture stress and the maximum compressive stress.

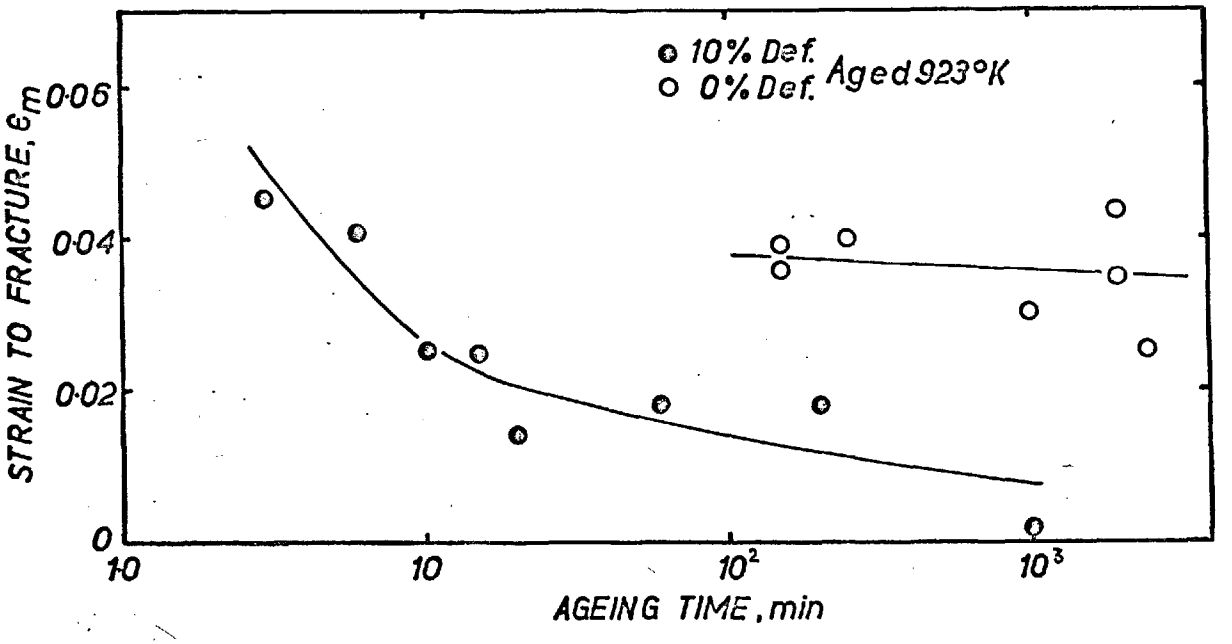

Fig. 4.6. The effect of ageing on the strain to fracture.

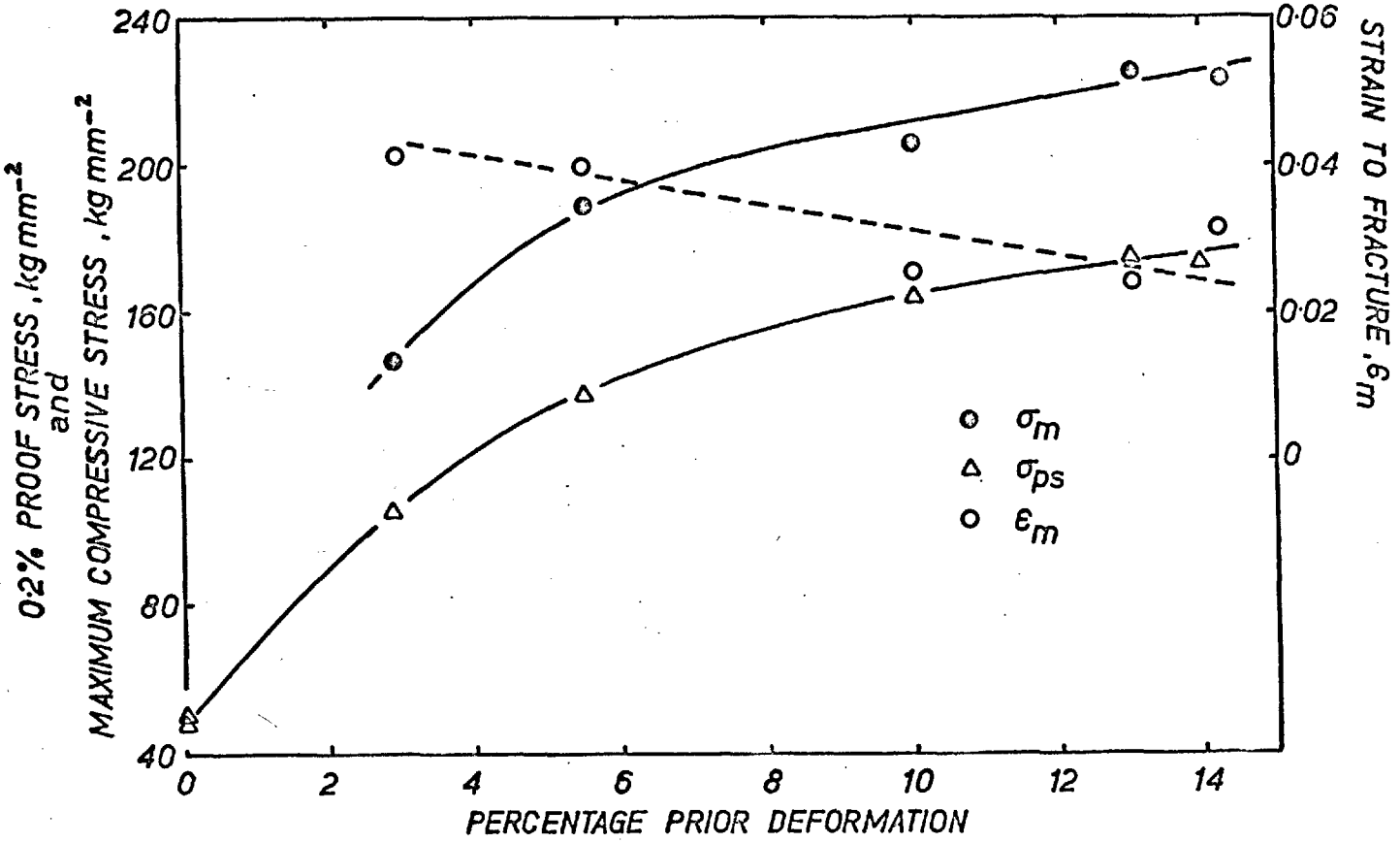

Fig. 4.7. Effect of prior deformation on the proof stress, maximum compressive stress and the strain to fracture of specimens aged for 10 minutes at 923°K.

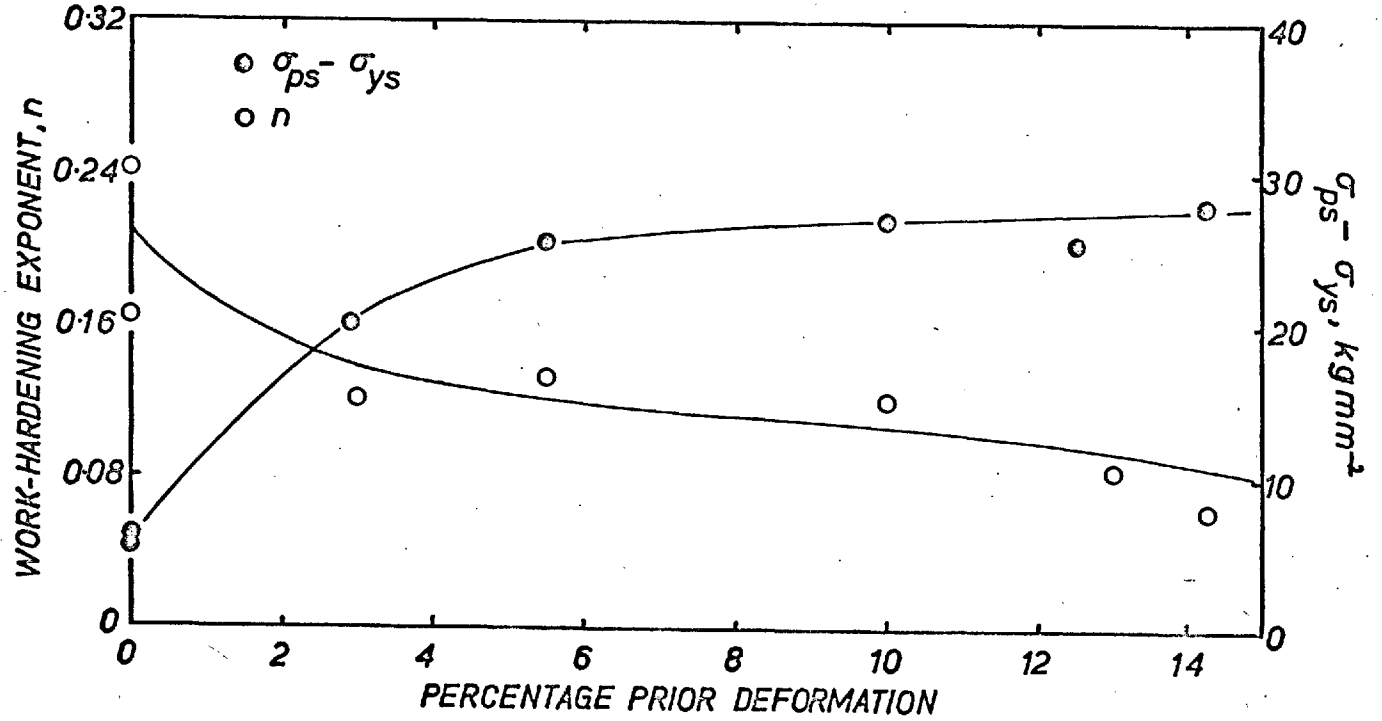

Fig. 4.8. Effect of prior deformation on the work-hardening exponent and the initial rate of work-hardening of specimens aged for 10 minutes at 923°K.

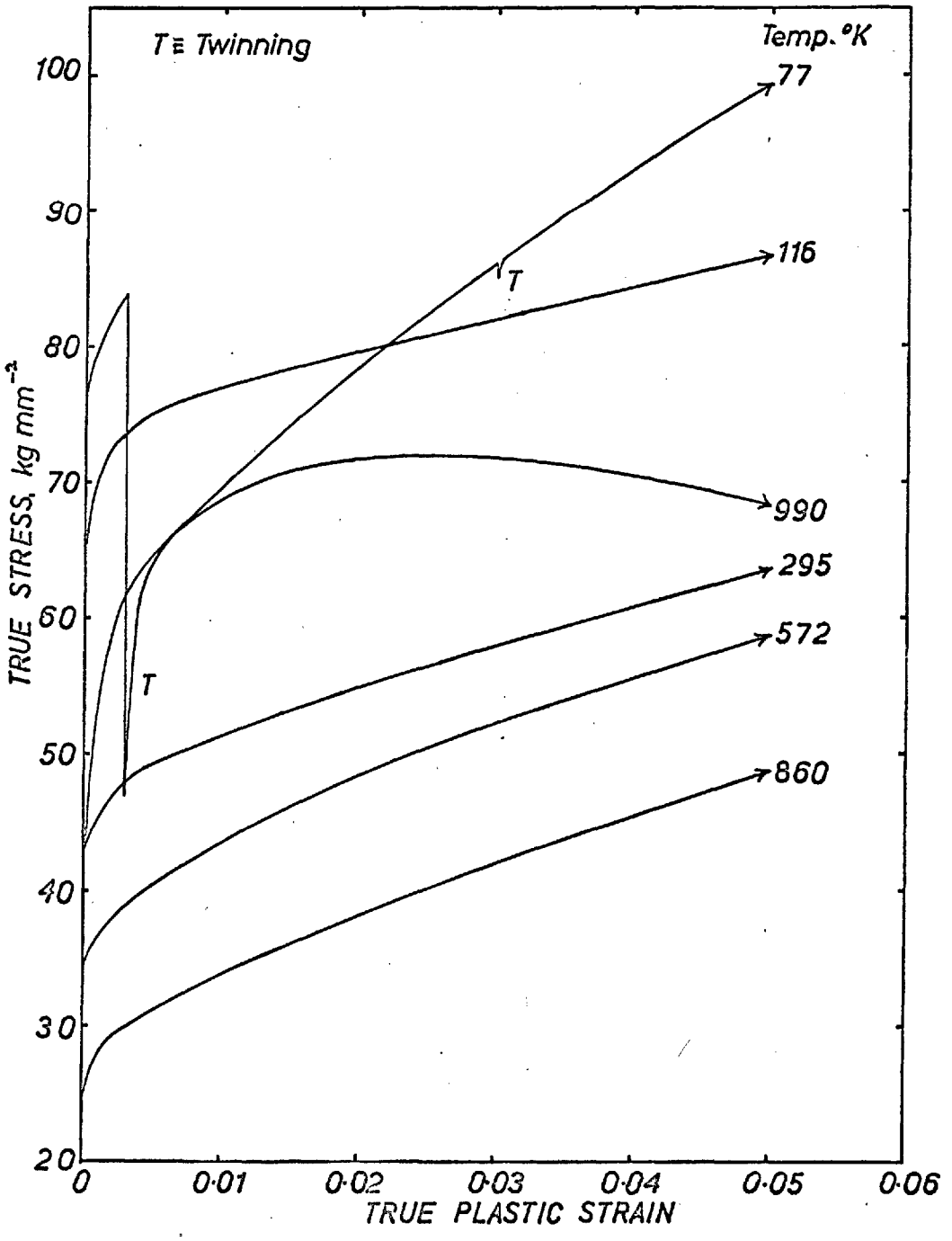

Fig. 4.9. Effect of temperature on typical stress-strain for the alloy in the solid solution condition.

Fig. 4.10. Straight slip bands produced in the solid solution when tested at 77°K. Interference contrast x 400.

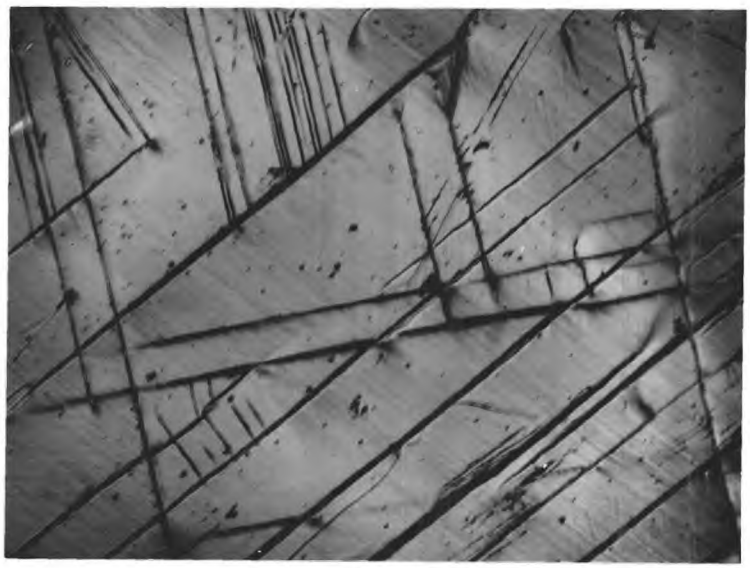

Fig. 4.11. Deformation twins produced in the solid solution when tested at 77°K. Interference contrast x 150.

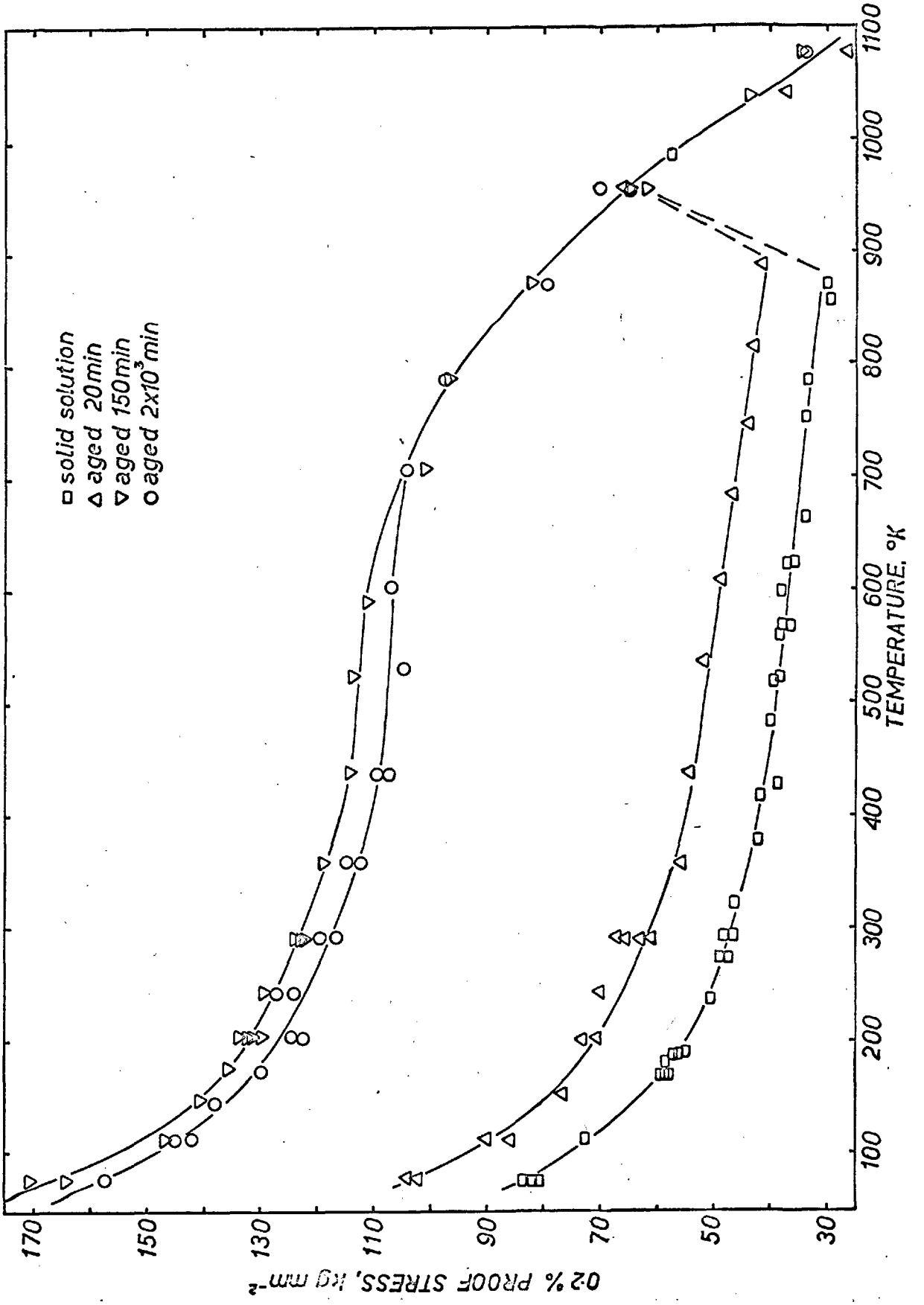

Fig. 4.12. Temperature dependence of the 0.2% proof stress of four different heat treated conditions of the alloy.

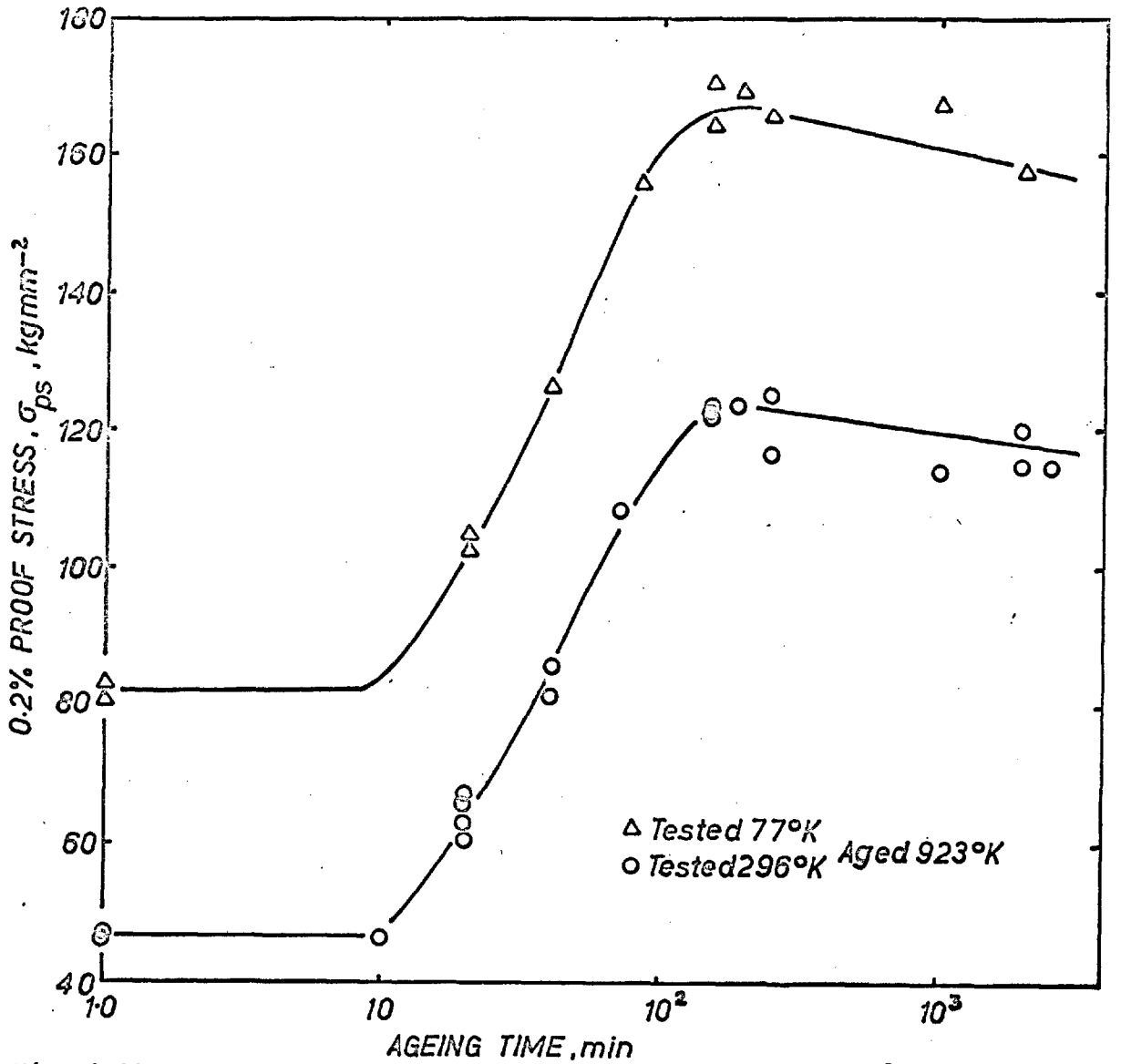

Fig. 4.13. Effect of ageing on the 0.2% proof stress at 77° and 296°K.

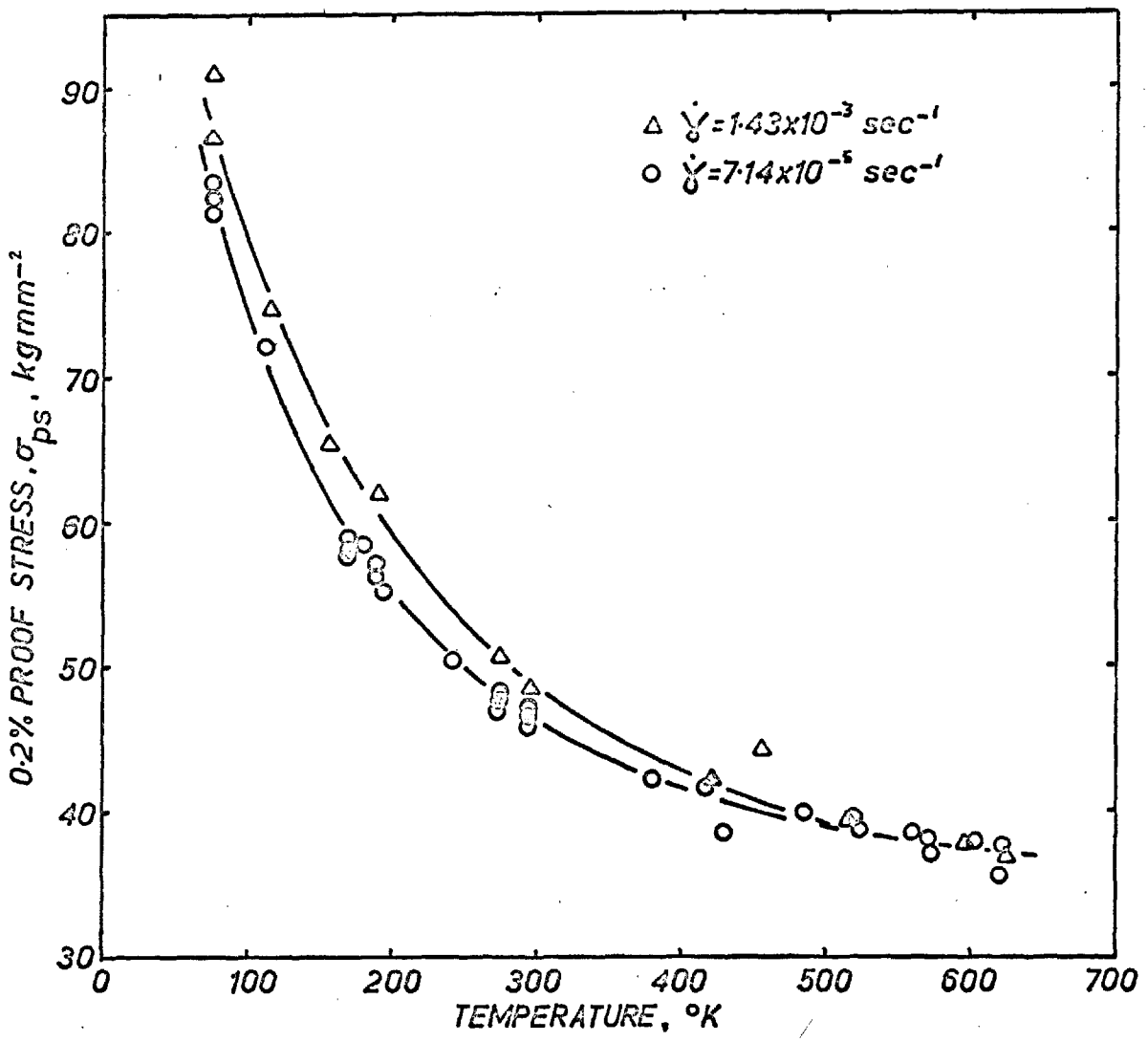

Fig. 4.14. Effect of strain rate on the 0.2% proof stress of the alloy in the solid solution condition.

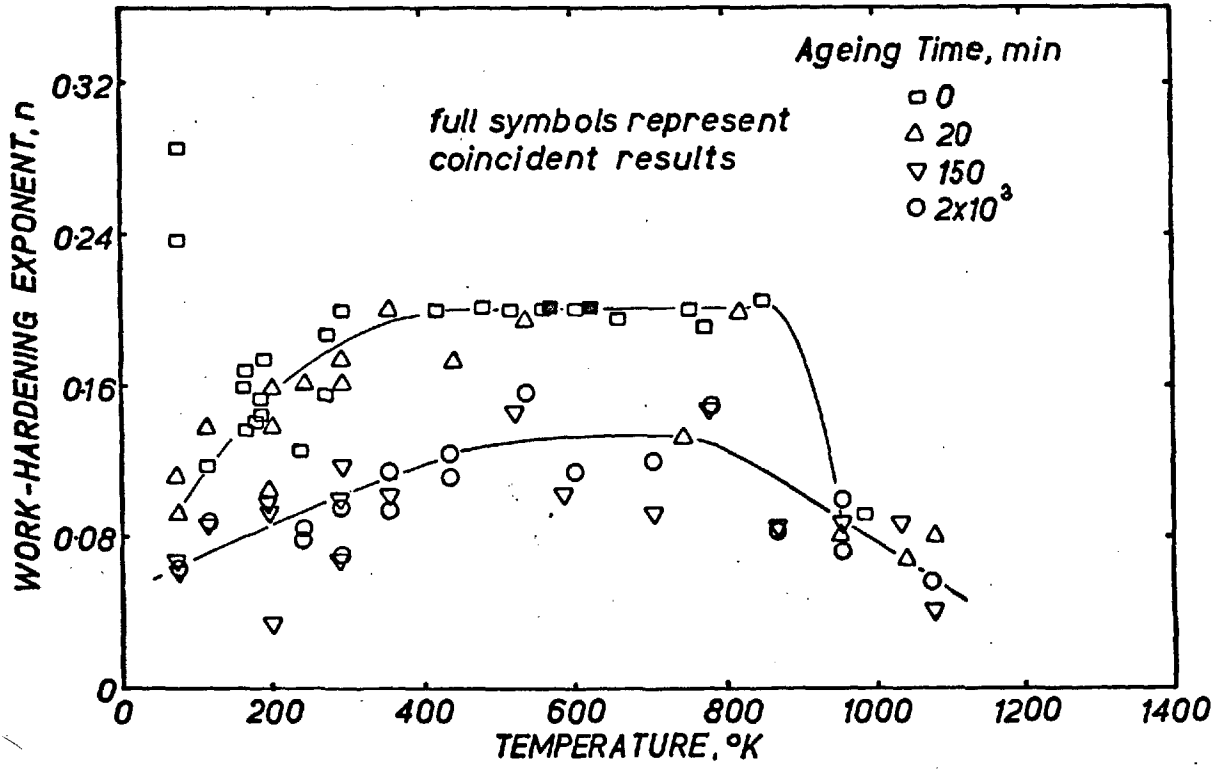

Fig. 4.15. The work-hardening exponent as a function of temperature for the alloy in four different heat treated conditions.

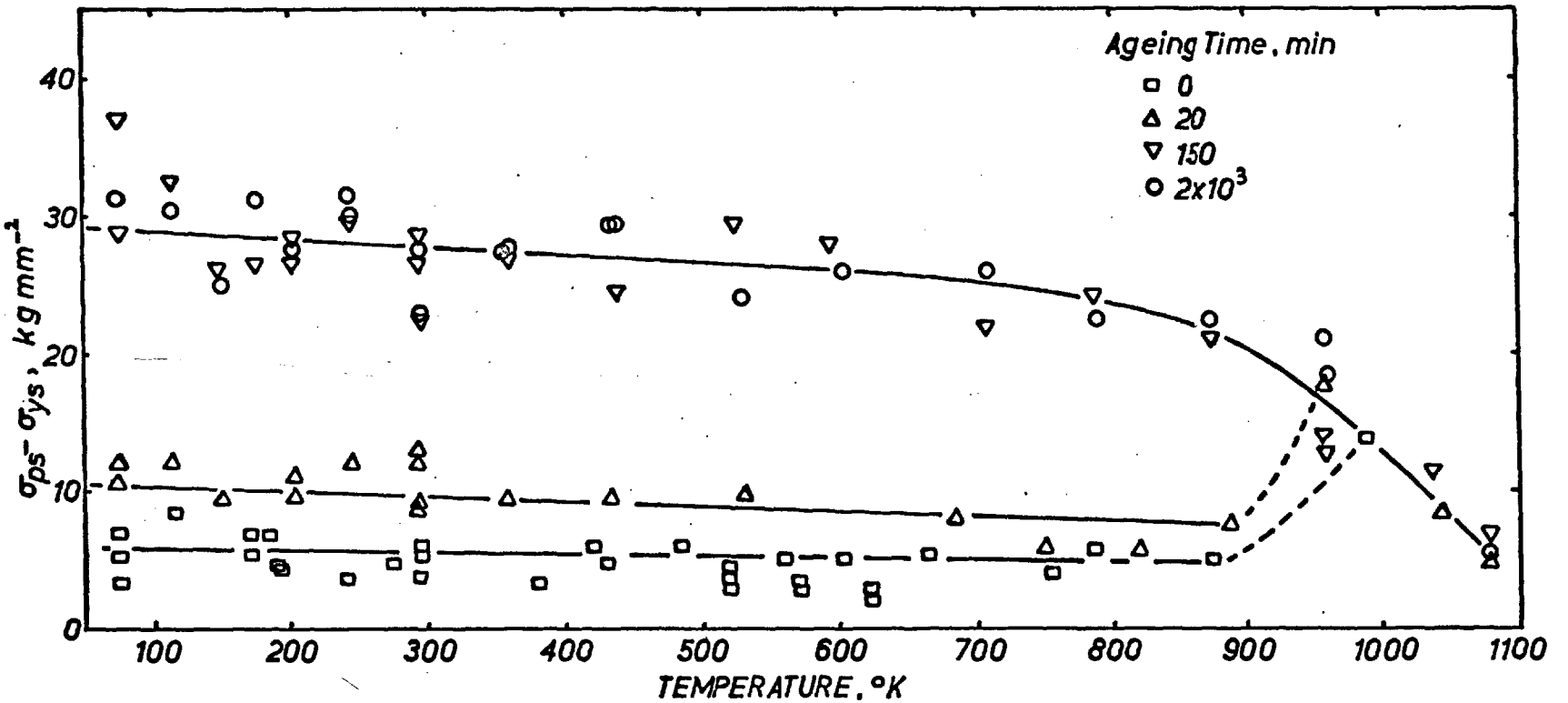

Fig. 4.16. Effect of temperature on the initial rate of work-hardening for the alloy in four different heat treated conditions.

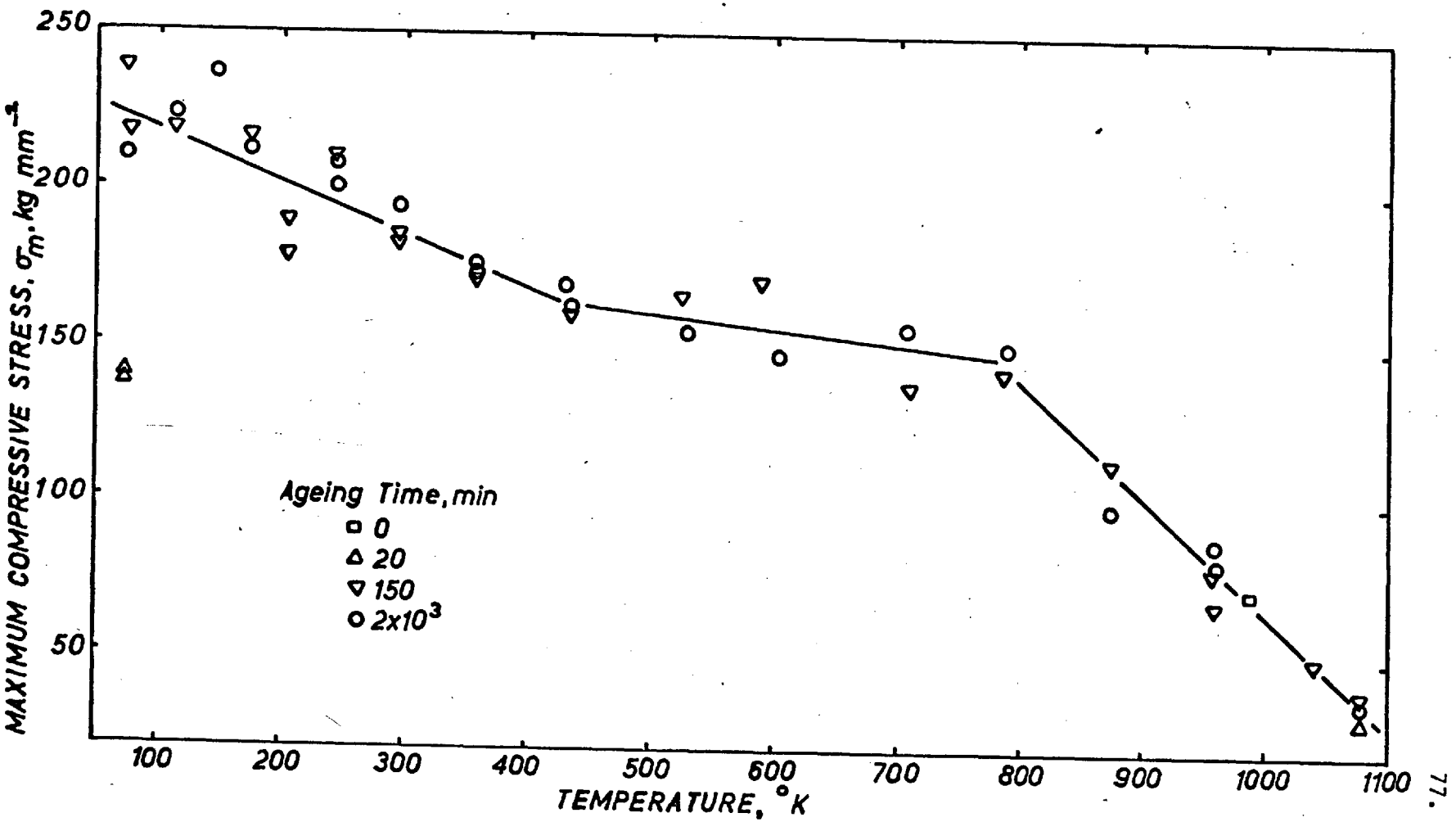

Fig. 4.17. The maximum compressive stress as a function of temperature for the alloy in four different heat treated conditions.

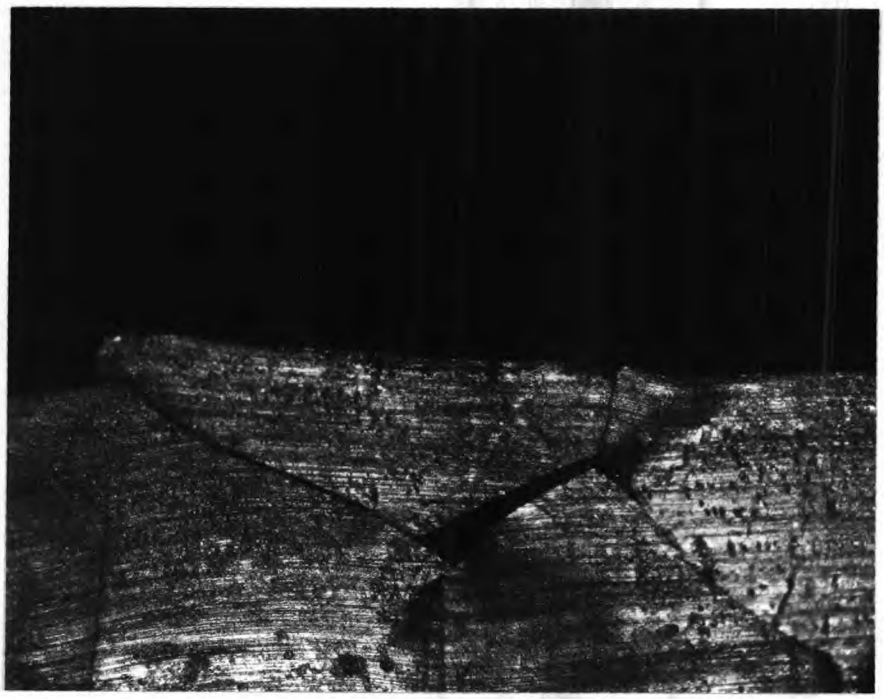

Fig. 4.18. Grain boundary cracking in a specimen aged 150 minutes and tested at 787°K. x 50.

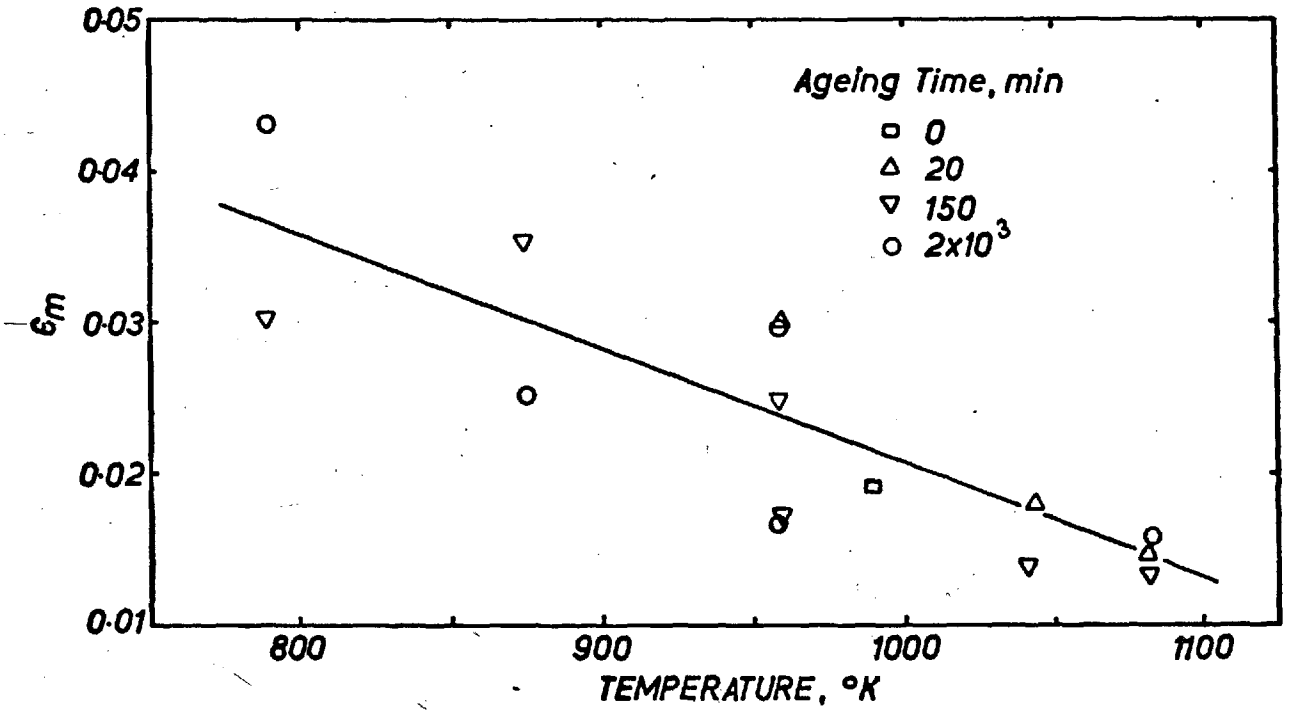

Fig. 4.19. The strain corresponding to the maximum compressive stress as a function of temperature.

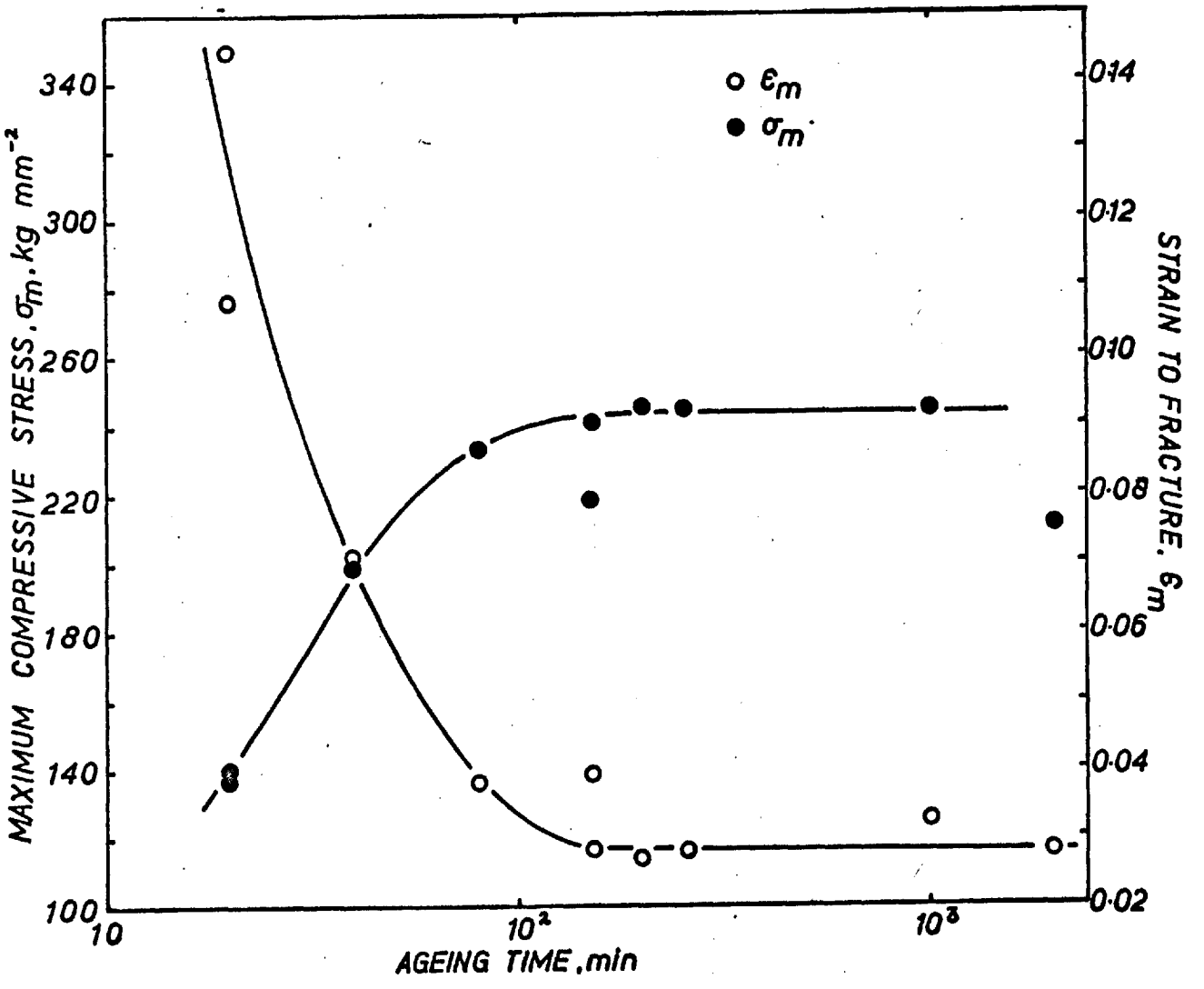

Fig. 4.20. Maximum compressive stress and strain to fracture at 77°K as a function of ageing time at 923°K.

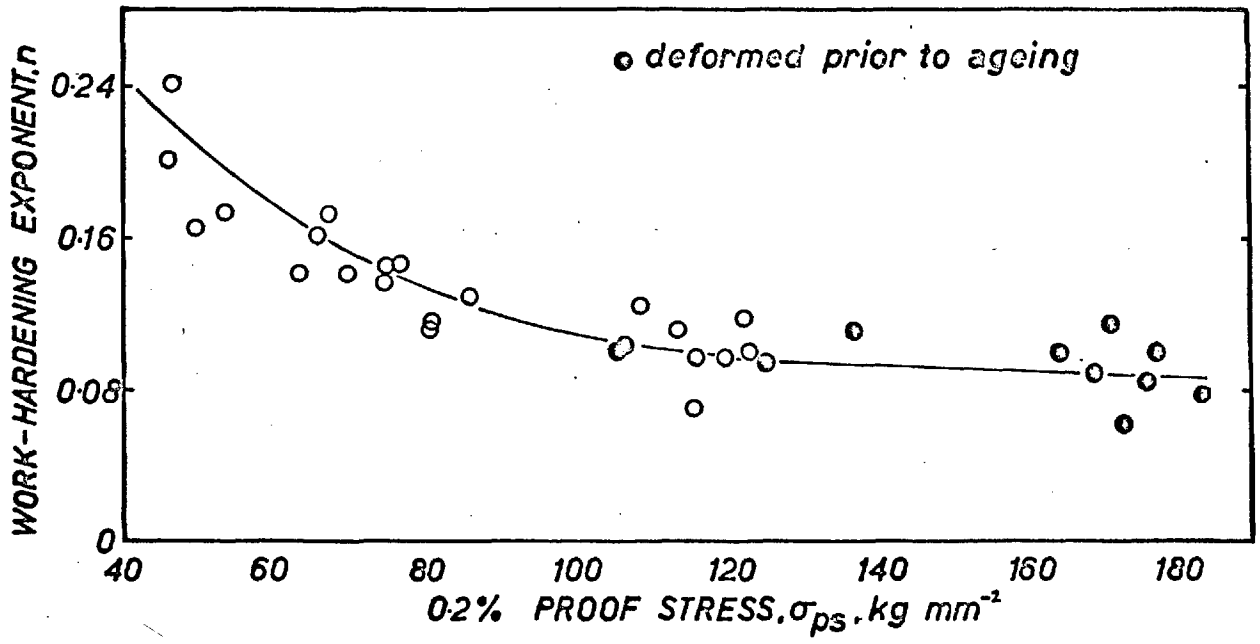

Fig. 4.21. Work-hardening exponent as a function of the proof stress for the alloy in various structural conditions.

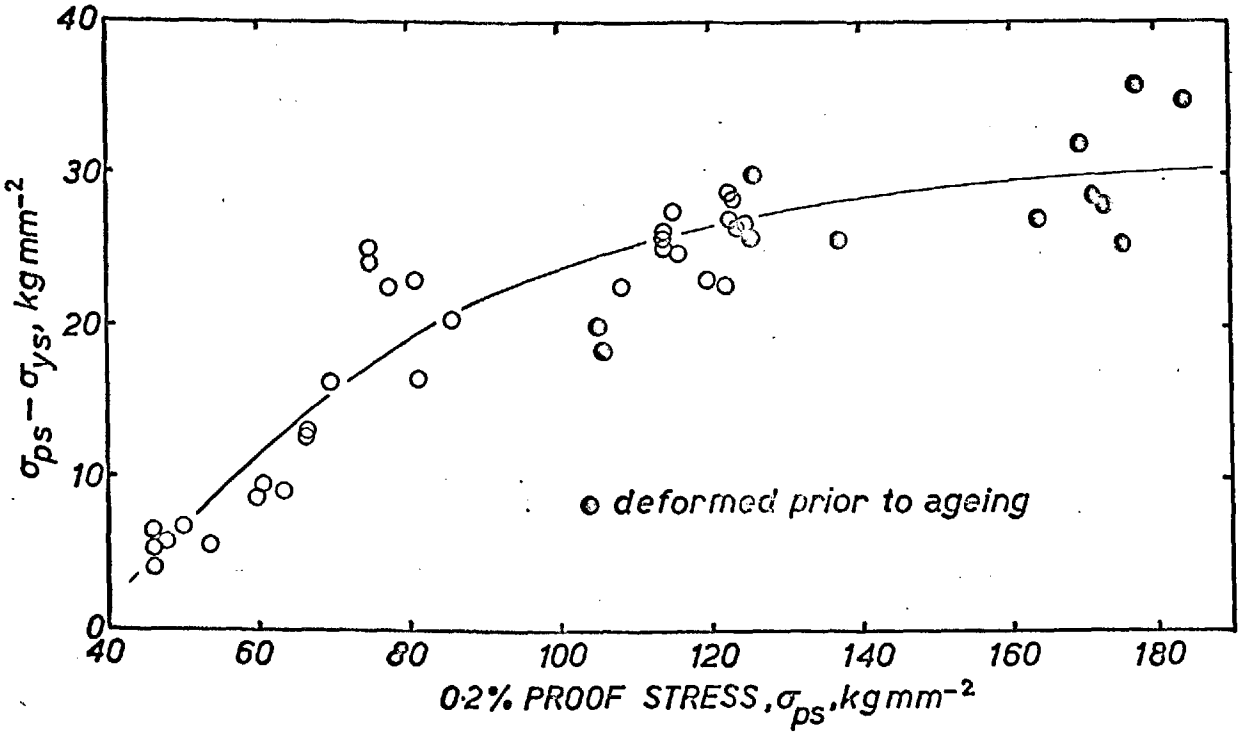

Fig. 4.22. The initial rate of work-hardening as a function of the proof stress for the alloy in various structural conditions.

Fig. 4.23. Cracking at twins and grain boundaries in a specimen deformed 10% prior to ageing for 3 minutes at 923°K. Tested at 296°K. x 65.

CHAPTER 5

DEFORMATION PROCESSES IN Fe-11 AT.% Mo ALLOY

5.1. Introduction

It has long been accepted that thermal fluctuations may assist the applied stress in moving dislocations past obstacles that possess short-range stress fields. A consequence of this phenomenon is that plastic deformation is time, temperature and strain rate dependent, and that the applied shear stress, τ, can be considered to be the sum of two components:

$$\tau = \tau^* + \tau_\mu \qquad (5.1.)$$

where τ_μ is the athermal component of stress and varies with temperature only through the shear modulus, μ, while the thermal component, τ^*, is temperature and strain rate dependent.

For a complete understanding of any deformation process it is necessary to determine the behaviour of the dislocations contributing to the deformation. This is achieved primarily by activation analysis, but an approach based on dislocation mobility may also be employed.

With the aid of activation analysis it is often possible to identify the thermal obstacles that are hindering dislocation motion. If a single activation process is rate controlling the shear strain rate, $\dot{\gamma}$, is given by an Arrhenius-type equation:

$$\dot{\gamma} = \dot{\gamma}_o \exp\left(\frac{-\Delta G}{kT}\right) \qquad (5.2.)$$

where $\dot{\gamma}_o$, the frequency factor, depends on the density of dislocations contributing to the deformation, the area swept out by a dislocation per successful fluctuation, and the frequency of vibration the dislocation segment involved in the thermal activation; k is Boltzmann's constant and T the absolute temperature. ΔG, the free energy of activation, is defined by:

$$\Delta G = \Delta H - T\Delta S \qquad (5.3.)$$

where ΔH and ΔS are the enthalpy (activation energy) and entropy of activation respectively. Generally it is assumed that the entropy is small compared with the free energy, thus $\Delta G \simeq \Delta H$. Hereafter, the usual practice of omitting the delta in the thermodynamical terms will be followed, i.e. $\Delta H = H$.

The activation energy is given by the expression due to Conrad and Wiedersich (1960):

$$H = -kT^2\left(\frac{\partial \ell n \dot{\gamma}}{\partial \tau}\right)\left[\left(\frac{\partial \tau}{\partial T}\right)_{\dot{\gamma}} - \left(\frac{\tau_\mu}{\mu}\frac{d\mu}{dT}\right)\right] \qquad (5.4.)$$

The activation volume, v*, which is the change in the activation free energy with respect to the shear stress, is given by:

$$v^* = -\left(\frac{\partial G}{\partial T}\right) = -\left(\frac{\partial H}{\partial T}\right)_T = kT\left(\frac{\partial \ell n \dot{\gamma}}{\partial \tau}\right)_T \qquad (5.5.)$$

Activation mechanisms are associated with characteristic values of H and v*, and therefore these parameters may be used for the identification of rate controlling processes.

The alternative approach to the investigation of dislocation motion is based on the empirical relationship between stress and dislocation velocity, v:

$$v = \left(\frac{\tau}{\tau_o}\right)^m \qquad (5.6.)$$

where τ_o is the shear stress for $v = 1$ cm sec^{-1} and m, the dislocation velocity exponent, is a constant. The physical significance of m is in doubt, nevertheless, it has been correlated with the occurrence of yield points (Johnston 1962 , Hahn 1962) and crack propagation (Hahn et al. 1963, Tetelman 1963).

The average dislocation velocity is related to the strain rate by:

$$\dot{\gamma} = \rho b v \qquad (5.7.)$$

where ρ is the density of mobile dislocations and b the Burgers

vector. Differentiating the logarithmic form of this equation and using equation 5.6. (Guard 1961):

$$m' = \frac{\partial \log \dot{\gamma}}{\partial \log \tau} = \frac{\partial \log \rho}{\partial \log \tau} + m \qquad (5.8.)$$

where m' may be called the apparent value of m. Johnston and Stein (1963) showed that if m' was extrapolated to zero strain, good agreement was obtained between m' and m determined from direct dislocation velocity measurements. The extrapolated value of m' will be referred to in the present work as m'_o.

The type of activation analysis outlined has been applied to a wide variety of materials, e.g. b.c.c. metals (Conrad 1961, Christian and Masters 1964), intermetallic compounds (Rosen et al. 1964, Pascoe 1966), solid solutions (Dorn and co-workers 1965 A and B, Rawlings and Newey 1967, Appendix IV) and ceramics (Conrad et al. 1965). However, except for work on alloys containign G.P. zones and coherent precipitates (Byrne et al. 1961, Kelly 1958), there is a dearth of data on age hardening materials, particularly with b.c.c. matrices, Similarly, the only evaluation of m'_o for a precipitate hardened material was by Felberbauer et al. (1964) for Fe-Al_2O_3.

This chapter reports the results of an analysis of the effect precipitation in an Fe-11 at.% Mo alloy on the deformation behaviour. In addition, the athermal stress of the solid solution is discussed.

5.2. Experimental Procedure

Specimen production was as described in the previous chapter.

Tests were performed in compression at a basic shear strain rate of 7.14×10^{-5} sec^{-1}. The strain rate was changed several times during a test between the basic strain rate and 7.14×10^{-4} sec^{-1} and the change in the shear stress, $\Delta\tau$, produced by an increment in strain rate recorded. Shear stresses were taken to be equal to half the compressive stresses.

Room temperature measurements were made as a function of time of ageing at 923 and 1073°K. Also, the temperature dependence of the activation parameters and m'_o, for the solid solution, slightly aged (20 minutes at 923°K), aged to peak hardness (150 minutes at 923°K) and overaged (2×10^3 minutes at 923°K) conditions of the alloy was studied over a considerable temperature range.

5.3. Results

5.3.1. Temperature Range 77-500°K

At room temperature, for all conditions of the alloy, the increase in the shear flow stress, $\Delta\tau$, produced by an increment in $\dot{\gamma}$ was fairly constant with stress (or strain); however, $\Delta\tau$ was greater for the aged conditions of the alloy (Fig. 5.1.).

This change in $\Delta\tau$ with ageing was observed at all temperatures below 500°K. Typical $\Delta\tau$ vs. τ curves for the alloy in the slightly aged condition at different test temperatures are shown in Fig. 5.2. The number of times that the strain rate could be changed during a test on the well-aged conditions of the alloy, i.e. 150 and 2×10^3 min, was limited by the lack of ductility of the specimens and generally only about four changes could be made.

In the later stages of tests performed above room temperature small yield drops occurred after a change in strain rate; in these cases, the difference between $\Delta\tau$ measured to the peak and by extrapolation through the transient was negligible and consequently the extrapolation procedure was adopted.

Activation volumes were calculated from the average value of $\Delta\tau$ during a test. At room temperature, precipitation resulted in a decrease in v*, but at 113 and 77°K, due to the smallness of the activation volumes, there was little absolute change in v* with ageing (Fig. 5.3.). Activation volume plotted against the thermally activated component of flow stress (the effective stress) is given in Fig. 5.4. τ_μ was taken as the proof stress at 500°K; the change in τ_μ with temperature, due to the temperature dependence of the elastic modulus, was ignored as it was negligible compared with the temperature dependence of τ^*. The full line in Fig. 5.4. is from the work on the solid solution reported

elsewhere (Rawlings and Newey 1967, Appendix IV) and it can be seen that within experimental error the results for the aged material fall on the same curve.

The effect of ageing on the room temperature values of m'_o is shown in Fig. 5.5., and some typical room temperature m' vs. true plastic strain plots for specimens aged for various times at 1073°K are given in Fig. 5.6. For the solid solution and the slightly aged material the variation of m'_o with temperature exhibited a minimum around room temperature and increased more rapidly at temperatures above room temperature than below (Fig. 5.7.). The behaviour of the two well-aged conditions of the material was similar above room temperature but the scatter was too great at the lower temperatures to distinguish any trend.

5.3.2. Temperature Range 500-1100°K

For all heat treated conditions, over a temperature range commencing about 500°K, the temperature dependence of the proof stress was very small (see Fig. 4.12.) and the material was not strain rate sensitive. As Fig. 4.12. shows this athermal behaviour terminated at about 700°K for the well aged states but extended to 875°K for the solid solution and slightly aged material.

Above 700°K the strength of the well-aged material was very temperature dependent and the material was again strain rate sensitive. Except for one test, as at low temperatures, $\Delta\tau$ was approximately constant with strain. The exception was at 890°K where the specimen that had been aged 20 minutes showed a marked increase in $\Delta\tau$ during the test (Fig. 5.8.). The same specimen also exhibited an appreciable amount of work-hardening and it is thought that the two phenomena are the result of precipitation during the test. Solid solution, and slightly aged specimens tested at, and above, 960°K had exactly the same strength and activation volume as the well-aged material. Fig. 5.9. shows the variation of v^* with τ for all conditions of the alloy except for the specimen aged 20 minutes and tested at 890°K.

Tests below 800°K on the well-aged specimens gave m' values which increased with strain; above 800°K, because of the very small amount of work hardening, m' was virtually independent of strain. The effect of temperature on m'_o is illustrated in Fig. 5.10.

5.4. Discussion

5.4.1. Behaviour Below 500°K

The small increase in m_o' with decreasing temperature below room temperature is comparable to the temperature dependence of m, evaluated by the dislocation etch pit technique, for a Fe-Si solid solution (Stein and Low 1959). The values of m_o' obtained in the present investigation for the solid solution were some 50% greater than m for Fe-Si. The increase in m_o' above room temperature may be associated with dislocation pinning due to the increasing mobility of the molybdenum or interstitial atoms, although no jerky flow, which often accompanies dislocation pinning, was detected in the stress-strain curves.

The increase in m_o' with ageing cannot be correlated with a reduction in the molybdenum content of the matrix as this would indicate that m_o' for iron is high which contradicts the work of Michalak (1965). Also, it is unlikely that the difference in the maximum values of m_o' obtained at the ageing temperatures of 923 and 1073°K (corresponding to matrix concentrations of 2.4 and 2.9 at.% Mo respectively) would be about the same as that between matrix concentrations of 2.9 and 11 at.% Mo if m_o' were governed solely by the molybdenum concentration. It is concluded that the large values for m_o' for the aged alloy are the result of either the high stress levels or the high initial rate of work-

hardening (Schadler 1964).

Explanations for the variation in v* with ageing based on the change of the carbon or molybdenum content of the matrix, or on the change in precipitate size and distribution, during ageing are found to be unsatisfactory in detail. The possibility that the change in v* may be due to small variations in the effective stress for the different conditions of the alloy cannot be disregarded. The fact that the activation volumes as a function of the effective stress fall on the same curve for all conditions of the alloy and that the temperature dependences of the proof stresses were similar indicates that, although there may be some differences in fine detail, the rate controlling mechanisms are the same for all conditions of the alloy.

The small activation volumes obtained for the deformation at the lower temperatures suggest that the rate controlling mechanism at these temperatures is the overcoming of the Peierls' barrier. Dorn and Rajnak's theory (1964) for the Peierls' mechanism was found to hold for the solid solution over a limited temperature range (Rawlings and Newey 1967, Appendix IV) and it is therefore of interest to apply the same theory to the aged material.

According to Dorn and Rajnak (1964) the thermal component of the flow stress for the Peierls' process is given by:

$$\frac{\tau^*}{\tau^*_p} = f_1\left(\frac{Un}{2U_k}\right) \simeq f_1\left(\frac{T}{T_c}\right) \qquad (5.9.)$$

where τ^*_p is the Peierls' stress, Un is the activation energy for nucleating a pair of kinks, U_k is the energy of an isolated kink, T is the test temperature, T_c is the critical temperature at which thermal fluctuations with energy $2U_k$ are frequent and is defined by:

$$\dot{\gamma} = \frac{\rho ab\nu\, L}{w} \exp\left(\frac{-2U_k}{kT_c}\right) \qquad (5.10.)$$

where ρ is the dislocation density, a is the distance between adjacent Peierls' valleys, ν is the Debye frequency, L is the length swept out by a pair of kinks and w is the length of the embryonic kinks.

Extrapolation of graphs of log proof stress against temperature gave values for τ^*_p of 50, 54 and 54 kg mm^{-2} for the material aged 20, 150 and 2 x 10^3 min respectively, compared with 49 kg mm^{-2} obtained for the solid solution. Theoretical calculations of the Peierls' stress, e.g. Foreman, Jawson and Woods 1951, predict that it is proportional to the shear modulus and therefore to Young's modulus. Hence, the similarity in the τ^*_p values are in agreement with molybdenum in solution having very little effect on the elastic properties of iron (Chapter 3). Using

these values for τ^*_p, together with the measured values of τ^* and T, the low temperature data were fitted to the universal $\frac{T}{T_c}$ versus $\frac{\tau^*}{\tau^*_p}$ curves by the appropriate choice of critical temperatures. As Fig. 5.11. shows a good fit with theory with the pertubation factor, α, which describes the shape of the Peierls' barrier, equal to unity was obtained for tests performed at and below 175°K using critical temperatures of 290 and 320°K, 290 and 320°K and 285 and 315°K for ageing times of 20, 150 and 2×10^3 min respectively and for strain rates of 7.14×10^{-5} and 7.14×10^{-4} sec^{-1}. τ^* values for $\dot{\gamma} = 7.14 \times 10^{-4}$ sec^{-1} were taken to be equal to τ^* for $\dot{\gamma} = 7.14 \times 10^{-5}$ sec^{-1} plus $\Delta\tau$. Above 200°K the experimental points deviated from the theoretical curve suggesting that the Peierls' mechanism was no longer rate controlling.

Using equation 5.10. the energy of an isolated kink, U_k, was calculated to be 0.31, 0.31 and 0.30 eV for ageing times of 20, 150 and 2×10^3 min respectively. The small difference in these values and that of 0.29 eV for the solid solution again correlates with only a small change in the modulus of the matrix with ageing.

Values of $\frac{\tau^*_p v^*}{2U_k}$ plotted against $\frac{\tau^*}{\tau^*_p}$ and of Un, calculated from equation 5.9., against τ^* fitted the theoretical curves for temperatures below 200°K (Figs. 5.12. and 5.13.). The theoretical curve of Un vs. τ^* varies with the value of τ^*_p

and U_k, but the change is negligible for the small differences in τ_p^* and U_k for the aged conditions of the alloy so only one theoretical curve has been drawn.

Ignoring the temperature dependence of the shear modulus in equation 5.4. gives:

$$H = -kT^2 \left(\frac{\partial \ell n \dot{\gamma}}{\partial \tau}\right) \left(\frac{\partial \tau}{\partial T}\right)_{\dot{\gamma}} = -v^*T \left(\frac{\partial \tau}{\partial T}\right)_{\dot{\gamma}} \qquad (5.11.)$$

H, evaluated from this equation, and also the low temperature values of Un are plotted against temperature in Fig. 5.14. for $\dot{\gamma} = 7.14 \times 10^{-5}$ sec^{-1} and the 2×10^3 min heat treatment. Similar curves were obtained for the other conditions of the alloy. The graph consists of two distinct regions; a low temperature linear region (below about 200°K) and a higher temperature region of greater slope in which a process or processes other than the Peierls' mechanism are operative. As for other b.c.c. materials (Basinski and Christian 1959; Christian and Masters 1964) the slope of the low temperature region gives a value of about 25-26 for $(\ell n\dot{\gamma}_o - \ell n\dot{\gamma})$.

Using

$$\frac{2U_k \pi}{a\Gamma_o} \Big/ \left(\frac{\tau^*_p ab}{\pi \Gamma_o}\right) \simeq 5.75$$

for $\alpha = +1$ (Dorn and Mitchell 1964) the line energy of a dislocation, Γ_o, was evaluated for the aged conditions of the

alloy. The values of Γ_o obtained were similar to that of 2.8×10^8 eV cm^{-1} found for the solid solution.

From the above analysis it would appear that below about 200°K the Peierls' mechanisms is rate controlling for all conditions of the alloy.

It has been suggested (Guyot and Dorn 1966) that at intermediate temperatures, i.e. 200-500°K, the rate controlling mechanism in the deformation of an Fe-Mn solid solution is the recombination of sessile, dissociated screw dislocations (Escaig 1966). According to Escaig, at low stresses where $\tau^* << \tau_o^*$ the following equations apply:

$$\tau^* = \frac{\mu^2 b^3}{150\ KC} \left\{ - \left[15 \frac{\tau_o^*}{\mu} + \ell n \left(1 - 15 \frac{\tau_o^*}{\mu}\right) \right] \right\}^{\frac{3}{2}} \frac{1}{T} \qquad (5.12.)$$

$$H = \frac{\mu^2 b^3}{150} \left\{ - \left[15 \frac{\tau^*}{\mu} + \ell n \left(1 - 15 \frac{\tau_o^*}{\mu}\right) \right] \right\}^{\frac{3}{2}} \frac{1}{\tau^*} \qquad (5.13.)$$

$$v_T^* = \frac{2k\,T}{\tau^*} + v^* \simeq \frac{8b^3 \tau_o^{*3}}{\mu \tau^{*2}} \qquad (5.14.)$$

where C is a constant approximately equal to 45 and τ_o^* is the flow stress at absolute zero. For all conditions of the alloy at intermediate temperatures, linear relationships exist between

τ^* and $\frac{1}{T}$, H and $\frac{1}{\tau^*}$, and v_T^* and $\frac{1}{\tau^{*2}}$ in accordance with the above equations (e.g. Figs. 5.15. and 5.16. and 5.17.). However, straight line plots are also obtained at the lower temperatures where the Peierls' mechanism is operative (Figs. 5.15. and 5.16.). τ_o^* values, calculated from the slopes of the graphs in the low temperature range, were 160-175 kg mm^{-2}. These values are considerably greater than τ_p^* values obtained by extrapolation of the log proof stress-temperature curves, and preclude any possibility that the recombination mechanism is operative at these temperatures. In the intermediate temperature range, the τ_o^* values obtained from the different graphs were not consistent, i.e. τ^* vs. $\frac{1}{T}$, τ_o^* = 190-205 kg mm^{-2}; H vs. $\frac{1}{\tau^*}$, τ_o^* = 125-140 kg mm^{-2}; v^* vs. $\frac{1}{\tau^{*2}}$, τ_o = 80 kg mm^{-2}. This inconsistency, and the fact that no significance can be placed on obtaining linear relationships in accordance with Escaig's theory as these are also found at the lower temperatures where the Peierls' mechanism is operative, indicates that it is unlikely that the recombination mechanism is rate controlling in the temperature range 200-500°K in Fe-Mo.

5.4.2. Athermal Behaviour

The high athermal stress level for the aged conditions of the alloy was due to the precipitate particles acting as obstacles to

dislocation movement. As a thorough study of precipitate size and separation as a function of ageing time was not made it was not possible to compare experimental yield stresses with stresses predicted by theories.

The theories of Mott and Nabarro (1948) and Mott (1952) for the strengthening due to misfit stresses were applied to the solid solution. The shear stress is given by:

$$\tau' = \mu\varepsilon^2 c \{c^{\frac{2}{3}} (\ell nc)^2\} \qquad (5.15.)$$

or

$$\tau'' = \mu\varepsilon^{\frac{4}{3}} c \{\frac{c^{\frac{2}{3}}}{2\pi} (\ell n\frac{1}{c})^4\}^{\frac{1}{3}} \qquad (5.16.)$$

depending on the flexibility of the dislocation. c is the fractional atomic concentration of solute and ε is the misfit of the solute atom in the lattice and is given by the change in the lattice parameter, a, with concentration:

$$\varepsilon = \frac{1}{a} \frac{da}{dc} \qquad (5.17.)$$

Substituting $\mu_{500^oK} = 6.9 \times 10^{11}$ dyne cm^{-2}, $c = 0.11$ and $\varepsilon = 0.11$ gave

$$\tau' = 11.2 \times 10^8 \text{ dyne cm}^{-2} = 11.4 \text{ kg mm}^{-2}.$$

and $$\tau'' = 42.7 \times 10^8 \text{ dyne cm}^{-2} = 43.5 \text{ kg mm}^{-2}.$$

The experimental value for τ at 500°K was 17 kg mm^{-2}, which is in fair agreement with τ'.

In the concentration range c = 0.01-0.20 the terms $\{c^{\frac{2}{3}} (\ell nc)^2\}$ and $\{ \frac{c^{\frac{2}{3}}}{2\pi} (\ell n \frac{1}{c})^4 \}^{\frac{1}{3}}$ of equations 4.16. and 4.17. vary between 0.89 and 1.22, and 0.72 and 1.54 respectively. Thus the expressions approximate to:

$$\tau' \simeq \mu\varepsilon^2 c \qquad (5.18.)$$

$$\tau'' \simeq \mu\varepsilon^{\frac{4}{3}} c \qquad (5.19.)$$

i.e. in both cases the shear stress varies linearly with c. Owing to the lack of yield data for Fe-Mo solid solutions, this relationship was tested by plotting hardness values collected from many sources as a function of molybdenum concentration. As Fig. 5.18. shows, a reasonable linear relationship between H.V. and c was obtained. Davies and Ku (1966) found that stress was directly proportional to the solute concentration for Fe-C and Fe-Ni alloys. The theory due to Fleischer and Hibbard (1963), which considers the effect of the shear modulus mismatch as well as the size misfit of the solute atoms, is unlikely to be applicable as H.V. does not vary linearly with $c^{\frac{1}{2}}$ (Fig. 5.19.).

5.4.3. High Temperature Behaviour

In the high temperature region the flow stress decreased with increasing temperature. The possible causes of this loss in strength are, (i) grain boundary sliding, (ii) change in structure, and (iii) thermally activated flow.

(i) is eliminated by the fact that, even though grain boundary sliding was observed at the higher temperatures, the proof stresses of the single crystal, the two bi-crystals and the polycrystals tested at 960°K were similar. Iron-molybdenum alloys overage very slowly and it is unlikely the marked decrease in strength is caused by the overageing phenomenon. In particular, the fall-off in strength for the well-aged material began at about 700°K a temperature at which structural changes would take several weeks.

The most satisfactory explanation is in terms of the thermally activated motion of dislocations past the large precipitate barriers. Although there is the possibility that high temperatures and grain boundary sliding could affect the validity of an activation analysis, the activation parameters obtained in the present investigation were of reasonable magnitudes and compared favourably with those from other studies. The activation energy, which was calculated in the same manner as for the low temperature results, was only slightly temperature dependent at first but rapidly increased with temperature above

950°K (Fig. 5.20.). At these temperatures diffusion is relatively rapid and the rate controlling mechanism is probably associated with diffusion. If so, the activation energy for deformation should be comparable to the activation energy for diffusion. Unfortunately, there is no data available on diffusion in Fe-Mo solid solutions. However, Mokrov (1964) found that molybdenum in iron increased the activation energy for the formation of vacancies, Q_v. The molybdenum concentration of the matrix after precipitation is about 2.4 at.% which, according to Mokrov, increased Q_v some 27% above that of pure iron. Assuming a vacancy mechanism, the activation energy for diffusion, Q_D, would be increased by a similar amount and, taking the energy for self diffusion in iron as 2.6 eV $atom^{-1}$ (≈60 kcal $mole^{-1}$) gives an approximate value of 3.3 eV $atom^{-1}$ (≈76 kcal $mole^{-1}$) for Q_D in Fe-Mo. This value of Q_D is similar in magnitude to the activation energy for deformation in the temperature range 750-950°K.

Two possible activation mechanisms involving diffusion are climb, and non-conservative motion of jogs on screw dislocations. Activation volumes in this temperature range were greater than those generally associated with the climb mechanism, i.e. 110 to 33 b^3 compared with 1 b^3 for climb. On the other hand the distance between jogs in a b.c.c. material has been calculated to be about 50 b (Schoeck 1961) which gives an activation volume of 50 b^3.

Thus the activation volumes obtained were of the magnitude expected for the non-conservative motion of jogs.

Above 950°K H rapidly increased to a maximum value of about 8.1 eV at 1050°K, but the activation volumes remained the same magnitude. It should be noted, however, that there is a discrepancy between the measured v* values and those calculated from the slope of the curve of H against τ in this region. The latter method gave v* values considerably higher than the measured values. A similar rapid increase in the activation energy for creep has been reported for nickel (Landon et al. 1959) and for iron (Ishida et al. 1966) in the region of the Curie temperature and has been attributed to effects arising from the Curie transformation (Garofalo 1965, Ishida et al. 1966).

Ishida et al. found that the secondary creep rate, $\dot{\varepsilon}_s$, for iron in the temperature range 750-1050°K is given by:

$$\dot{\varepsilon}_s = k\sigma^n \qquad (5.20.)$$

where n = 6.9. Reference to equation 4.8. shows that n may be compared with m'_o. Above 800°K m' was independent of strain and decreased with increasing temperature tending to values of 10-20. These values are slightly greater than n for iron but agree quite well with n, measured from the slopes of log stress vs. log minimum creep rate curves, for Fe-Mo alloys, i.e. Fe-6.5 at.% Mo tested at 922°K, n ≃ 11 (Reiter and Hibbard 1955), Fe-5.4-5.7 at.% Mo tested at 922°K, mean value of n ≃ 14 (Coldren et al. 1964).

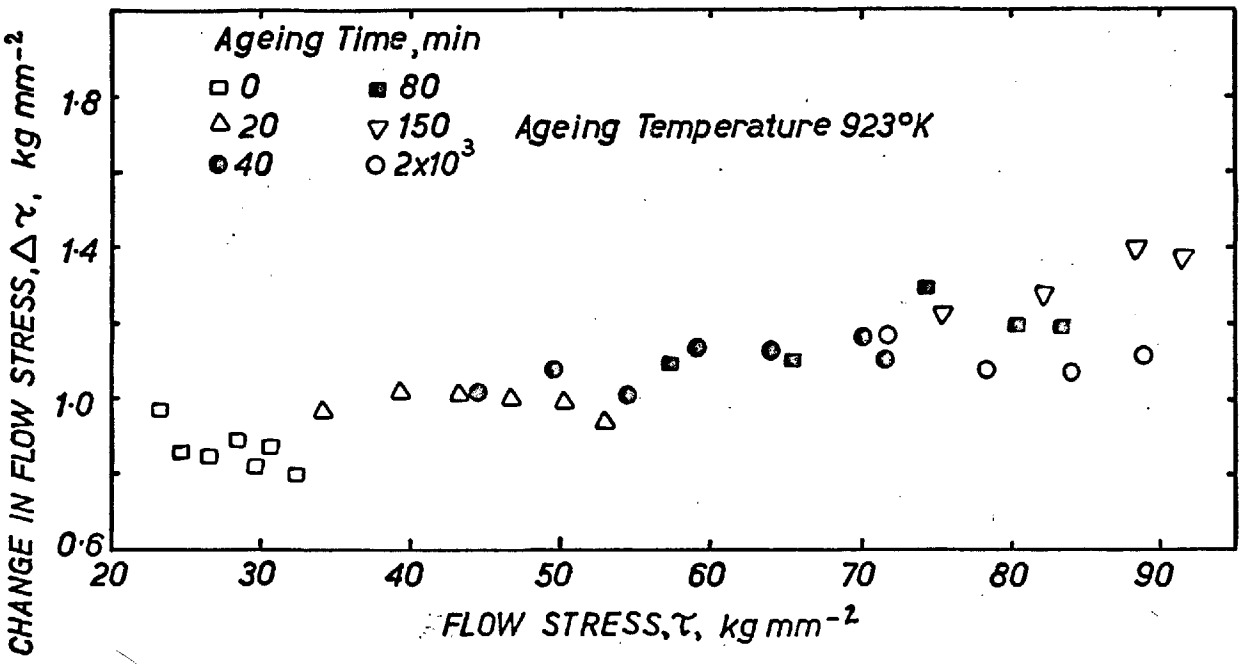

Fig. 5.1. Effect of ageing on the change in flow stress produced by an increment in strain rate as a function of the flow stress at 296°K.

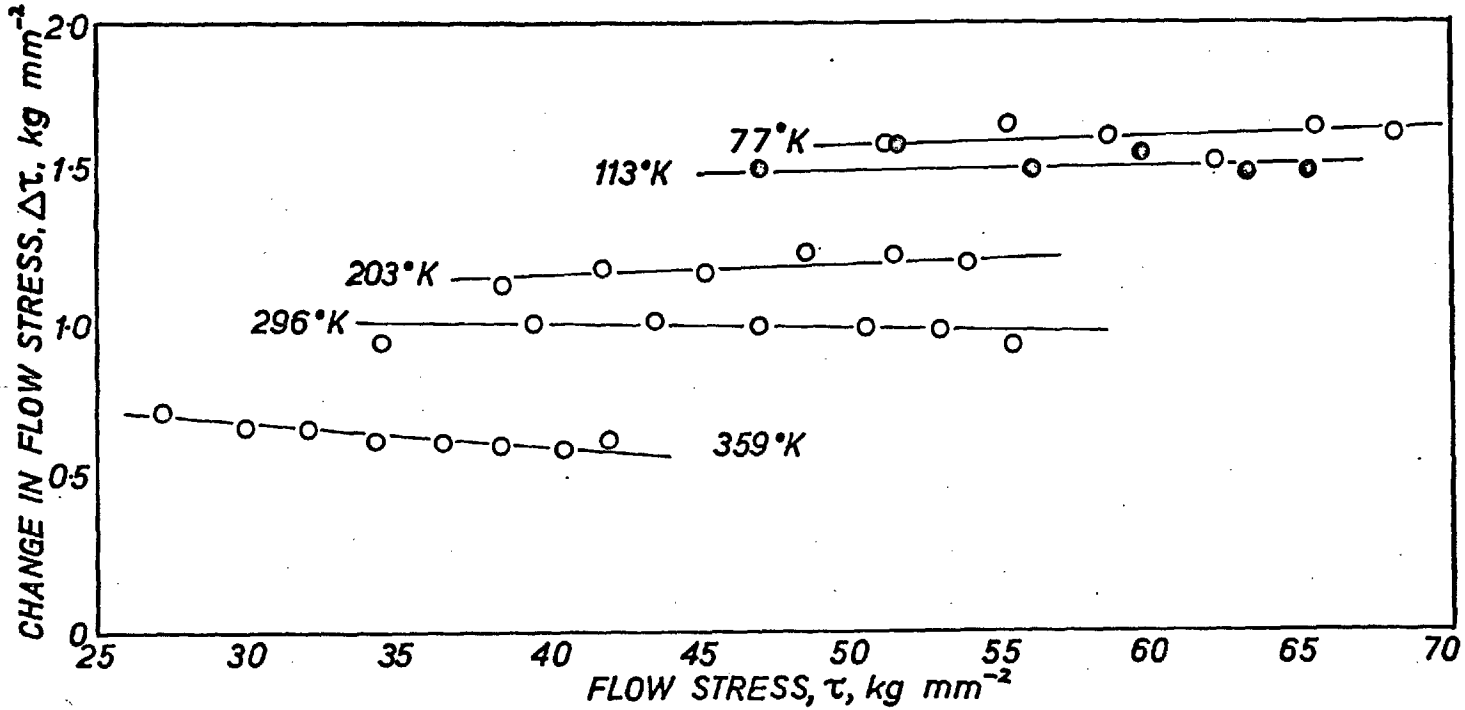

Fig. 5.2. Effect of temperature on typical change of flow stress versus flow stress plots for the alloy aged 20 minutes at 923°K.

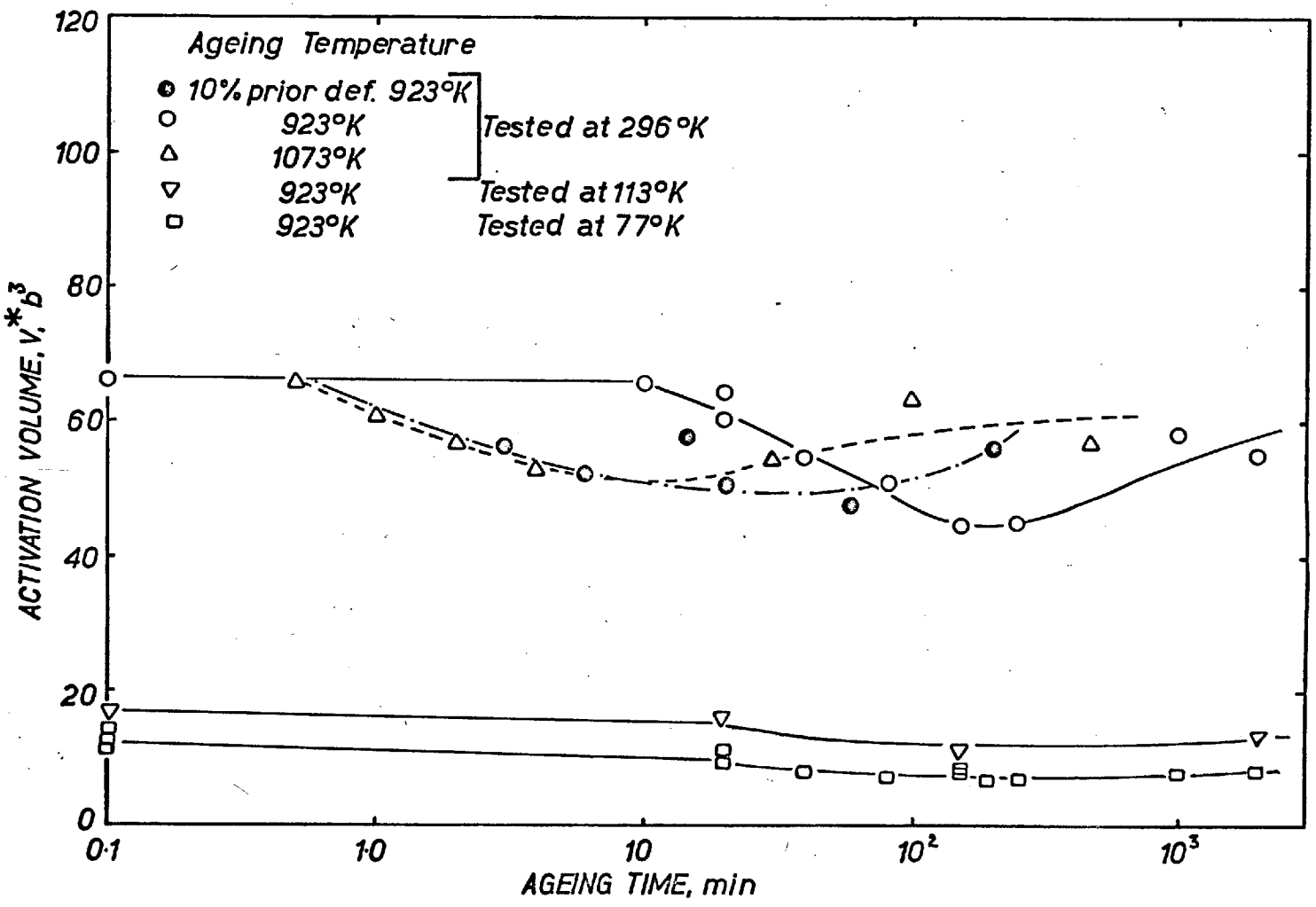

Fig. 5.3. Effect of ageing and test temperature on the activation volume.

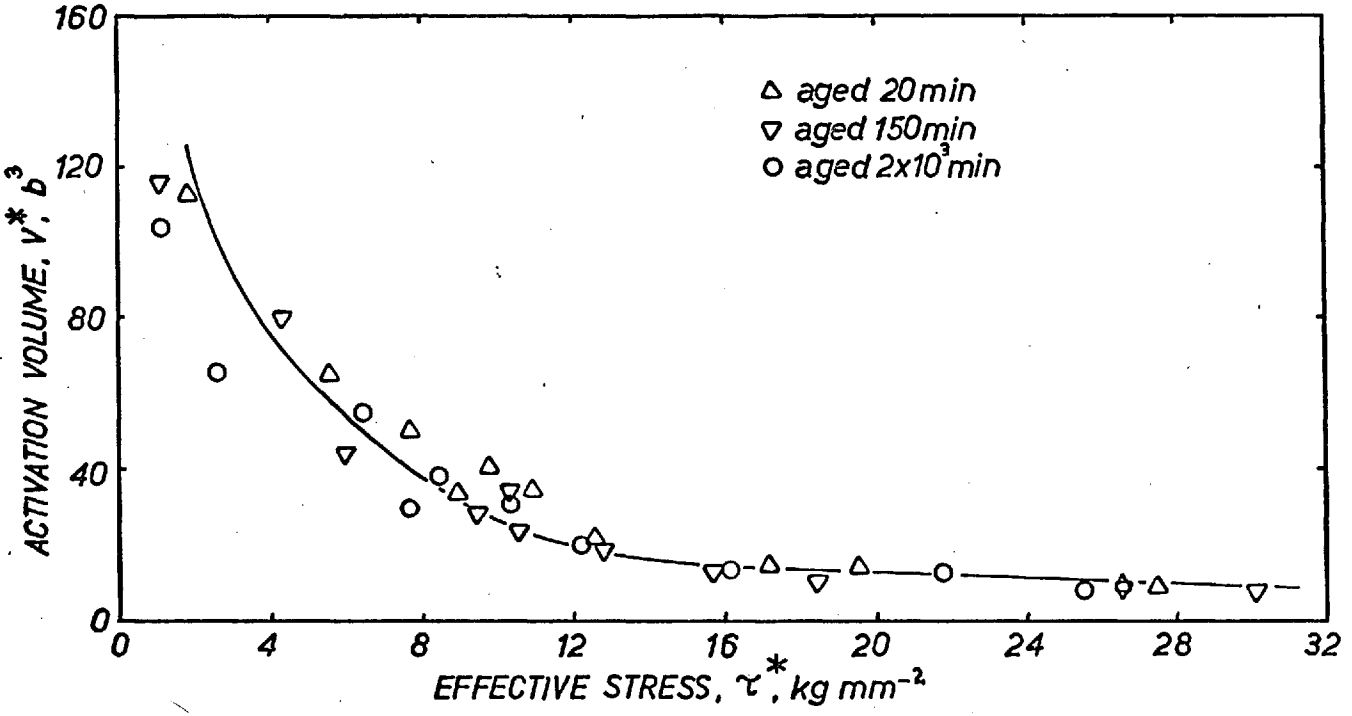

Fig. 5.4. Activation volume for the aged conditions of the alloy as a function of the effective stress.

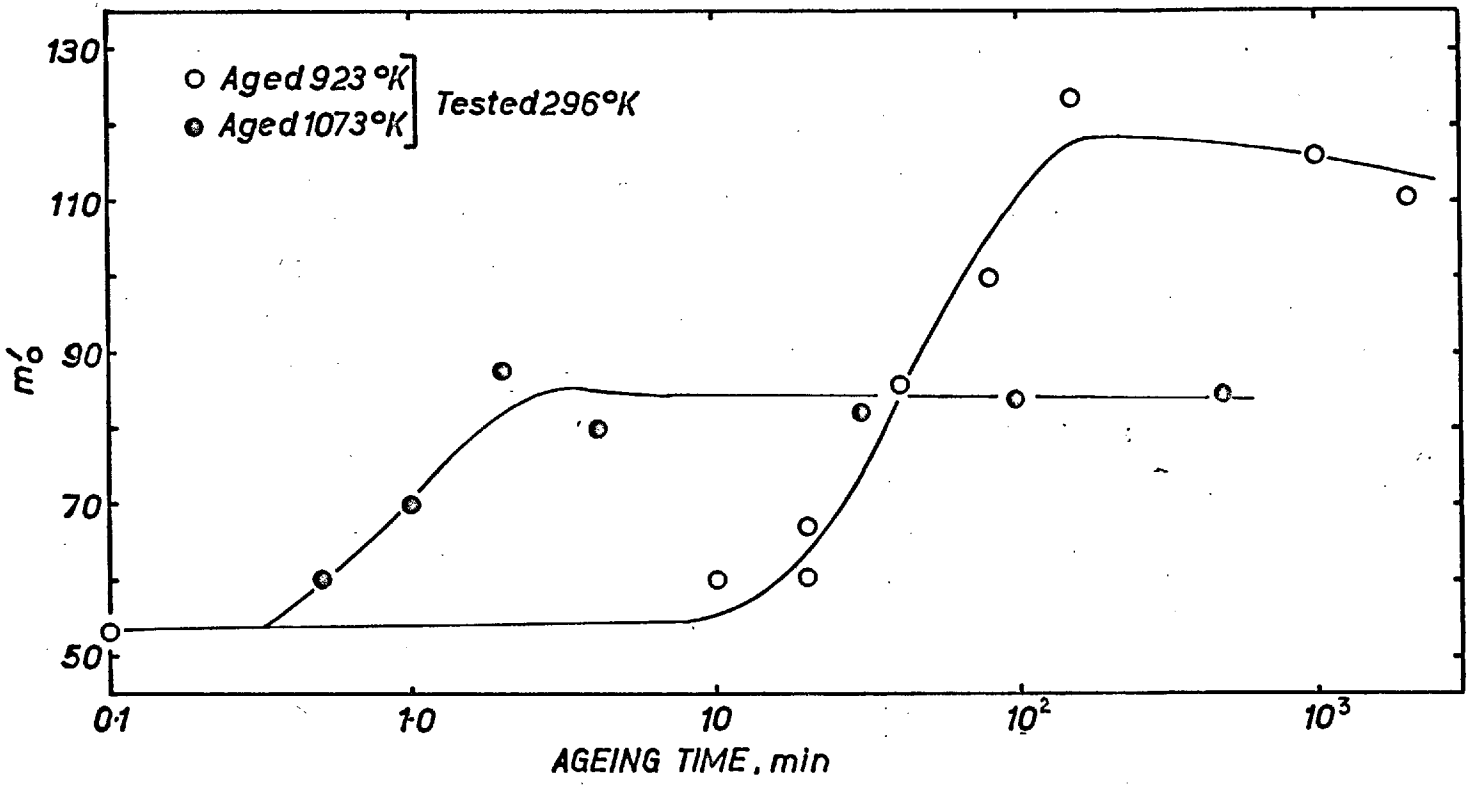

Fig. 5.5. Effect of ageing on the extrapolated value of m', i.e. m'_o.

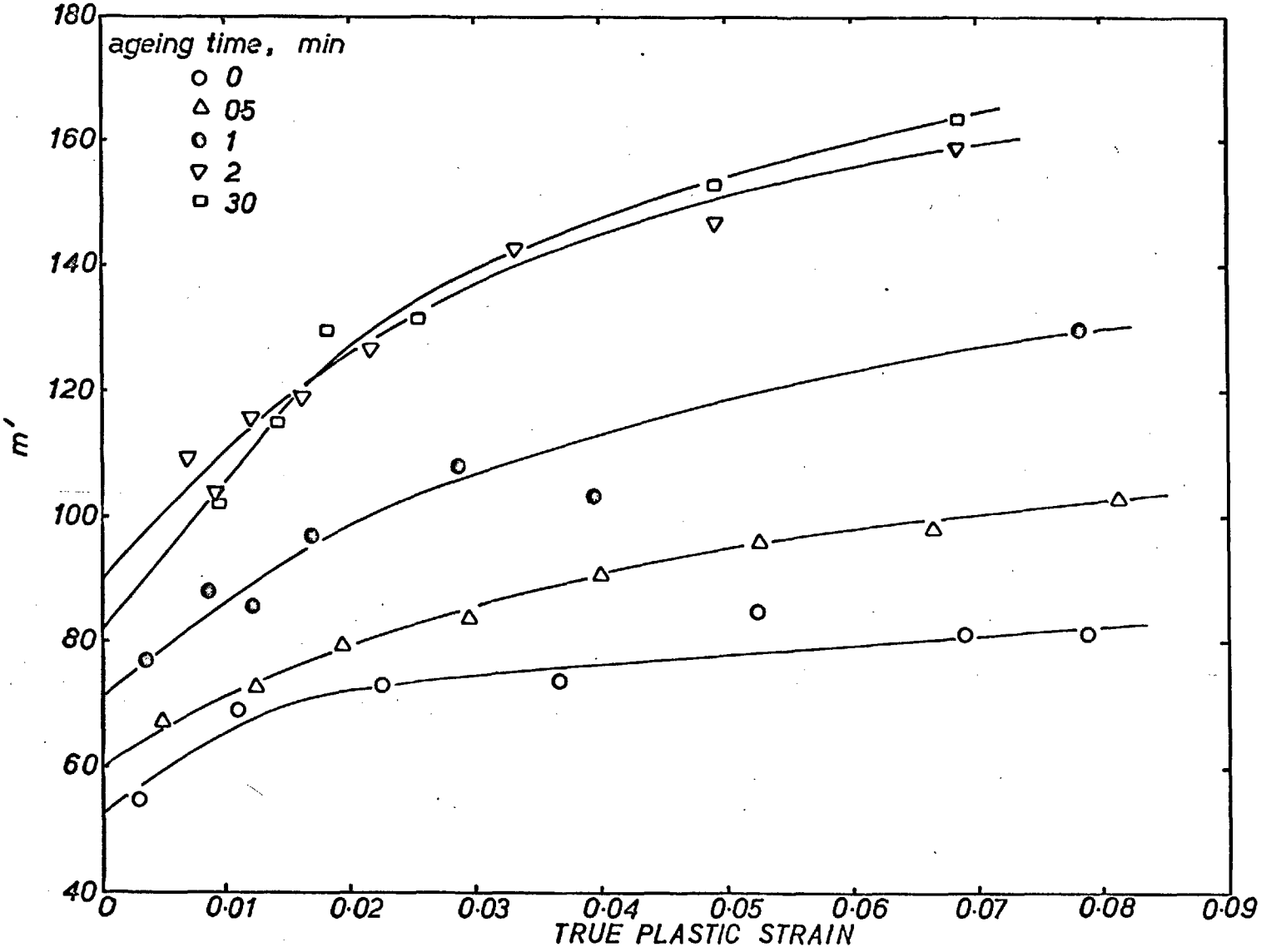

Fig. 5.6. Typical room temperature m' versus true plastic strain plots for the alloy aged at 1073°K.

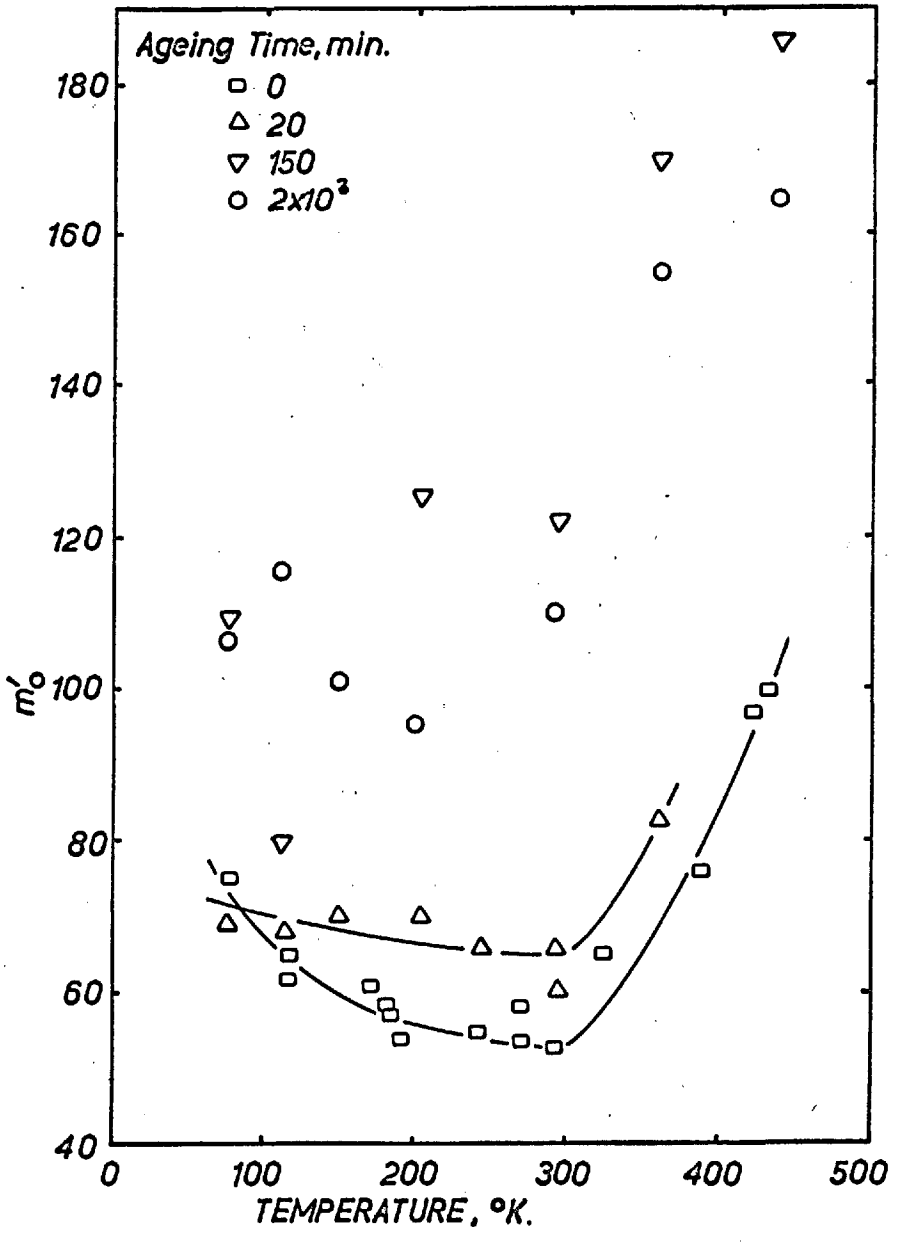

Fig. 5.7. Effect of temperature on the extrapolated value of m', m'_o, for the alloy in four different heat treated conditions.

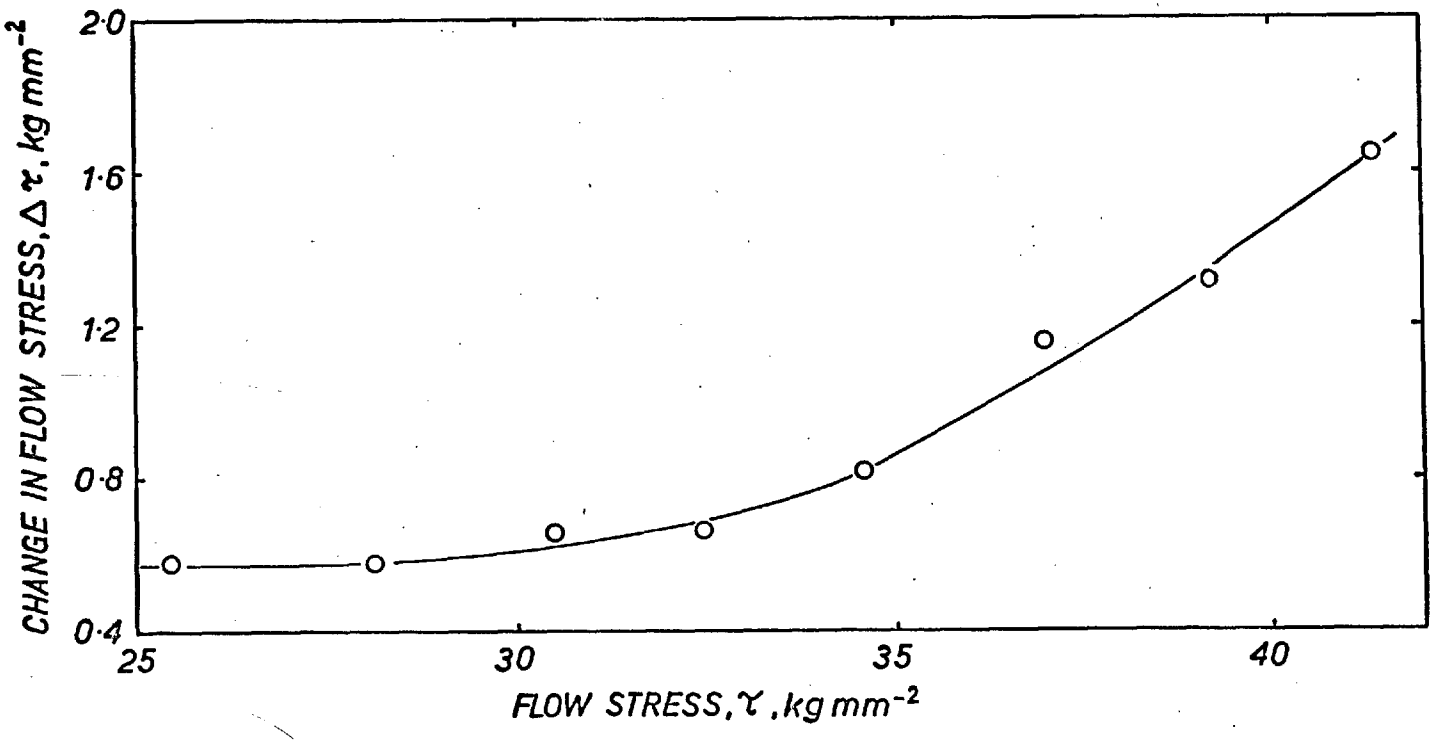

Fig. 5.8. The change in flow stress produced by an increment in strain rate as a function of flow stress for the alloy aged 20 minutes at 923°K and tested at 890°K.

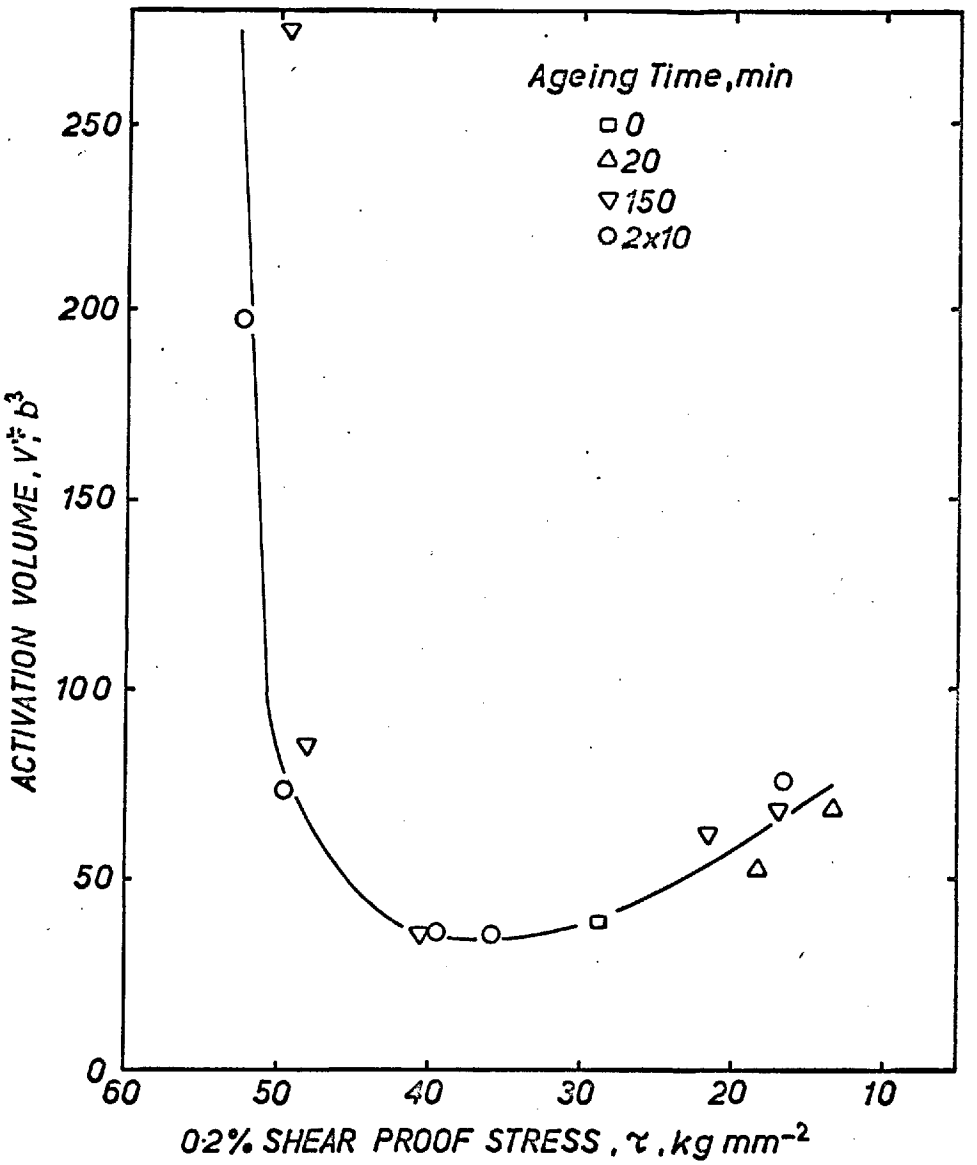

Fig. 5.9. Activation volume as a function of the proof stress for the alloy in four different heat treated conditions.

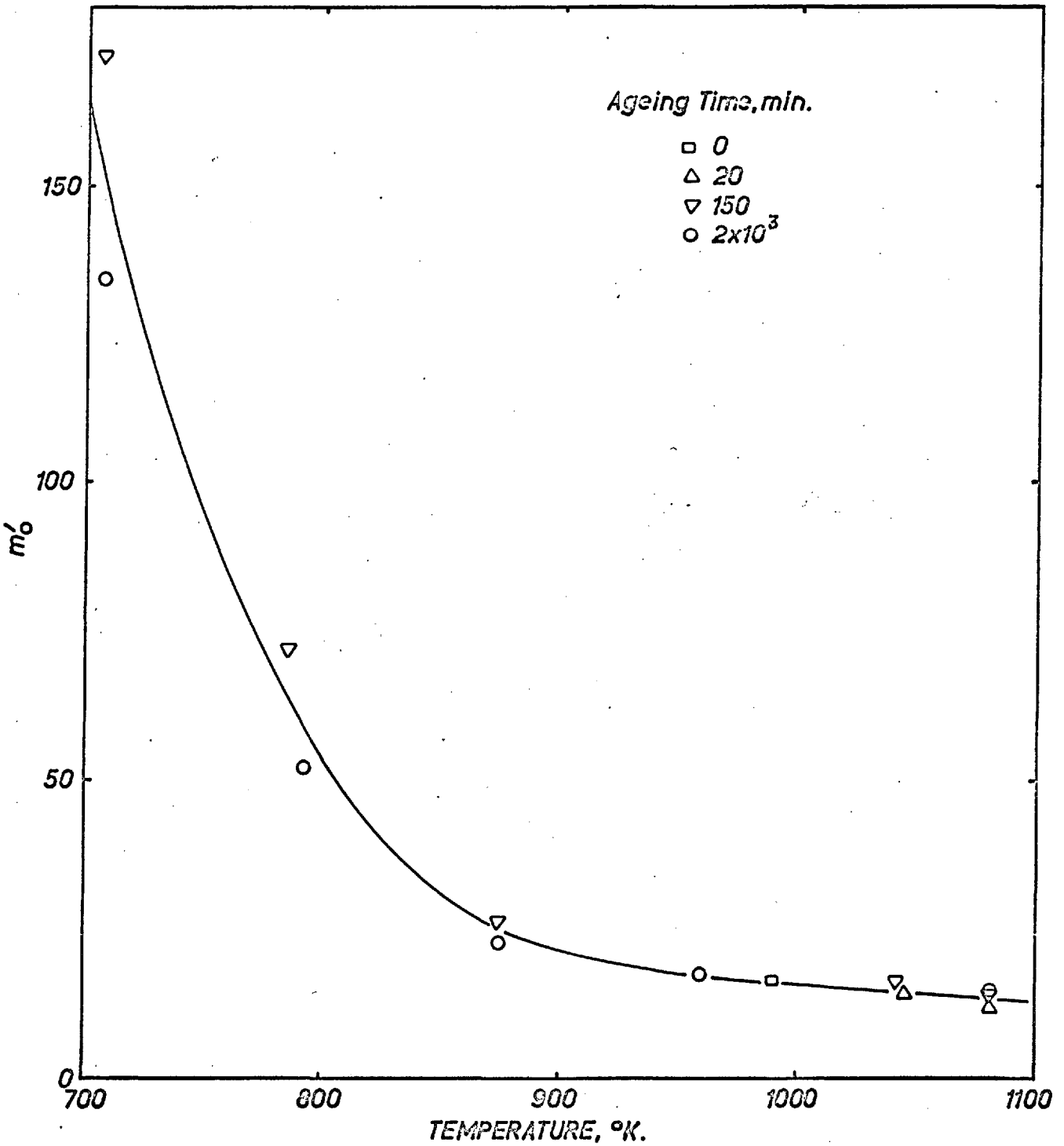

Fig. 5.10. Effect of temperature on the extrapolated value of m', m'_o, for the alloy in four different heat treated conditions.

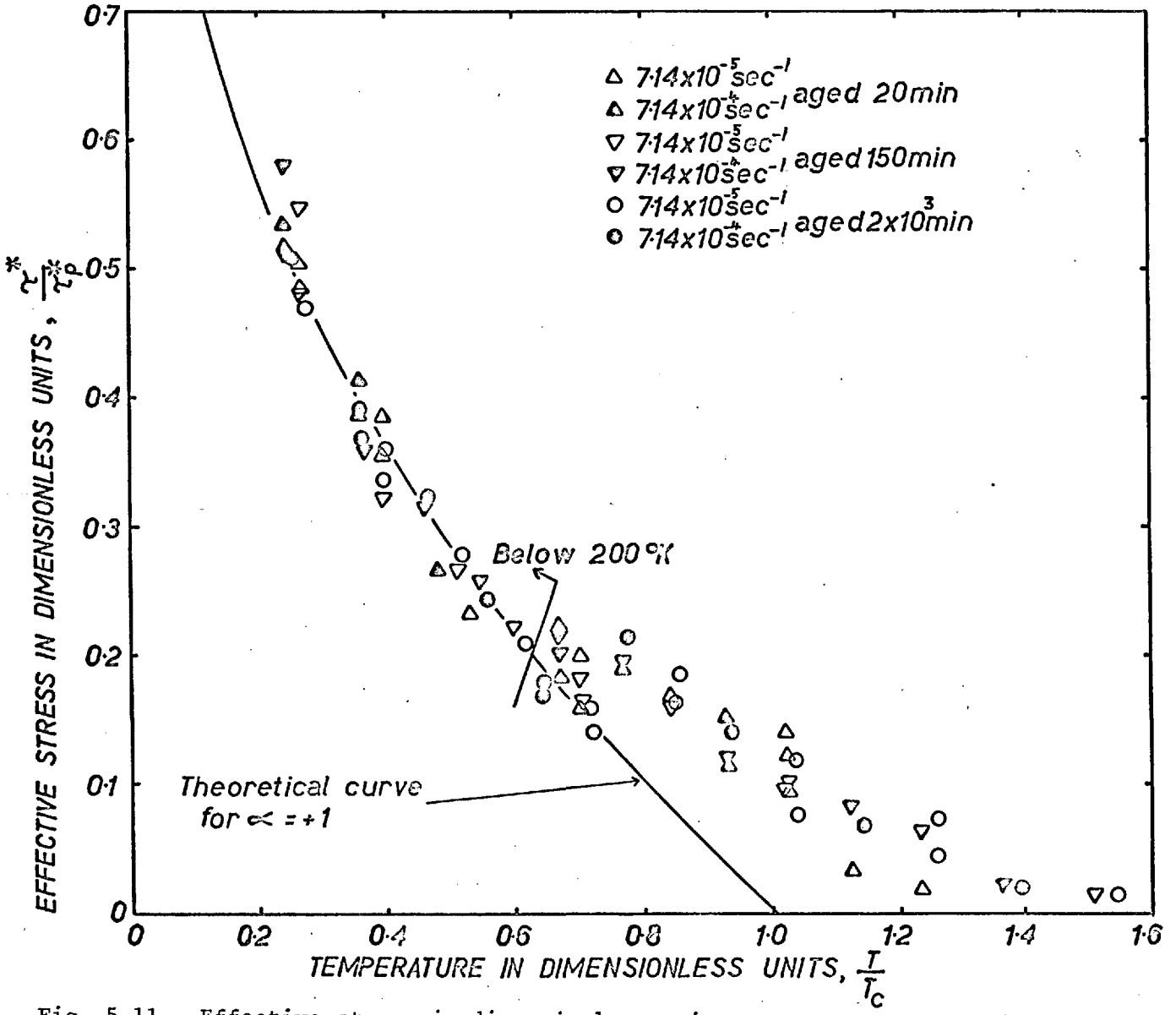

Fig. 5.11. Effective stress in dimensionless units versus temperature in dimensionless units.

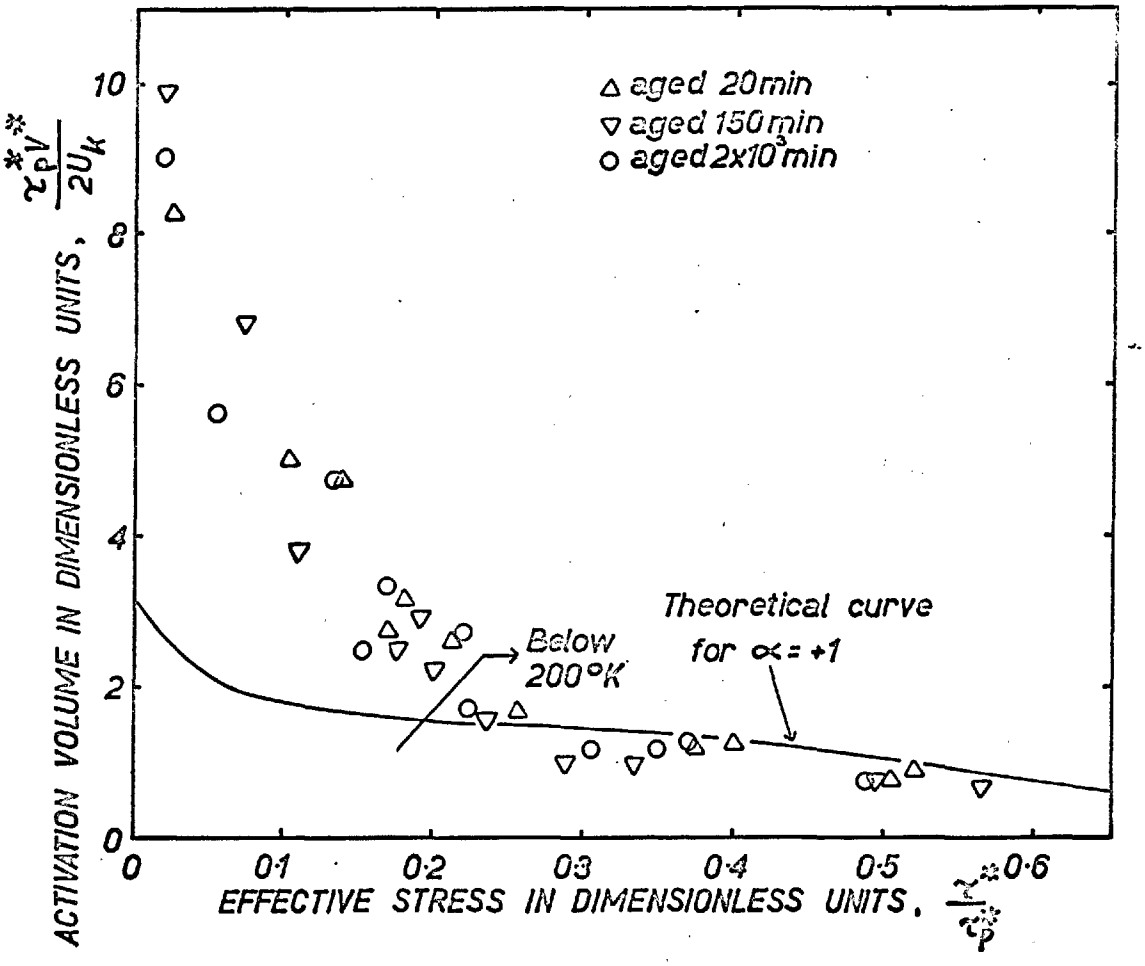

Fig. 5.12. Activation volume in dimensionless units versus effective stress in dimensionless units.

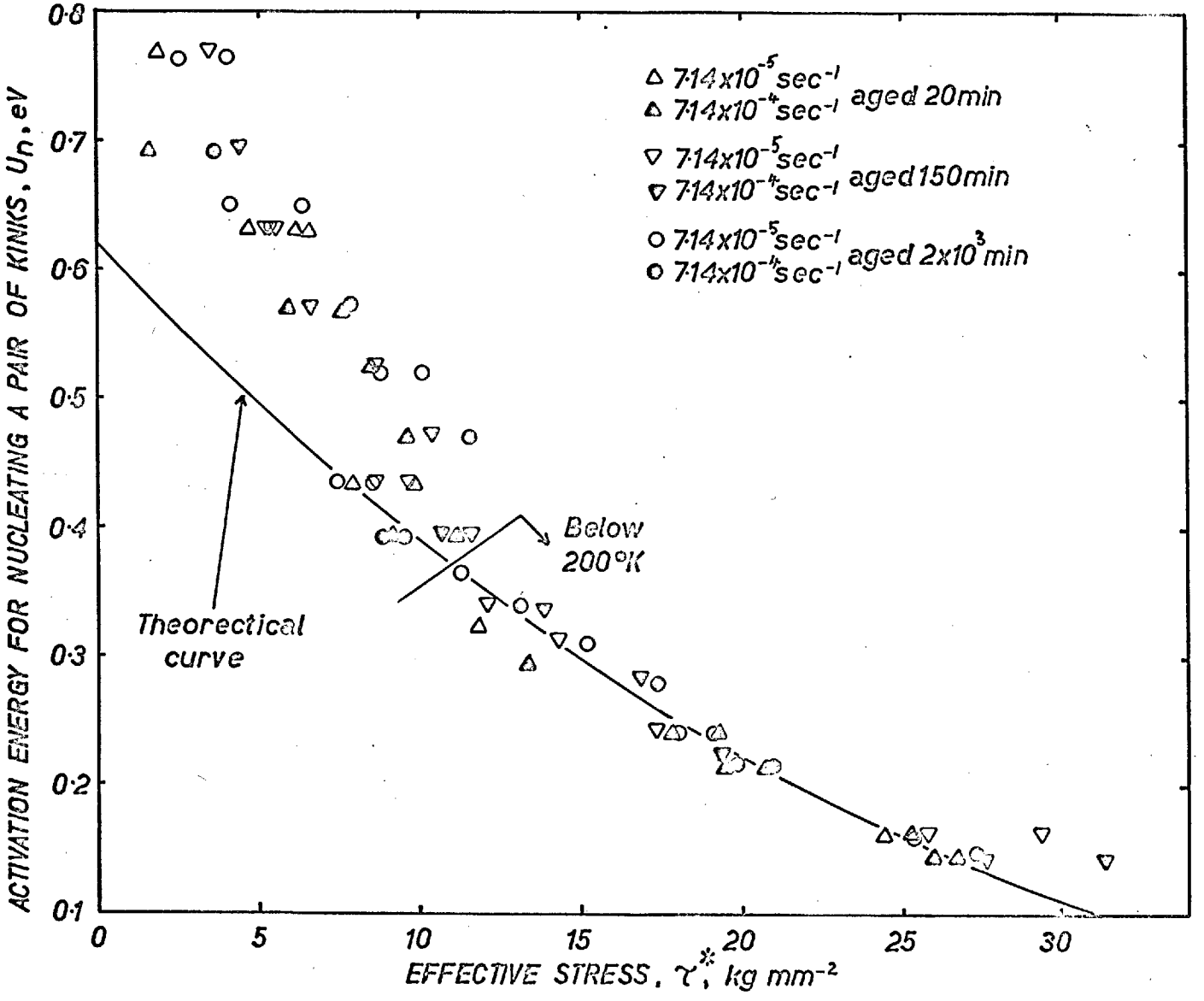

Fig. 5.13. Activation energy for nucleating a pair of kinks versus effective stress.

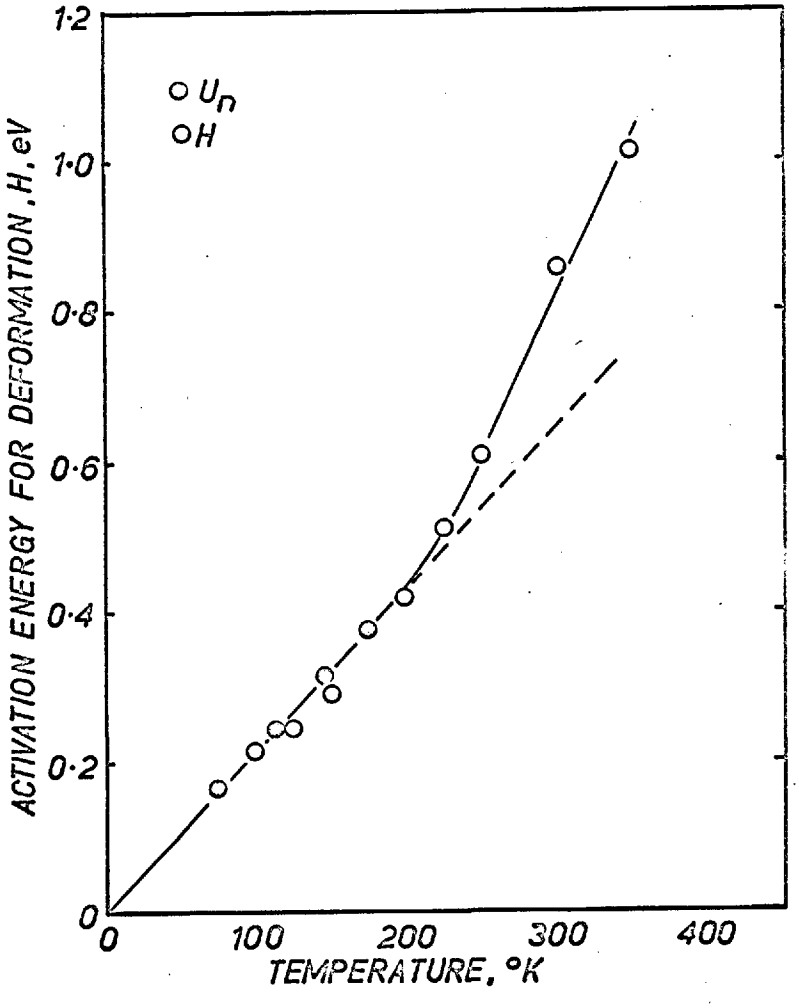

Fig. 5.14. Effect of temperature on the activation energy for deformation for the alloy aged 2×10^3 minutes at 923°K.

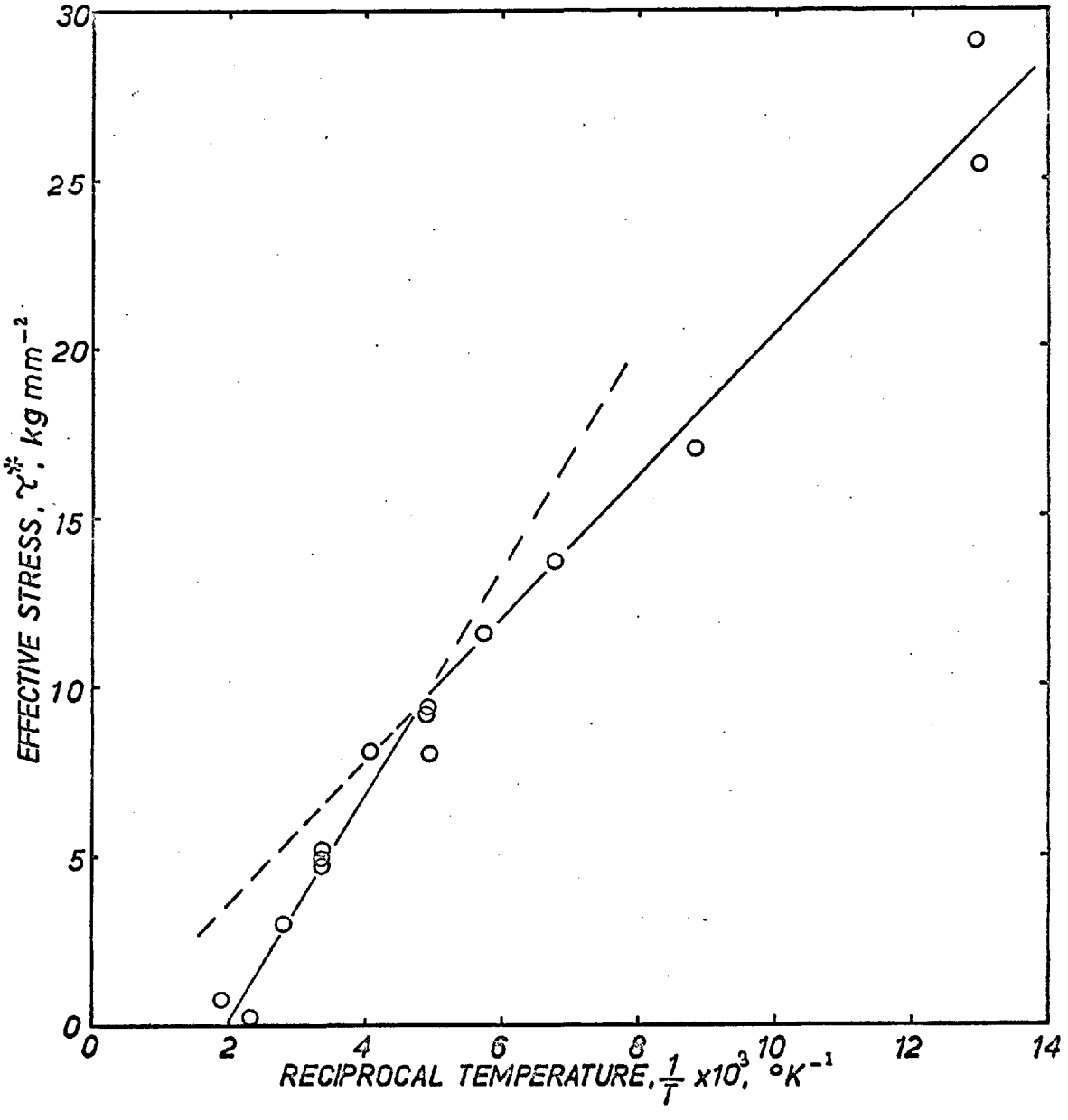

Fig. 5.15.. Effective stress versus reciprocal temperature for the alloy aged 150 minutes at 923°K.

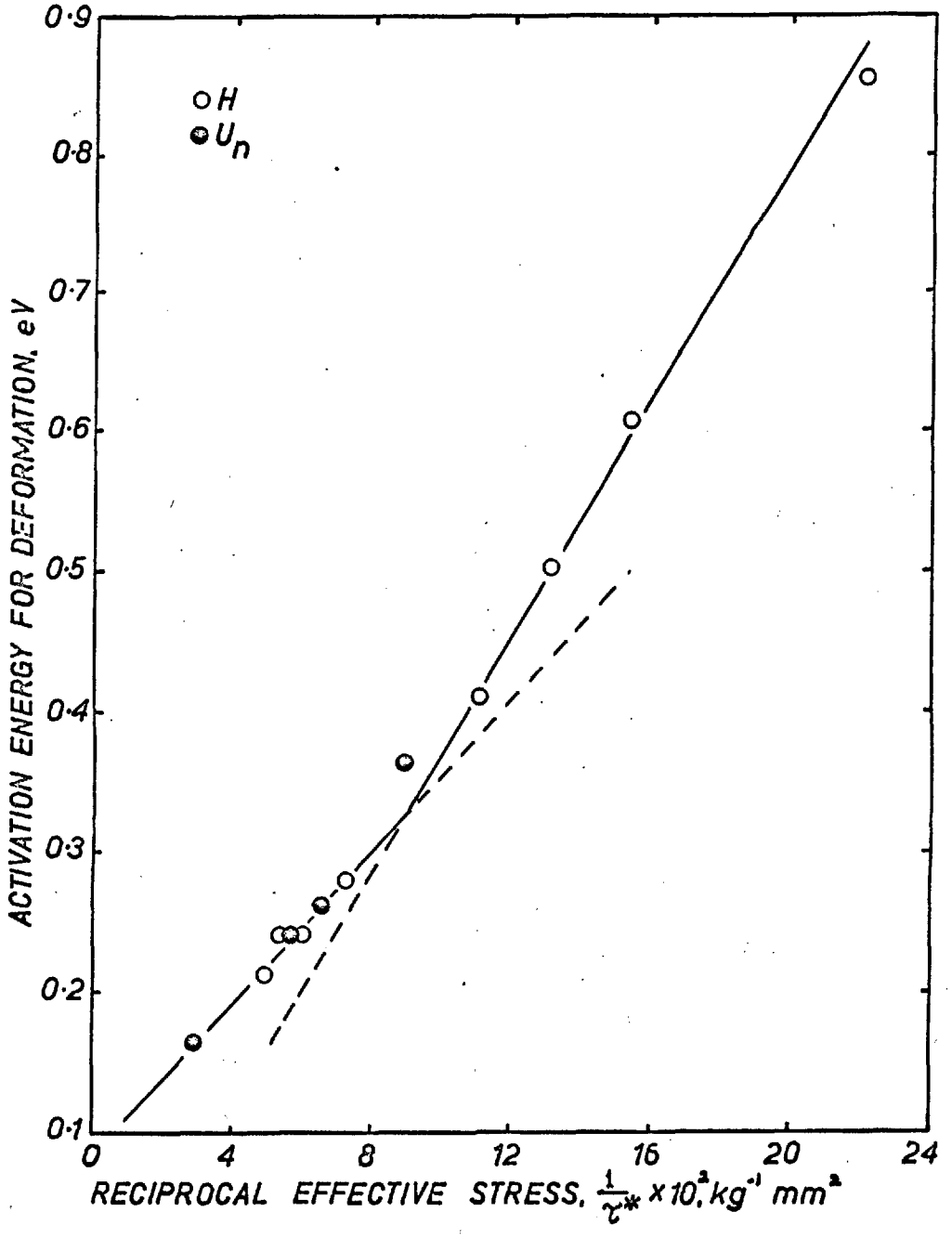

Fig. 5.16. Activation energy for deformation versus reciprocal effective stress for the alloy aged 2×10^3 minutes at 923°K.

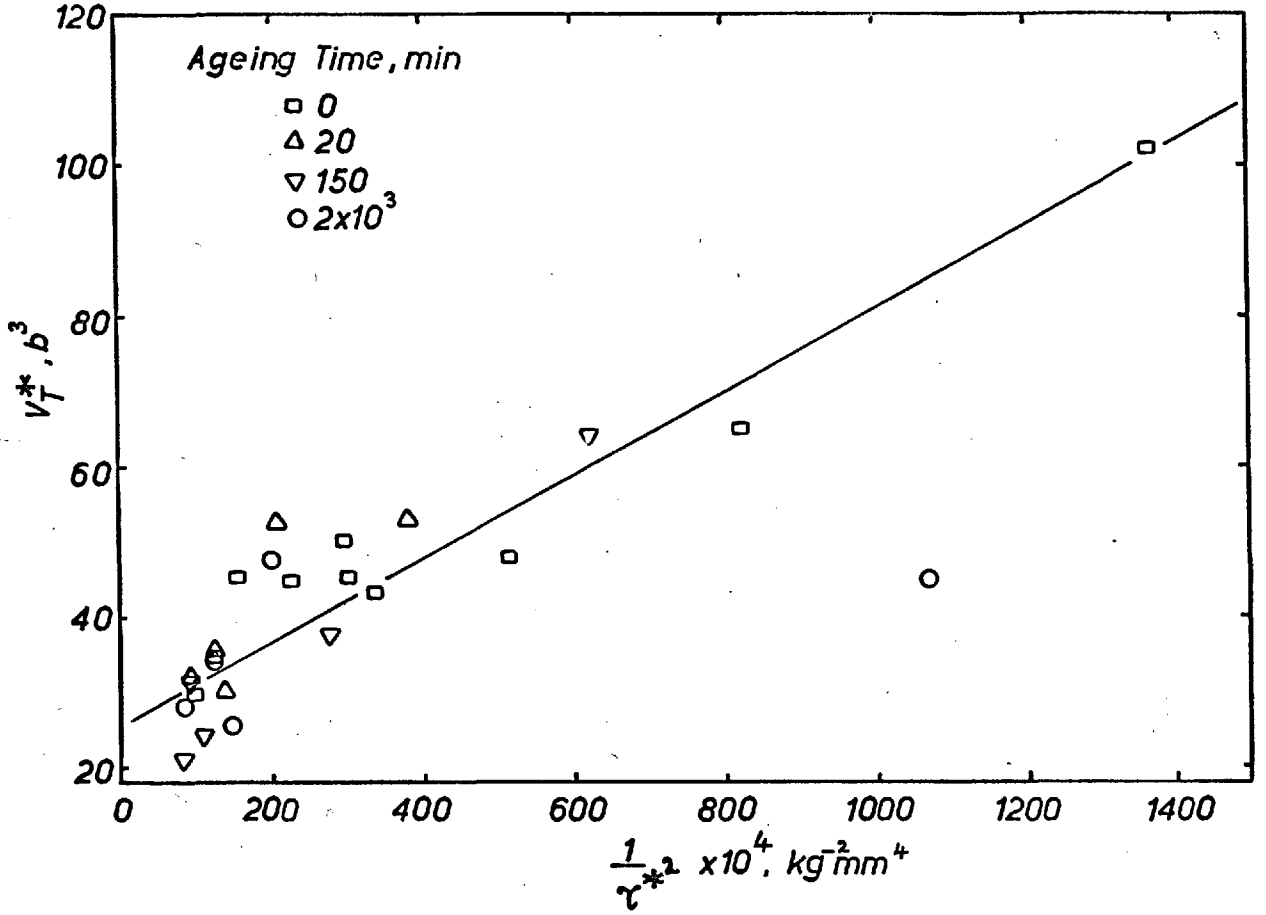

Fig. 5.17. v_T^* versus $\frac{1}{\tau^{*2}}$ for four different heat treated conditions of the alloy.

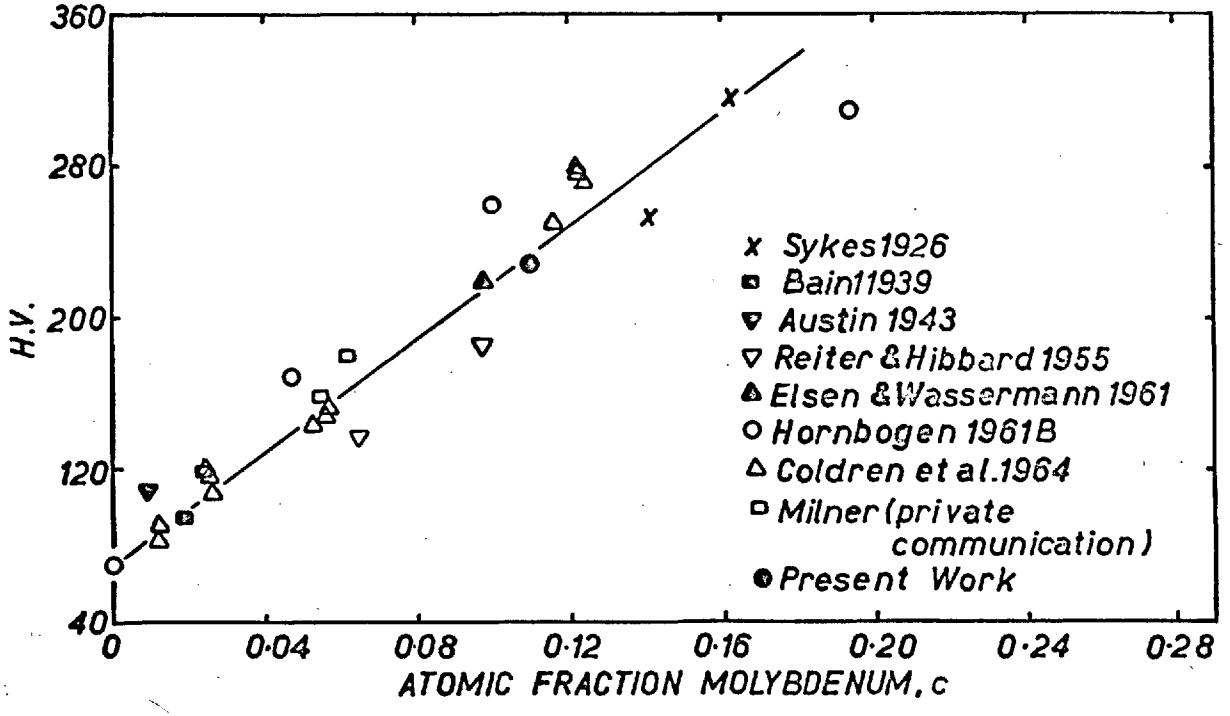

Fig. 5.18. Graph showing a linear relationship between hardness and molybdenum concentration.

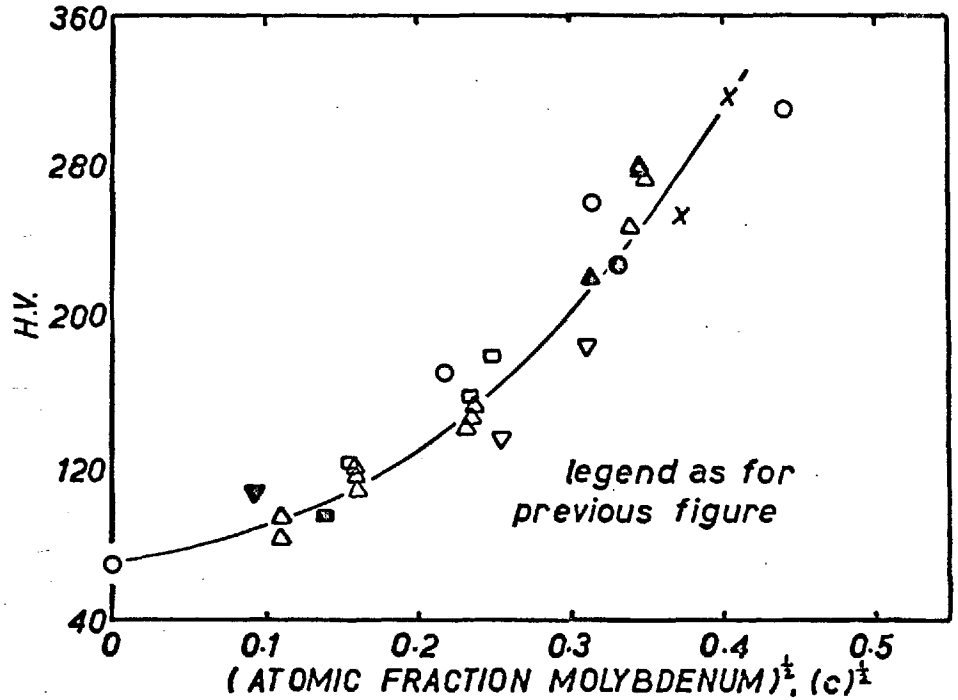

Fig. 5.19. Graph showing a non-linear relationship between hardness and the square root of the molybdenum concentration.

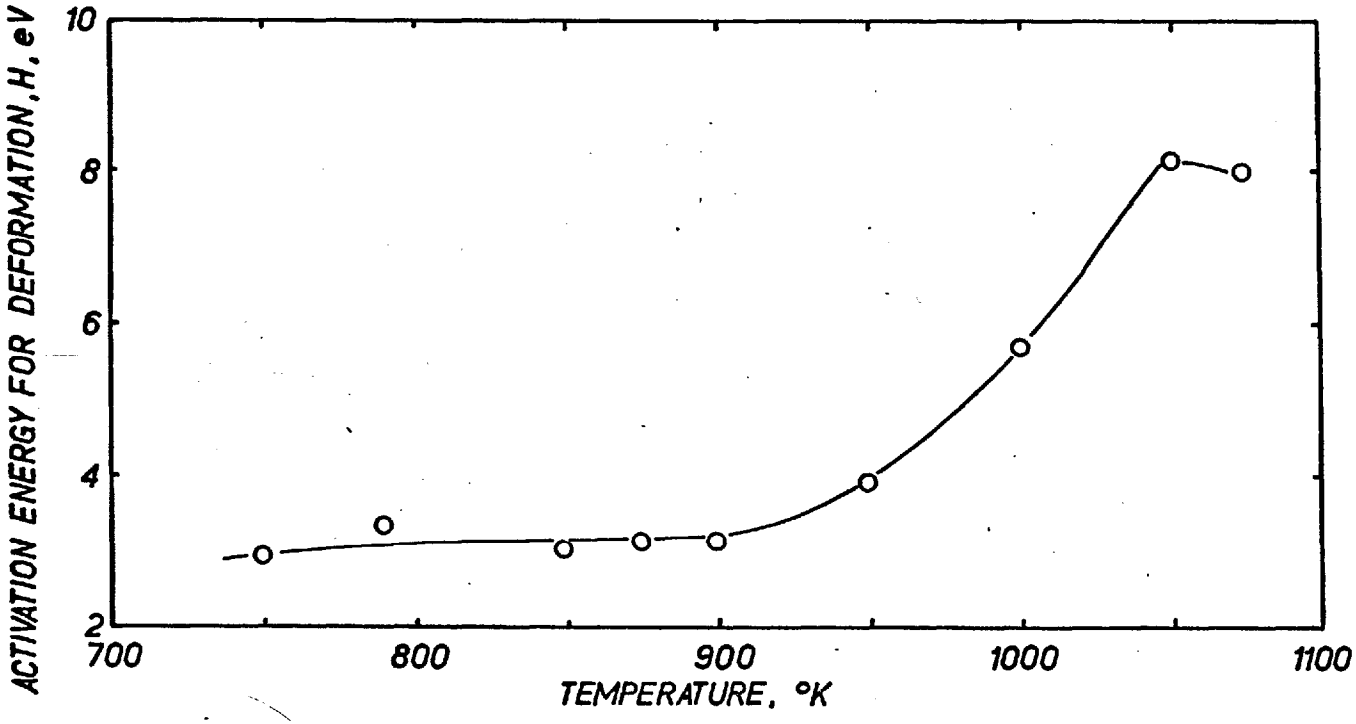

Fig. 5.20. Effect of temperature on the activation energy for deformation.

CHAPTER 6

SUGGESTIONS FOR FURTHER WORK

The object of this investigation was to make a general survey of the ageing characteristics and mechanical properties of the b.c.c. based precipitation hardening system, iron-molybdenum. During the investigation it became evident that there were many topics associated with the present work which, if studied, would produce results of value and interest. These include:

a. An X-ray diffraction and chemical analysis examination of the extracted precipitate phase. This is required to determine whether the λ or ε-phase is precipitated in Fe-11 at.% Mo at normal ageing temperatures.

b. An electron microscopy study of precipitate size and distribution as a function of time and temperature of ageing, coupled with a parallel investigation of the effect of test temperature on precipitate-dislocation and dislocation-dislocation interactions would give information that could be correlated with the mechanical properties data obtained in the present work.

c. It would be of value to know if the trends in the mechanical property parameters as a function of ageing and temperature are general to age-hardening b.c.c. materials. Thus,

similar surveys on an Fe-Mo alloy of different molybdenum concentration and on another binary system, where an intermediate phase is precipitated in a b.c.c. matrix, would be relevant.

d. The deformation of Fe-Mo solid solutions of varying molybdenum content as a function of temperature would confirm whether or not strength inversion takes place for certain molybdenum concentrations. In addition, if this investigation was performed for three carbon concentrations, i.e. normal purity c ≈ 30 ppm, wet hydrogen purified c ≈ 5 ppm and Zr-H purified c ≈ 0.005 ppm information on the topical and controversial role played by carbon in the deformation of b.c.c. materials would be obtained.

e. Solute diffusion is an important factor in precipitation and high temperature deformation phenomena. Unfortunately, very little diffusion data are available for solutes in low carbon iron alloys, including the alloy used in the present work. The chemical diffusion of molybdenum in Fe-Mo solid solutions of varying molybdenum content could be investigated using diffusion couples and the electron probe microanalyser to measure the diffusion profiles. Also, a radio-active isotope of molybdenum, Mo^{99}, is available so the self-diffusion characteristics of molybdenum in these alloys can be determined by a radio-active tracer technique.

f. The creep behaviour of the alloy should be investigated in order that a comprehensive assessment of the mechanical properties may be made. Creep measurements should provide comparative and complementary data to that from compression testing. In particular, it would be of interest to compare the high temperature activation parameters obtained from the two modes of deformation and to study the stability of the precipitate during creep.

ACKNOWLEDGEMENTS

The author wishes to thank his supervisor, Dr. C. W. A. Newey for valuable advice and assistance and Professor J. G. Ball for the provision of research facilities.

Thanks are also due to Mr. N. Ware for assistance given with the Electron-Probe Microanalyser and to Mr. D. C. Phillips, whose apparatus was used for the Young's Modulus measurements.

Finally, the author is indebted to the Science Research Council for a research studentship during the period 1964-1966 and B.I.S.R.A. for a grant-in-aid.

APPENDIX I

Calculation of the Error Involved in a Typical Density Measurement

Source of Error	Absolute Error	Fractional Error
$W_D + W_{DC} = 3.20964$	$\pm 5.0 \times 10^{-5}$	
$W_{DC} = 0.13766$	$\pm 5.0 \times 10^{-5}$	
$\therefore W_D = 3.07198$	$\{(5.0\times10^{-5})^2 + (5.0\times10^{-5})^2\}^{\frac{1}{2}} = \pm 7.1 \times 10^{-5}$	
$W_A = 4.18601$	$\pm 5 \times 10^{-5}$	1.2×10^{-5}
$W_A - W_D = 1.11403$	$\{(7.1\times10^{-5})^2 + (5 \times10^{-5})^2\}^{\frac{1}{2}} = 8.7 \times 10^{-5}$	7.6×10^{-5}
$\frac{W_A}{W_A-W_D} = 3.755$	$\pm 2.9 \times 10^{-4}$	$\{(1.2\times10^{-5})^2 + (7.6\times10^{-5})^2\}^{\frac{1}{2}} = 7.7 \times 10^{-5}$

Assuming there is no error in the density of the standard, then, the error in the evaluation of the density of the dibromo-ethane, ρ_D, will be similar to the error in $\frac{W_A}{W_A-W_D}$. Therefore:

$\rho = \frac{W_A}{W_A-W_D} \rho_D = 8.152$ gm cm^{-3}	$\pm 8.96 \times 10^{-4}$	$\{(7.7\times10^{-5})^2 + (7.7\times10^{-5})^2\}^{\frac{1}{2}} = 1.1 \times 10^{-4}$

W_A and W_D are the weights of the specimen in air and in dibromo-ethane respectively, W_{DC} is the weight of the cradle in dibromo-ethane. ρ is the density of the specimen and ρ_D the density of dibromo-ethane.

APPENDIX II

Calculation of the Error Involved in a Typical Young's Modulus Measurement

Measurement

Source of Error	Absolute Error	Fractional Error
$t = 0.356$	$\pm 5.0 \times 10^{-4}$	1.4×10^{-3}
$\therefore r = \frac{t}{\sqrt{12}} = 1.028$		1.4×10^{-3}
$\ell = 4.950$	$\pm 2.0 \times 10^{-3}$	4.1×10^{-4}
$\therefore (\frac{r}{\ell})^2 = 4.316 \times 10^{-4}$		$(2\left[\{(4.1\times10^{-4})^2 + (1.4\times10^{-3})^2\}^{\frac{1}{2}}\right]^2)^{\frac{1}{2}}$ $= 2.06 \times 10^{-3}$
$T_1 \simeq 1 + 88.12(\frac{r}{\ell})^2 = 1.038$		2.06×10^{-3}
$\frac{\ell}{t} = 1.3904 \times 10^{1}$		$\{(1.4\times10^{-3})^2 + (4.1\times10^{-4})^2\}^{\frac{1}{2}}$ $= 1.45 \times 10^{-3}$
$\therefore (\frac{\ell}{t})^3 = 2.688 \times 10^{3}$		$\{(1.45\times10^{-3})^2+(1.45\times10^{-3})^2$ $+(1.45\times10^{-3})^2\}^{\frac{1}{2}} = 2.52\times10^{-3}$
$b = 0.801$	$\pm 5.0 \times 10^{-4}$	6.2×10^{-4}
$\therefore \frac{1}{b} = 1.248$		6.2×10^{-4}
$W = 11.50796$	$\pm 5.0 \times 10^{-5}$	4.3×10^{-6}
$f = 7.127 \times 10^{3}$	± 3	4.2×10^{-4}
$f^2 = 50.794 \times 10^{6}$		$\{(4.2\times10^{-4})^2+(4.2\times10^{-4})^2\}^{\frac{1}{2}}$ $= 5.9 \times 10^{-4}$
$E=9.467\times10^{-1} (\frac{\ell}{t})^3 \frac{T_1}{b} Wf^2$ $= 19.26 \times 10^{11}$ dynes cm^{-2}		$\{(2.52\times10^{-3})^2+(2.06\times10^{-3})^2$ $+(6.2\times10^{-4})^2+(4.3\times10^{-6})^2$ $+(5.9\times10^{-4})^2\}^{\frac{1}{2}} = 3.3\times10^{-3}$

APPENDIX III

Instrumental Modifications for Compressive Testing at Temperatures up to 1800°C.

J. SCI. INSTRUM., 1967, VOL. 44

Instrumental modifications for compressive testing at temperatures up to 1800 °C

R. T. PASCOE, K. C. RADFORD, R. D. RAWLINGS and C. W. A. NEWEY
Department of Metallurgy, Imperial College, London
MS. received 20th December 1966

Abstract. The three basic designs of compression apparatus which can be used in conjunction with an Instron testing machine are considered and assessed in general terms. The construction and operation of two compression jigs, based on one of these designs, for operation in the temperature ranges −196 °C to 250 °C and room temperature to 1800 °C, respectively, are then described.

1. Introduction

Compression testing is becoming increasingly important as a means of investigating the plastic deformation of materials, particularly of ceramics and other brittle materials. It offers a number of advantages over testing in tension:

(i) More plastic strain can be introduced into a brittle material by compression since, in general, the applied stress inhibits the propagation of cracks.

(ii) Relatively small specimens may be used. This is important for studies of costly materials and of those not available in bulk form. In addition it is a considerable asset for tests at elevated temperatures since the whole specimen is more easily maintained at constant temperature.

(iii) Specimen grips are not required—this is particularly advantageous for tests at high temperatures.

(iv) Specimens are of a simple shape and can be prepared more easily than the common form of tensile specimen.

On the other hand it should be noted that compression testing has one major disadvantage. To prevent buckling of the specimen during deformation its length-to-area ratio must be small. As a consequence the inhomogeneous deformation which occurs at the ends of the specimen, due to friction and imperfect matching of the specimen ends and the compression surfaces, becomes significant. Unless very careful precautions are taken to counter these effects, for example by means of a lubricant at the compression faces, the assumption that the specimen deforms homogeneously does not hold for plastic strains greater than about 10%.

A considerable amount of experience in the design and operation of compression equipment has been built up in recent years but, rather surprisingly, very little of this information has appeared in the literature. It is felt that an appreciation of the various possible basic designs, together with useful technical and operational details of jigs based on these designs, would be of use to new and established workers in this field. To this end, this paper describes the basic types of compression jig which can be used in conjunction with an Instron-type testing machine, and the prime factors which influence the choice of design are considered. A description is then given of two compression jigs, based on one of these designs, which have been developed and operated successfully over a wide range of loads and temperatures.

2. Basic designs of compression apparatus

Straining frames of the Instron type (see figure 1) consist essentially of two coupled beams one of which, the crosshead, is driven at a constant rate relative to the other by means of two lead screws. In its usual tensile form the other beam of the Instron carries the load cell which senses the load applied to the specimen. The machine must be adapted for compression testing and the position of the load cell then depends on

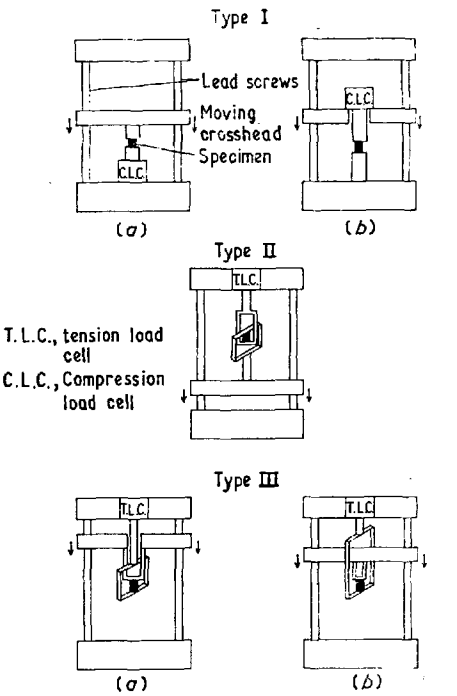

Figure 1.

the form of modification. The Instron is a 'hard' machine, i.e. it has a high elastic stiffness. This is an important feature for most investigations because the higher the elastic stiffness of the machine, the greater is the strain transmitted to the material, and thus the greater is the registered change of load for a given crosshead movement.

The basic designs of compression jig which can be used in a machine of the Instron type are illustrated schematically in figure 1 where the crosshead is considered to move in a downward direction in each case. Designs of type I may be reversed with an upward-moving crosshead and a compression load cell located in the top beam. The main features affecting the choice of design are:

(i) Load capacity.
(ii) Elastic stiffness. In order to obtain maximum sensi-
vity from the load-weighing system of the testing machine
e elastic stiffness of the jig must be comparable with that of
e machine.
(iii) Testing temperature.
(iv) Homogeneity of deformation. To achieve this the
mpression faces must remain accurately parallel to one
nother during a test; this normally requires an alignment
cility on the jig.
(v) Specimen size.
(vi) Ease of introduction and removal of specimens. This
ctor is particularly important for tests at high and low
mperatures.

Each type of jig shown in figure 1 has particular advantages
nd disadvantages and the final choice of design depends on
e relative importance of the above factors to the investi-
ation for which it is constructed. However, the following
eneral comparisons can be made.
Designs of type I can be expected to have the greatest
astic stiffness and load capacity but their alignment facilities
re unsatisfactory. They are difficult to use for low tempera-
re tests and considerable problems are encountered in testing
t elevated temperatures. In the latter case two-part furnaces
at split in the vertical plane have been used with some
ccess (Hulse and Copley 1966).
Jigs of type II can be fitted with effective alignment systems
ratt 1951 Dissertation, University of Cambridge, Newey
959 Thesis, University of Birmingham) but the design is not
itable for modification for operation below room tempera-
re or above about 500 °C.
Jigs of type III are the compression equivalents of the
olanyi tensile jig (see Schmid and Boas 1950). Alignment
cilities can be fitted and these jigs are particularly useful
r tests at low temperatures because they can be immersed
controlled temperature baths.
For the present deformation studies (on the intermediate
hases NiAl and Ni_3Al, Fe–Mo alloys and spinel, $MgAl_2O_4$)
compression apparatus was required that would deform
latively small specimens at temperatures between −196 and
800 °C; homogeneity of deformation was of considerable
portance. It was considered that a jig of type III would fit
ese primary requirements and offer the best combination of
e remaining factors outlined above. As a result, two jigs
ased on this design have been developed, one for use between
om temperature and 1800 °C and the other for the range
196 to 300 °C. Both have a designed load capacity of
000 kg.

. High temperature compression jig

The jig consists of two interpenetrating stainless-steel cages;
e upper cage is bolted to the underside of the Instron cross-
ead and the lower cage hangs, via a connecting rod which
asses through the crosshead, from a tension load cell in the
pper beam of the straining frame (figures 2 and 3). Each
age has upper and lower plates separated by three radially
sposed vertical rods. The compression rams are attached
the lower plates of each cage; details of the design and pre-
aration of the compression rams and of the various ram
aterials used are discussed later. A downward movement
f the crosshead, and hence of the upper cage and ram,
pplies a compressive load to the specimen; this load is
ansmitted to the load cell as a tensile load via the lower ram
nd lower cage.

Accurate alignment of the jig is achieved by precision machining and construction of the jig components; by careful preparation of the ends of the rams; and by means of a series of adjustable roller bearings housed on the lower plate of the upper cage and the top plate of the lower cage—the greater the

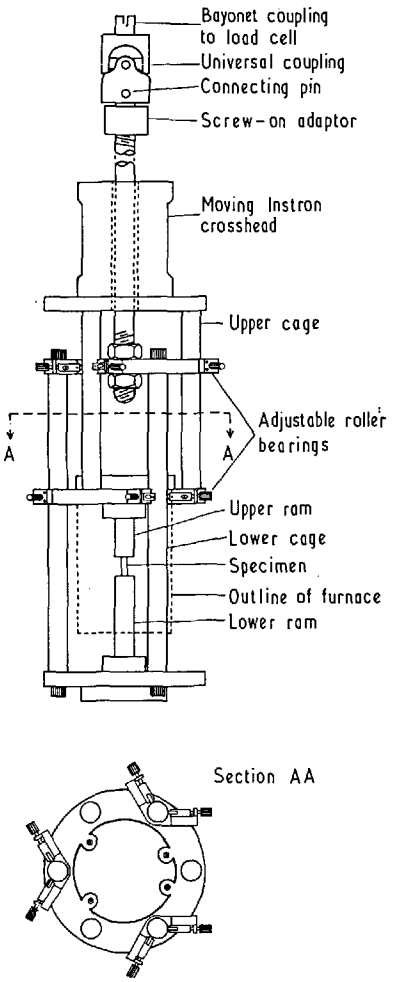

Figure 2.

distance between the two sets of bearings the better is the alignment between the two frames. A pair of roller bearings on one cage locates on one of the three vertical rods of the other cage (see figure 2). This particular arrangement of the bearings prevents any lateral or twisting motion of the two cages relative to one another during straining.

The elastic stiffness of the jig, as measured by compressing the rams together, was $7{\cdot}0 \times 10^{-4}$ mm kg^{-1} up to 500 kg load with alumina rams at room temperature.

One of the main features of this design is that the furnace can be incorporated within the lower cage. Consequently, this jig has a considerable advantage over other types of compression arrangement, since with an efficiently cooled furnace the only load bearing members of the jig exposed to elevated temperatures are the rams, and these can be constructed of any suitable metallic or ceramic materials. Further advantages are gained from the fact that the furnace is attached to the upper cage of the jig. Thus, the load-weighing system is unaffected by the furnace and its accessories, and

any problems arising from heat convection are avoided. In addition this facilitates the rapid changing of specimens because the furnace and top compression cage can be raised,

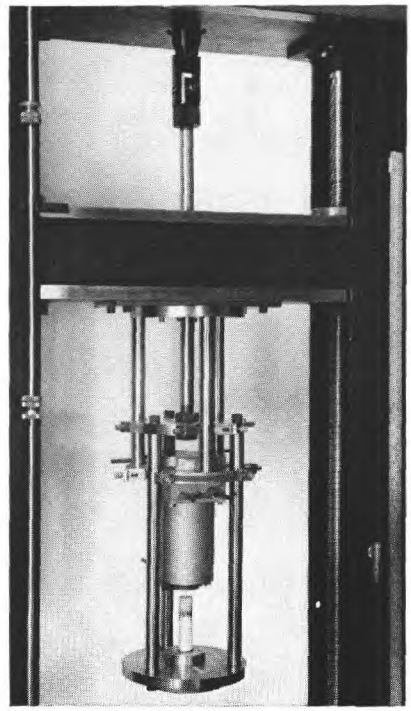

Figure 3.

using a fast crosshead speed, until the specimen is exposed standing on the lower ram; the specimen having been changed, the cage and furnace can be lowered until the top ram makes contact with the specimen, as indicated by a load being registered on the recorder.

The overall width of the compression frame was chosen to give a reasonale compromise between the elastic stiffness of the jig and the thermal capacity of the furnace. The length of the jig was determined by the working distance required for th introduction and removal of specimens.

Three furnaces which have been designed and operate successfully are illustrated in section in figures 4, 5 and Furnace I has a double wound Nichrome heating elemen with fewer windings near the centre of the work tube t minimize temperature gradients in the furnace; it has wate cooled brass end-plates and is insulated thermally wit vermiculite. The furnace is used for tests at temperatur up to 1000 °C. Three methods have proved successful fo carrying out tests in atmospheres other than air. A conti uous stream of argon, with a small gap between the bottom the furnace and the stem of the lower ram, works sati factorily. With a static atmosphere the gap between th furnace and the lower plate of the jig can be sealed with plastic tube or a flexible copper bellows. The latter is mor successful but its use depends on the importance of th contribution of the load required to compress the bellows t the overall applied load. A modification to the internal ga seals of the furnace would allow tests to be made in vacuu using these bellows.

Furnace II incorporates a specially designed Crusilite heatin element in a water-cooled shell. It is very convenient for test up to 1575 °C because, unlike furnace III, it is not affecte by rapid heating and cooling cycles. In addition the heatin element can be replaced very easily. However, the temper ture gradients in the furnace are rather severe because th heated zone of the element is only 2 cm long; the gradie over a typical specimen length (7·5 mm) was measured a 20 degC at 1300 °C. In comparison the gradient in furnace I wa only 2 degC over 7·5 mm at 750 °C using a pyrophyllite ran

Furnace III has a heating element of 0·85 mm diamete molybdenum wire wound on an alumina work tube an protected by a forming gas (25% H_2–75% N_2) atmospher The furnace casing is again a water-cooled shell. Thi furnace operates successfully for long periods at temperature up to 1800 °C; when not in use during a prolonged series o experiments it is maintained at 1100 °C. For tests at tempera tures above about 1300 °C additional cooling of the jig i necessary. This is achieved by water cooling the plates o the frame that are in contact with the compression ram (see figure 2). The measured gradient was 10 degC ove 7·5 mm at 1500 °C.

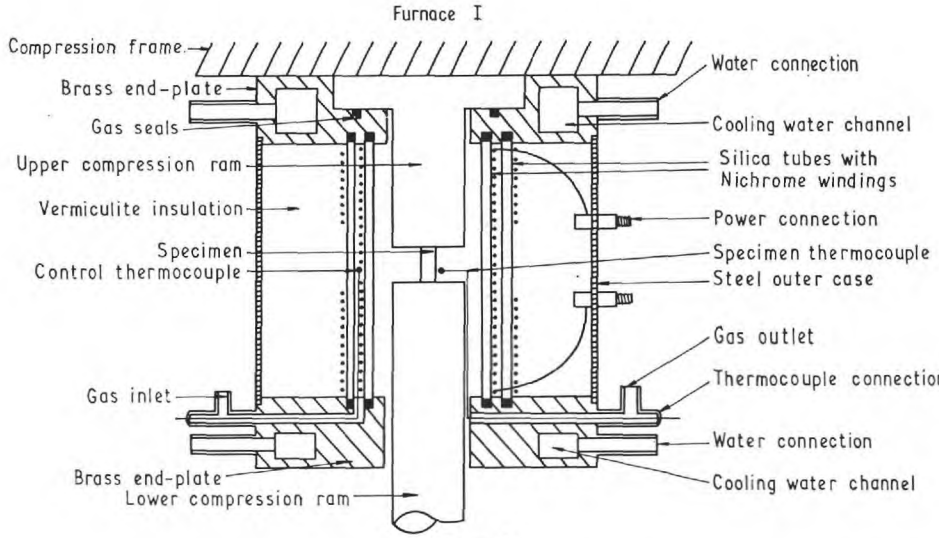

Figure 4.

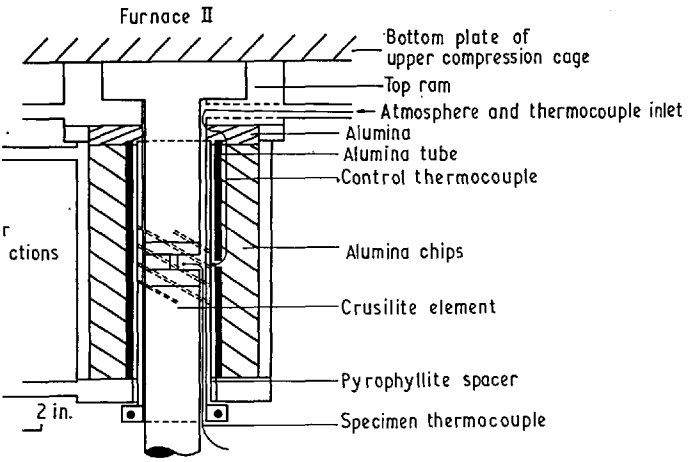

Figure 5.

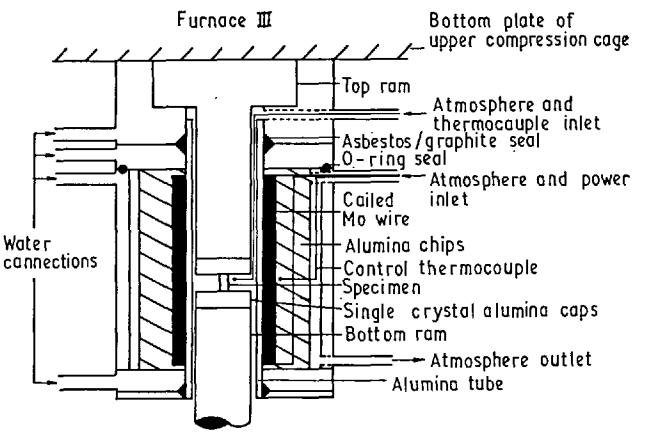

Figure 6.

Low temperature jig

The low temperature jig (figure 7) is based on the same nciples of two interpenetrating frames as is the high mperature jig, but it differs in other aspects of design.

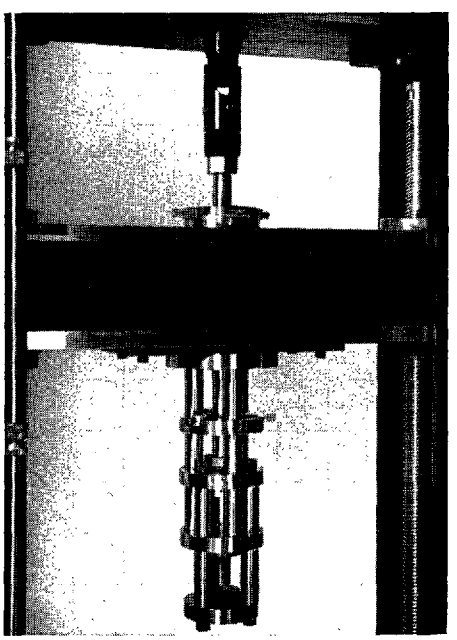

Figure 7.

The jig was designed to fit into a Dewar flask containing uid coolants for tests below room temperature or into a ntrolled temperature oil bath for use up to 300 °C. This eans that, unlike the high temperature jig, parts of the frame her than the rams are at the testing temperature. Thus the was built with a smaller overall diameter to reduce its ermal mass and to enable it to be fitted into a Dewar flask convenient size. This reduction in diameter increases the astic stiffness to 5 $\times$ 10^{-4} mm kg^{-1} for loads of up to 500 kg room temperature.

To avoid 'icing-up' of the roller bearings during low temrature deformation the two plates holding bearings are tuated as far as possible from the bottom of the jig whilst ing sufficiently widely spaced to ensure that accurate alignment and stability is achieved. The upper set of bearings is housed on a plate bolted to the top face of the crosshead; the bearings locate on the load cell connecting rod. The other bearing plate is attached to the upper cage and the bearings locate on the connecting rod. This arrangement has proved to be satisfactory, but it is thought that even better stability could be achieved if the lower bearing plate were attached to the connecting rod with the roller bearing making contact with the vertical rods of the upper cage. As an added precaution against icing-up a stream of warm air is passed over the lower bearing housing during low temperature tests.

5. Compression rams

The compression rams are the only stressed members to be heated and being very simple in design and construction they can be interchanged readily or, if necessary, easily removed to regrind the compression faces.

The ideal ram material is one which does not itself undergo plastic deformation during compression or react chemically with the specimen or testing atmosphere. In addition, using short furnaces at elevated temperatures, materials of low thermal conductivity are desirable in order to reduce heat losses and temperature gradients. Materials which have been used successfully are listed in the table.

Most of the tests above 1000 °C have been performed on spinel single crystals which cause significant indentation of the alumina rams at all temperatures. This problem was largely overcome by using $\frac{1}{4}$ in. thick spacers of single crystal spinel between the rams and the specimen. This technique of using spacers of the same material as the specimen is possible because of the constraint offered by the bulk of the spacer to deformation. It can be shown by slip line field theory that about three times the yield stress is required before plastic indentation of the spacers occurs (see, for example, Dieter 1961). For certain specimens, the alumina rams were capped with slices of single crystal α-alumina orientated so that the basal planes (the primary slip planes) were perpendicular to the compression axis. These caps proved very effective and no indentation of the alumina was observed.

Each ram consists of a long stem which fits inside the furnace and is attached to a flange fixed to the compression cage. Various methods are used to join the flange and stem; some rams are machined as an integral unit whilst others have a screw thread cut into the base of the stem and the two components are bolted together. Whilst the former arrangement gives a better gas seal between the flange and stem, the latter

Ram materials

Material	Hardness at 20 °C	Useful temperature range (degC)	Limitations
Nonvar tool steel	650 VPN	−196–100	tempering temperature 100 °C
Nimonic 80A	230–250 VPN	20–500	high thermal conductivity; loss of strength and oxidation resistance at higher temperatures
Nimonic 115	450–500 VPN	−196–500	high thermal conductivity although strength maintained to 1000 °C
Pyrophyllite (Al_2O_3: SiO_2) fired to 1050 °C	6 MOH	20–700	is prone to creep under small loads at 800 °C
Sintox (95% Al_2O_3)	9 MOH	400–1000	high thermal conductivity
Dense recrystallized alumina (99% Al_2O_3) fired to 1850 °C	9 MOH	800–1800	best for high temperatures; comparatively poor thermal shock resistance, requiring slow removal from the furnace; softer than spinel—requires end caps
Refrax (silicon carbide bonded with silicon nitride)	8 MOH	800–1500	poor surface finish; high thermal conductivity, reacts with spinel

method is more commonly used because it is more economical on material. Furthermore, large cross sections of pyrophyllite are very prone to cracking on firing. Alumina rams are cylindrical in shape, pass through a stainless-steel annulus (the flange) and abut against the jig plate; each ram is held in position by grub screws in the annulus. The top and bottom faces of each ram are made accurately flat and parallel by precision grinding, or by cutting with a diamond impregnated slitting wheel in the case of the alumina rams.

Rams for the low temperature modification are of a slightly different form to allow the specimen to be placed as far below the surface of the liquid bath as possible; the lower ram has no stem and the flange attached to the lower cage acts as the anvil.

Acknowledgments

The authors wish to thank Professor J. G. Ball for the provision of research facilities at Imperial College, t Science Research Council for a grant for Special Research, a the British Iron and Steel Research Association and t Ministry of Aviation for financial support during the peri of the work. Two of the authors (K.C.R. and R.D.R.) a indebted to the Science Research Council for Resear Studentships.

References

DIETER, G. E., 1961, *Mechanical Metallurgy* (New Yor McGraw Hill).

HULSE, C. O., and COPLEY, S. M., 1966, *Bull. Amer. Cera Soc.*, **45**, 530–4.

SCHMID, E., and BOAS, W., 1950 *Plasticity of Crystals* (Londo F. A. Hughes).

APPENDIX IV

The Plastic Deformation of Iron-11 At.% Molybdenum Solid Solution Alloy

Reprinted from Acta Metallurgica, Vol. 15, No. 2, 1967, pp. 440–443. Pergamon Press Ltd, Printed in Northern Ireland

The plastic deformation of iron–11 at.% molybdenum solid solution alloy*

The plastic deformation of an iron–11 at.% molybdenum solid solution has been investigated as a preliminary to a study of the effects of precipitation on the mechanical properties of this alloy.

The alloy was produced from deoxidised electrolytic iron and Murex sintered molybdenum. Analysis for minor constituents gave: C 0.003; Si 0.002; S 0.005; P < 0.002; O_2 0.0098 wt.%. The material, in the form of $\frac{1}{4}$ in. dia. swaged rod, was solution treated at 1300°C for 1 hr and quenched in iced water. Compression specimens of nominal size 2.5 × 2.5 × 6.0 mm were cut longitudinally from the rod. Yield and flow data were obtained using an Instron testing machine adapted for compression testing by means of jigs attached to the underside of the crosshead beam.[1] Change of strain rate tests and tests performed at shear strain rates, $\dot{\gamma}$, 7.14×10^{-5}, 1.43×10^{-4} and 1.43×10^{-3} sec^{-1} were carried out over a considerable temperature range.

The increase in the shear flow stress, $\Delta\tau$, produced by an increment in strain rate was fairly constant above about 240°K, but it increased slightly with stress below this temperature (Fig. 1). Activation volumes,[2] v^*, were calculated from the average value of $\Delta\tau$ obtained during a test and also from the yield stress data for the different strain rates. In Fig. 2 these activation volumes are plotted against the thermally activated component of the flow stress, τ^*. The small value of the activation volumes obtained for deformation at the lower temperatures, i.e. the region in which τ^* is high in Fig. 2, indicated that the rate-controlling mechanism at these temperatures was the overcoming of the Peierls' barrier. It was of interest, therefore, to apply these results to Dorn and Rajnak's theory[3] for the Peierls' mechanism.

According to Dorn and Rajnak the thermal component of the flow stress for the Peierls' process is given by

$$\frac{\tau^*}{\tau_p^*} = f_1\left(\frac{u_n}{2u_k}\right) \simeq f_1\left(\frac{T}{T_c}\right) \qquad (1)$$

where τ_p^* is the Peierls' stress, u_n is the activation energy for nucleating a pair of kinks, u_k is the energy of an isolated kink, T is the test temperature; T_c is the critical temperature defined by

$$\dot{\gamma} = \frac{\rho a b \nu L}{w} \exp\left(-\frac{2u_k}{kT_c}\right) \qquad (2)$$

where ρ is the dislocation density, a is the distance between adjacent Peierls' valleys, ν is the Debye frequency, L is the length swept out by a pair of kinks, w is the length of the embryonic pair of kinks, b is the Burgers' vector and k is Boltzmann's constant. Extrapolation of the graph of log yield stress against temperature gave a value of 49 kg . mm^{-2} for τ_p^*. Using this value of τ_p^*, together with the measured values of τ^* and T, and ignoring the change of τ_p^* with temperature, the low temperature data for the three strain rates employed were fitted to the universal T/T_c versus τ^*/τ_p^* curves by the appropriate choice of critical temperatures. A good fit with the theory of Dorn and Rajnak, with the perturbation factor $\alpha = +1$, was obtained below 170°K using critical temperatures of 255, 265 and 290°K for strain rates 7.14×10^{-5}, 1.43×10^{-4} and 1.43×10^{-3} sec^{-1} respectively. The results corresponding to temperatures greater than 170°K deviated considerably from the theoretical curve, thus suggesting that the Peierls' mechanism was no longer rate-controlling (Fig. 3).

Using equation (2), the energy of an isolated kink, u_k, is given by

$$u_k = k \ln\left(\frac{\dot{\gamma}_1}{\dot{\gamma}_2}\right) \Big/ 2\left(\frac{1}{T_{c2}} - \frac{1}{T_{c1}}\right) \qquad (3)$$

The substitutions $\dot{\gamma}_1 = 1.43 \times 10^{-3}$ sec^{-1}, $T_{c1} = 290$°K with $\dot{\gamma}_2 = 7.14 \times 10^{-5}$ sec^{-1} and $T_{c2} = 255$°K, and with $\dot{\gamma}_2 = 1.43 \times 10^{-4}$ sec^{-1} and $T_{c2} = 265$°K were made and the resulting average value for u_k was 0.29 eV; this is the same as that obtained for an Fe–2% Mn solid solution by Wynblatt *et al.*[4] The results for strain rates of 7.14×10^{-5} and 1.43×10^{-4} sec^{-1} were not coupled together as, due to the small difference in critical temperatures in this case, a small error in these would lead to a large error in the calculated value of u_k.

Values of $\tau_p^* v^*/2u_k$ were calculated using activation volumes from the yield stress curves and from the change of strain rate tests. The values so obtained plotted against τ^*/τ_p^* fitted the theoretical curve for temperatures below about 170°K (Fig. 4). Similarly, values of u_k, calculated from equation (1), are in good agreement with the theoretical values at low temperatures (Fig. 5).

The energies of activation for deformation, H, over the temperature range studied were evaluated from[2]

$$H = -v^* T \left(\frac{\delta\tau}{\delta T}\right)_{\dot{\gamma}} \qquad (4)$$

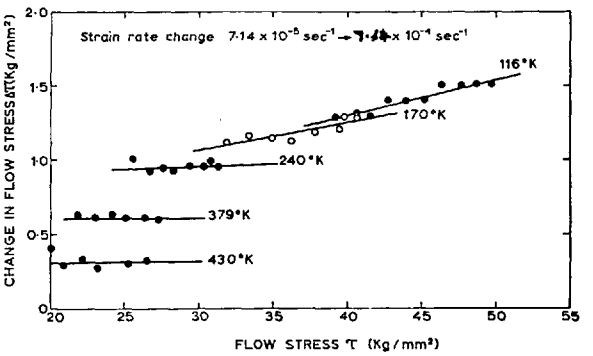

FIG. 1. Effect of temperature on the change of flow stress produced by an increment in strain rate versus flow stress.

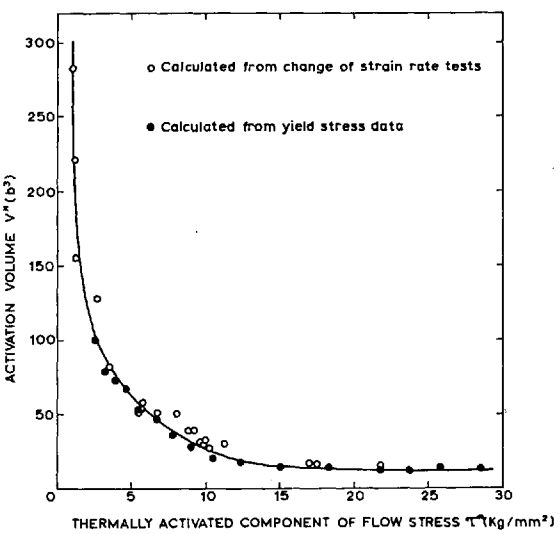

FIG. 2. Activation volume versus the thermally activated component of the flow stress.

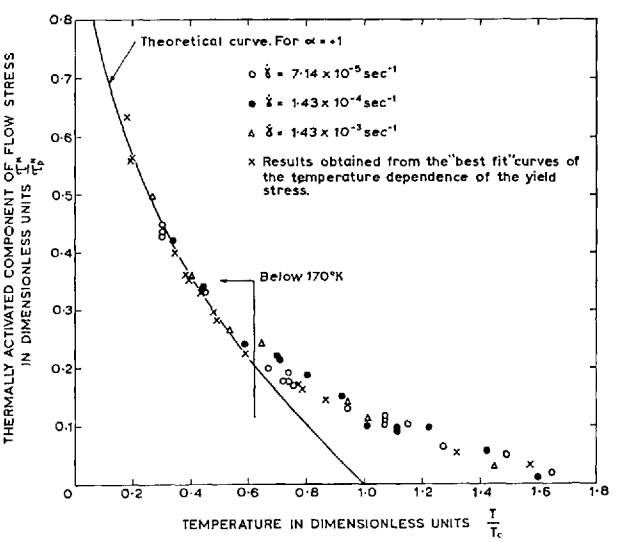

FIG. 3. Thermally activated component of the flow stress in dimensionless units versus temperature in dimensionless units.

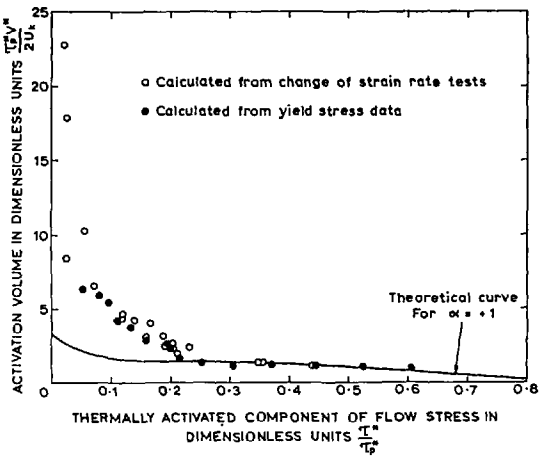

FIG. 4. Activation volume in dimensionless units versus thermally activated component of flow stress in dimensionless units.

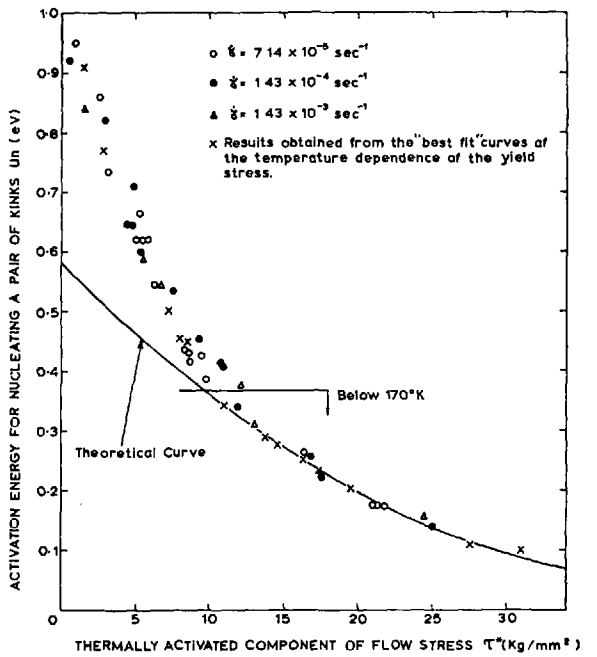

FIG. 5. Activation energy for nucleating a pair of kinks versus thermally activated component of flow stress.

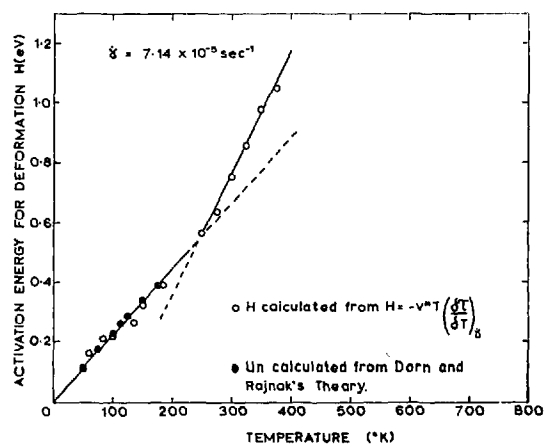

FIG. 6. Effect of temperature on the activation energy for deformation.

which is obtained by ignoring the temperature dependence of the shear modulus. H and also the low temperature values of u_n—the activation energy for the deformation in the Peierls' region—are plotted against temperature in Fig. 6 for a strain rate of 7.14×10^{-5} sec^{-1}. The graph consists of two distinct regions; a low temperature linear region, and a higher temperature region of greater slope in which a process or processes other than the Peierls' mechanism are operative. As found by other workers[5,6] the slope of the low temperature region gives a value of 26–27 for $(\ln A - \ln \dot{\gamma})$ where A is defined thus

$$\dot{\gamma} = A \exp\left(-\frac{H}{kT}\right) \tag{5}$$

For the Peierls' process[3]

$$\dot{\gamma} = \frac{\rho a b \nu L}{w} \exp\left(-\frac{u_n}{kT}\right) \tag{6}$$

Hence $A = (\rho a b \nu L)/w = 2.1 \times 10^7$ sec^{-1} and putting $w = 16b$, i.e. assuming $v^* = wb^2$, and $v = 10^{13}$ sec^{-1} a value of 1.4×10^3 cm^{-1} is obtained for ρL, which is of the expected order of magnitude.

Values of

$$\frac{2u_k\pi}{a\Gamma_0} \Big/ \left(\frac{\tau_p{}^* ab}{\pi\Gamma_0}\right)^{1/2}$$

where Γ_0 is the line energy of a dislocation, have been calculated as a function of α by Dorn and Mitchell.[7] For $\alpha = +1$ the function is equal to 5.75. Using this value the line energy was calculated to be 2.8×10^8 eV cm^{-1}. The generally accepted equation, which is derived from a formula due to Mott and Nabarro,[8] for Γ_0 is

$$\Gamma_0 \simeq 0.5\,\mu b^2 \tag{7}$$

where μ is the shear modulus; this gives a similar value for Γ_0 to that calculated above.

To summarise, the temperature dependence of the yield stress below about 170°K of an Fe–Mo solid solution can be interpreted satisfactorily in terms of Dorn and Rajnak's theory for the Peierls' mechanism.

The authors would like to thank the B.I.S.R.A. for providing a grant-in-aid for this research programme.

R. D. Rawlings
C. W. A. Newey

Department of Metallurgy
Imperial College
South Kensington
London, S.W.7

References

1. R. T. Pascoe, K. C. Radford, R. D. Rawlings and C. W. A. Newey (to be published).
2. H. Conrad, *J. Metals* **16**, 582 (1964).
3. J. E. Dorn and S. Rajnak, *Trans. Am. Inst. Min. metall. Engrs* **230**, 1052 (1964).
   P. Wynblatt, A. Rosen and J. E. Dorn, *Trans. Am. Inst.*
4. *Min. metall. Engrs* **233**, 651 (1965).
   Z. S. Basinski and J. W. Christian, *Aust. J. Phys.* **13**,
5. 299 (1960).
   J. W. Christian and B. C. Masters, *Proc. R. Soc.* **A281**,
6. 223 (1964).
7. J. E. Dorn and J. B. Mitchell, University of California Report, UCRL-11418 (1964).
8. N. F. Mott and F. R. N. Nabarro, *Bristol Conference on Strength of Solids* 1947. The Physical Society, London (1948).

* Received April 23, 1966.

REFERENCES

Abrahamson E. P. and Lopata S. L.; (1966) T.A.I.M.E. 236 76.

Arnfelt H. and Westgren A.; (1935) Jernkontorets Ann. 119 185.

Austin C. R.; (1943) T.A.S.M. 31 321.

Bain E. C.; (1939) Function of the Alloying Elements in Steel, A.S.M.

Basinski Z. S. and Christian J. W.; (1959) Aust. J. Phys. 13 299.

Bechtoldt C. J. and Vacher H. C.; (1957) J. Res. N.B.S. 58 7.

Bergman G. and Shoemaker D. P.; (1954) Acta Cryst. 7 857.

Byrne J. G., Fine M. E. and Kelly A.; (1961) Phil. Mag. 6 1119.

Cahn J. W.; (1957) Acta Met. 5 169.

Christian J. W. and Masters B. C.; (1964) Proc. Roy. Soc. A281 223.

Cleaves H. E. and Thompson J. G.; (1936) J. Res. N.B.S. 16 105.

Cleaves H. E. and Heigel J. M.; (1942) J. Res. N.B.S. 28 263.

Coldren A. P., Semchyshen M. and Scholz W. G.; (1964) T.A.I.M.E. 230 1236.

Conrad H. and Wiedersich H.; (1960) Acta Met. 8 128.

Conrad H.; (1961) J.I.S.I. 198 364.

Conrad H., Stone G. and Janowski K.; (1965) T.A.I.M.E. 233 889.

Corderoy D. J. H.; (1962) Acta Met. 11 1043.

Cottrell A. H. and Bilby B. A.; (1949) Proc. Phys. Soc. A62 49.

Davies R. G. and Ku R. C.; (1966) T.A.I.M.E. 236 1619.

Dorn J. E. and Rajnak S.; (1964) T.A.I.M.E. 230 1052.

Dorn J. E. and Mitchell J. B.; (1964) University of California Report UCRL-11418.

Dorn J. E., Wynblatt P. and Rosen A.; (1965A) T.A.I.M.E. 233 651.

Dorn J. E. and Wynblatt P.; (1965B) University of California Report UCRL-16601.

Dudzinski N., Murray J. R., Mott B. W. and Chalmers B.; (1948) J.I.M. 74 291.

Dudzinski N.; (1952) J.I.M. 81 49.

Edwards C. A., Phillips D. L. and Jones H. N.; (1940) J.I.S.I. 142 199.

Elsen G. and Wassermann G.; (1961) Z. Metallk. 52 263.

Escaig B.; (1966) Proc. La Physique des Dislocations Toulouse.

Farrell K. and Evans P. R. V.; (1965) J. Less-Common Met. 8 222.

Felberbauer F., Lautenschlager E. P. and Brittain J. O.; (1964) 230 1596.

Fisher J. C., Hart E. W. and Pry R. H.; (1953) Acta Met. 1 336.

Fleischer R. L. and Hibbard W. R.; (1963) The Relation between Structure and Mechanical Properties of Metals H.M.S.O. 262.

Foreman A. J., Jaswon M. A. and Wood J. K.; (1951) Proc. Phys. Soc. A64 156.

Forster F.; (1937) Z. Metallk. 29 109.

Garofalo F.; (1965) Fundamentals of Creep and Creep-Rupture in Metals, MacMillan New York 99.

Gensamer M.; (1946) T.A.S.M. 36 30.

Griffith A. A.; (1920) Phil. Trans. Roy. Soc. A221 163.

Guard R. W.; (1961) Acta Met. 7 163.

Guinier A. Z.; (1952) Electrochem. 56 468.

Guyot P. and Dorn J. E.; (1966) University of California Report UCRL-16992.

Hahn G. T.; (1962) Acta Met. 10 727.

Hahn G. T., Gilbert A. and Reid C. N.; (1963) Symposium on Role of Substructure on Mechanical Behaviour of Metals, ASD. TDR-63-324.

Ham F. S.; (1958) J. Phys. Chem. Sol. 6 335.

Ham F. S.; (1959) J.A.P. 30 915.

Hansen M.; (1958) The Constitution of Binary Alloys, McGraw-Hill New York 668.

Harper S.; (1951) Phys. Rev. 83 709.

Hart E. W.; (1953) Relation of Properties to Microstructure A.S.M. 95.

Hart E. W. and Hibbard W. R.; (1955) T.A.I.M.E. 203 200.

Holl H. A.; (1965) J.I.M. 93 364.

Hollomon J. H.; (1945) Met. Tech. 12.

Hollomon J. H. and Lubahn J. D.; (1947) Gen. Electric Rev. Feb. 28.

Hornbogen E.; (1961A) T.A.I.M.E. 221 711.

Hornbogen E.; (1961B) Z. Metallk. 52 47.

Ishida Y., Cheng C-Y and Dorn J. E.; (1966) T.A.I.M.E. 236 964.

Johnston W. G.; (1962) J.A.P. 33 2716.

Johnston W. G. and Stein D. F.; (1963) Acta Met. 11 317.

Jones M. P., Gavrilovic J. and Beaven C. H. J.; (1966) T.I.M.M. 75 274.

Kelly A.; (1958) Phil. Mag. 3 1472.

Koster W.; (1948) Z. Metallk. 39 145.

Landon P. R., Lytton J. L., Shepard L. A. and Dorn J. E.; (1959) T.A.S.M. 51 900.

Lankes J. C. and Wassermann G. Z.; (1950) Z. Metallk. 41 381.

Lenhart R.; (1955) W.A.D.C. Technical Report 55.

Lifshitz I. M. and Slezov V. V.; (1958) J.E.T.P. 35 479.

Lifshitz I. M. and Slezov V. V.; (1961) J. Phys. Chem. Solids 19 35.

Maiden C. J.; (1959) Acta Met. 7 297.

McLean D.; (1962) Mechanical Properties of Metals Wiley and Sons London 249.

Michalak J. T.; (1965) Acta Met. 13 213.

Mokrov A. P.; (1964) Fiz. Met. Metalloved 17 285.

Mott N. F. and Nabarro F. R. N.; (1948) Phys. Soc. Conference on Strength of Solids 1.

Mott N. F.; (1952) Imperfections in Nearly Perfect Crystals Wiley and Sons New York 173.

Nicholson R. B. and Lorimer G. W.; (1966) Acta Met. 14 1009.

Nunes J.; (1966) J.I.S.I. 204 371.

Oriani R. A.; (1964) Acta Met. 12 1399.

Orowan E.; (1948) Institute of Metals, Symposium on Internal Stresses in Metals and Alloys 451.

Pascoe R. T.; (1966) Ph.D. Thesis, London University.

Pascoe R. T., Radford K. C., Rawlings R. D. and Newey C. W. A.; (1967) J. Sci. Instruments 44 366.

Pickett G.; (1945) Proc. Amer. Soc. Testing Materials 45 846.

Rawlings R. D. and Newey C. W. A.; (1967) Acta Met. 15 440.

Rees W. P., Hopkins B. E. and Tipler H. R.; (1954) J.I.S.I. 177 93.

Reiter S. F. and Hibbard W. R.; (1955) T.A.I.M.E. 203 655.

Rosen A., Mote J. D. and Dorn J. E.; (1964) T.A.I.M.E. 230 1070.

Rosenbaum H. S. and Turnball D.; (1958) Acta Met. 6 653.

Rosenbaum H. S. and Turnball D.; (1959) Acta Met. 7 664.

Schadler H. W.; (1964) Acta Met. 12 861.

Schoeck G.; (1961) Acta Met. 9 382.

Seebold R. E. and Birks L. S.; (1960) J. Nucl. Mat. 3 260.

Sinha A. K., Buckley R. A. and Hume-Rothery W.; (1967) J.I.S.I. 205 191.

Smith R. L., Spangler G. and Brick R. M.; (1954) T.A.S.M. 46 973.

Stein D. F. and Low J. R.; (1959) J.A.P. 31 362.

Stein D. F.; (1966) Acta Met. 14 99.

Sykes W. P.; (1926) T.A.S.S.T. 10 839.

Sykes W. P.; (1940) T.A.S.M. 28 892.

Tetelman A. S.; (1963) Fracture of Solids, Interscience New York 461.

Thomas G.; (1961) J.I.M. 89 287.

Tietz T. and Wilson J.; (1961) Lockheed Missiles and Space Div. Rept. Code 2-36-61-1.

Wachtman J. B. and Lam D. G.; (1959) J. Amer. Ceram. Soc. 42 254.

Wagner C.; (1961) Z. Electrochem. 65 581.

Wert C.; (1949) J.A.P. 20 943.

Westgren A.; (1936) Sci. Repts. Tôhoku Univ. K. Honda Anniv. Vol. 852.